CR 112068

N72-31884

~~X72-10347~~

CASE FILE COPY

Final Report on Study of

Feedline Dynamic Effects on Shuttle POGO Stability

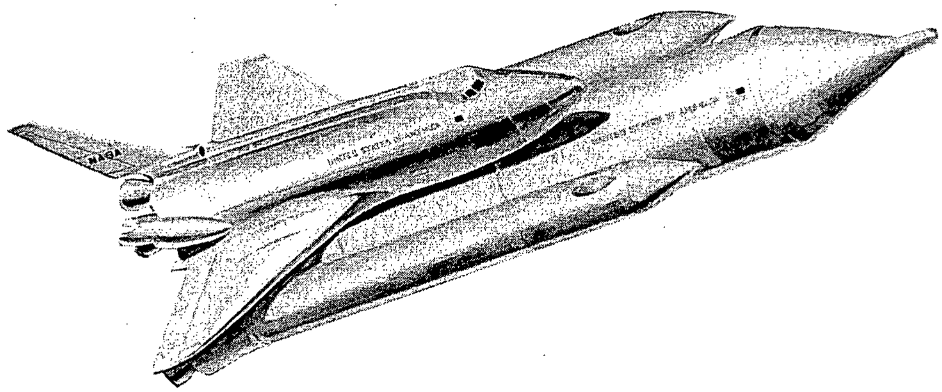

5 May 1972

Contract NAS1-10836 SD 72-SH-0039

FOR U.S. GOVERNMENT AGENCIES AND THEIR CONTRACTORS ONLY

Space Division
North American Rockwell

CR 112068

Final Report on Study of

Feedline Dynamic Effects on Shuttle POGO Stability

Prepared by O.D. DiMAGGIO
T. NISHIMOTO

R.H. Lassen

R.H. LASSEN
Study Manager

5 May 1972

Contract NAS1-10836

SD 72-SH-0039

Space Division
North American Rockwell

FOREWORD

This report is a description of work performed under Contract NAS1-10836, Study of Feedline Dynamic Effects on Shuttle POGO Stability, by the Space Division (SD) of North American Rockwell Corporation (NR) for the National Aeronautics and Space Administration, Langley Research Center, Hampton, Virginia, during the period of 25 June 1971 to 24 April 1972.

This work was conducted at NR/SD by O. DiMaggio and T. Nishimoto. Study Manager was R. H. Lassen of NR/SD and the Technical Monitor was L. D. Pinson of NASA Langley Research Center.

SUMMARY

The mathematical representation of a feedline is an important element in a POGO analysis. The dynamic characteristics of a feedline have been determined and the results presented in the form of transmission parameters. These transmission parameters include the effects of wall deformation, distributed damping, convective acceleration terms and the bulk modulus of the liquid. In order to reduce the characteristic equation associated with the system equations to a polynomial, it is necessary to approximate the transcendental terms appearing in the transmission parameters by appropriate polynomial expressions. The transmission parameters have been approximated using both power and product series expansions. The feedline transfer functions of a Shuttle Orbiter feedline configuration have been obtained using power and product series approximations of 60th, 120th, 180th, and 240th order. Bode plots using the above polynomial approximations have been obtained and the results compared with the "exact" solution. The "exact" solution to the feedline transfer function have been obtained by using the transcendental terms appearing in the transmission parameters.

The results show that the Shuttle Orbiter feedline may be modeled adequately by using polynomial approximations for the transcendental functions appearing in the transmission parameters. The power series approach has been shown to be preferable to the product series method.

CONTENTS

ILLUSTRATIONS

TABLES

I. INTRODUCTION

In order to perform a POGO stability analysis on the Shuttle Orbiter vehicle an accurate model of the propellant feedline is required. The model of the feedline must be made compatible with the stability program. The current stability program at NR can handle up to 40 fourth order differential equations with constant coefficients. It determines the characteristic polynomials associated with the stability equation and extracts the roots from these polynomials. Experience has shown that the program gives good numerical results for systems up to about 80th order. The transmission parameters for an elemental section of a feedline have been obtained by solving the linearized wave equation in the LaPlace domain. The transmission parameters include the effect of the convective acceleration terms and distributed damping. The "exact" transmission parameters have been used for obtaining results in the frequency domain and are useful in checking the numerical accuracy of the polynomial approximations required for inclusion into the stability program.

Bode plots of the feedline transfer functions have been obtained for a simplified feedline and a Shuttle Orbiter feedline configuration, using both a power series and product series approximation to the transmission parameters. The results have been compared with the "exact" solution.

The stability of the system and the solution vector were determined using both the power and product series approximations for the transmission parameters and the results compared.

II. SYSTEM EQUATIONS

The POGO stability equations deal with the interaction of the elements of the propulsion system and the structural system. Current Shuttle Orbiter designs use bipropellant (LO_2/LH_2) rocket engines. For the present study only the LO_2 system will be considered and the hydrogen system will be neglected. Although experience gained in the S-II stage of the Apollo Saturn V launch vehicle showed this approximation valid, it may or may not be true for the Shuttle Orbiter.

Since the present study is concerned primarily with modeling of the feedline and not with demonstrating the stability of the Shuttle, the hydrogen system has been neglected. The stability analysis to be performed will be meaningful only in that it may be used to compare the results for different approximations for the feedlines. The stability results themselves are not necessarily indicative of actual POGO tendencies. The system equations for the POGO stability analysis are given below:

$$\ddot{x}_o = \frac{4 T_{ess.}}{M} \qquad W_{SA} = \dot{W}_s - \rho A g \dot{x}$$

$$x_g = x_o + \sum \phi_i(x_g) q_i \qquad P_t = A(s) P_s + B(s) \ddot{W}_{SA}$$

$$\frac{T}{P_s} = H(s) \qquad P_t = \sum \gamma_i \ddot{q}_i + \rho h \ddot{x}_o$$

$$\frac{P_s}{\dot{W}_s} = G(s) \qquad \ddot{q}_i + 2\zeta\omega_i \dot{q}_i + \omega_i^2 q_i = \frac{4\phi_i(x_g) T_{ess.}}{\mathcal{M}_i}$$

In an attempt to account for the dynamic effects of the flow through the bulkhead and the feedline, the effective thrust $T_{ess.}$ may contain terms which include the pump inlet pressure P_s and the tank bottom pressure P_T.

The most common procedure is to draw a free body diagram of the engine system as shown in Figure 1,

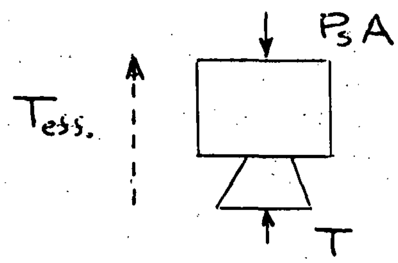

Figure 1. Engine Free Body Diagram

and obtain $T_{ess.}$ as the resultant force on the system.

$$T_{ess.} = T - P_s A$$

It should be noted that the factor 4 appearing with the effective thrust results from assuming that the feedlines to each engine are identical. This was the case for the four engine orbiter configuration used in this study.

III. FEEDLINE DYNAMICS

Feedline Dynamics concerns itself with wave propagation in the propellant lines and the dynamic characteristics of the pump. The approximate wave equations for the lines are developed in Appendix A. The solutions of these equations have been obtained and the results presented in the form of transmission parameters. The effect of the convective acceleration terms and distributed damping have been investigated using a simplified feedline and the "exact" or transcendental form of the transmission parameters. The transmission parameters have been approximated by polynomial expressions using both the power series and product series approach. The feedline transfer functions for a simplified feedline and a Shuttle Orbiter configuration have been determined using these polynomial approximations and the results compared with the "exact" solution.

1. Transmission Parameters For a Line Segment

The equations of motion of a compressible liquid in an elastic pipe are shown in Appendix A. The effect of distributed damping and the convective acceleration terms have been included in analysis. The results are presented in terms of transmission parameters and are given by the following equations:

$$\begin{Bmatrix} P_A \\ \rho a U_A \end{Bmatrix} = \begin{bmatrix} A(s) & B(s) \\ C(s) & D(s) \end{bmatrix} \begin{Bmatrix} P_B \\ \rho a U_B \end{Bmatrix}$$

where P_A, P_B, U_A, U_B are the pressure and fluid velocity at the upstream and downstream end, respectively, and A, B, C and D are the transmission parameters given by the following expression:

$$A(s) = \exp.\left\{-\frac{u_o}{a}\cdot\frac{s\ell}{a}\right\} ch\left[\sqrt{s(s+c)}\left(\frac{\ell}{a}\right)\right]$$

$$B(s) = \exp.\left\{-\frac{u_o}{a}\,\frac{s\ell}{a}\right\}\sqrt{\frac{s+c}{s}}\; sh\left[\sqrt{s(s+c)}\left(\frac{\ell}{a}\right)\right]$$

$$C(s) = \exp.\left\{-\frac{u_o}{a}\cdot\frac{s\ell}{a}\right\}\sqrt{\frac{s}{s+c}}\; sh\left[\sqrt{s(s+c)}\left(\frac{\ell}{a}\right)\right]$$

$$D(s) = \exp.\left\{-\frac{u_o}{a}\,\frac{s\ell}{a}\right\} ch\left[\sqrt{s(s+c)}\left(\frac{\ell}{a}\right)\right]$$

a. Convective Acceleration Terms

The linearized equations of motion for a compressible fluid in an elastic pipe are given by the following equations:

$$U_o \frac{\partial P}{\partial x} + \beta_e \frac{\partial U}{\partial x} + \frac{\partial P}{\partial t} = 0$$

$$\frac{\partial U}{\partial t} + u_o \frac{\partial U}{\partial x} + \frac{1}{\rho} \frac{\partial P}{\partial x} + c u = 0$$

where $C = \dfrac{f\, U_o}{D(1+.866\sqrt{f})}$ = damping parameter

β_e = equivalent bulk modulus

u_o = nominal fluid velocity

U, P = perturbed velocity and pressure

The effect of the convective acceleration terms $U_o \frac{\partial P}{\partial x}$ and $u_o \frac{\partial U}{\partial x}$ can be determined from the transmission parameters A, B, C and D given in the previous section. The effect of these terms is to introduce a lag term $e^{-\tau s}$ into the transmission parameters.

The effect of Mach No. $\frac{U_o}{a}$ and nondimensional frequency $\frac{\omega l}{a}$ on phase shift due to the convective acceleration term is given in Figure 2.

b. Power Series Representation

Neglecting the convective acceleration terms and the damping, the transmission equation for a segment of the feedline is given by:

$$\begin{Bmatrix} P_1 \\ \rho a U_1 \end{Bmatrix} = \begin{bmatrix} ch\frac{sl}{a} & sh\frac{sl}{a} \\ sh\frac{sl}{a} & ch\frac{sl}{a} \end{bmatrix} \begin{Bmatrix} P_2 \\ \rho a U_2 \end{Bmatrix}$$

The simplest procedure for reducing the hyperbolic functions to polynomials is to use a Taylor series.

$$ch\frac{sl}{a} = 1 + \frac{1}{2!}\left(\frac{sl}{a}\right)^2 + \frac{1}{4!}\left(\frac{sl}{a}\right)^4 + \cdots$$

$$sh\frac{sl}{a} = \frac{sl}{a} + \frac{1}{3!}\left(\frac{sl}{a}\right)^3 + \frac{1}{5!}\left(\frac{sl}{a}\right)^5 + \cdots$$

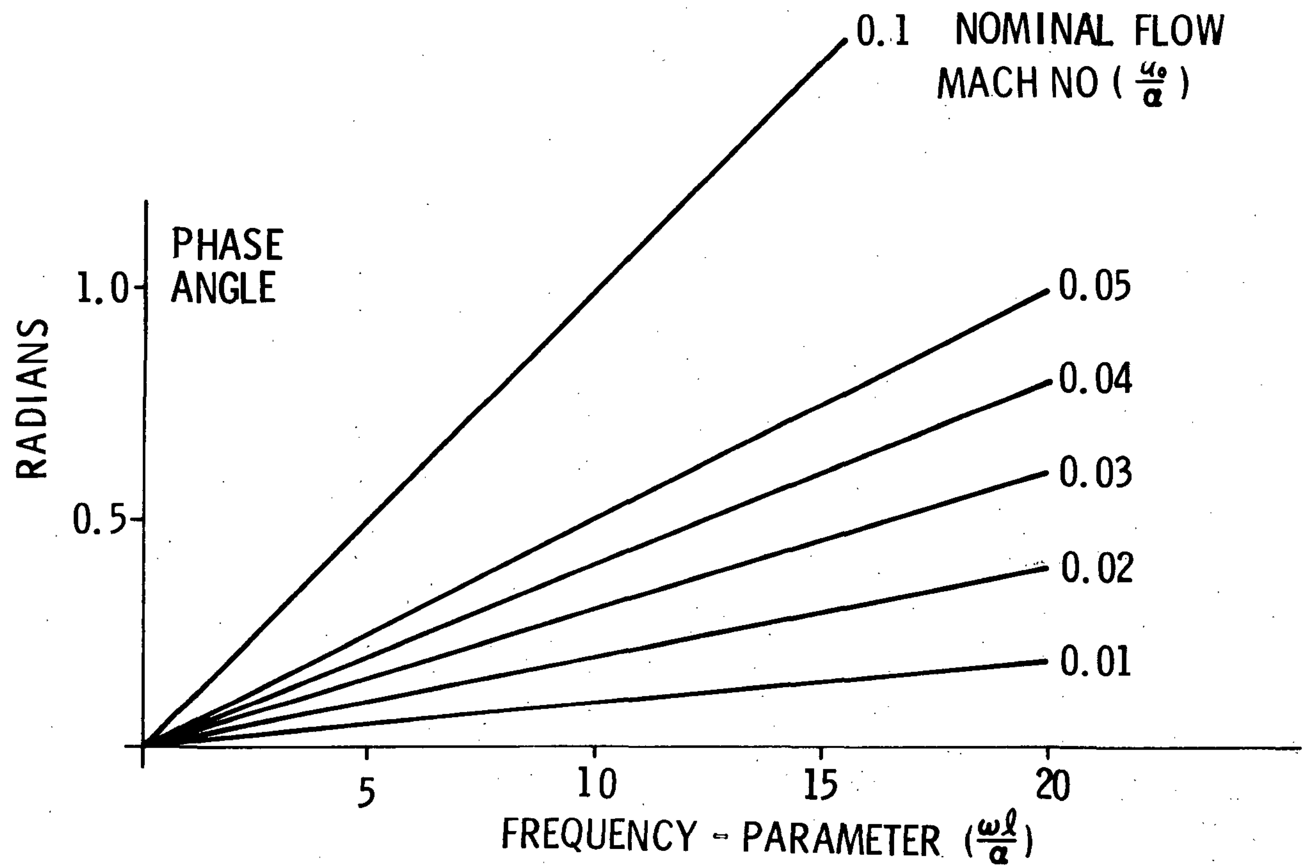

FIGURE 2 PHASE SHIFT DUE TO CONVECTIVE ACCELERATION TERM

$$\Phi = - \frac{u_o}{a} \frac{\omega \ell}{a}$$

In order to better understand the errors associated with using a Taylor series, Bode plots of $ch\frac{s\ell}{a}$ have been obtained using polynomials of different order and are shown in Fig. 3 - 8. It becomes clear that increasing the order of the polynomial approximation is not a very satisfactory method of expressing the hyperbolic functions. The results indicate reasonably good approximations for $\frac{\omega\ell}{a}<1$, but inaccurate results for larger values of the argument. It should be noted that when using this procedure some of the roots fail to appear. If a single Taylor series for the feedline were used, it would be possible to introduce instabilities due to the inaccuracies of the roots of polynomial approximation. This problem can be alleviated by using a segmented line and using terms no higher than the fourth order.

The transmission equations for a segmented line without damping will then be given by the following equations:

$$A_i = 1 + \frac{1}{2!}\left(\frac{s\ell}{a}\right)^2 + \frac{1}{4!}\left(\frac{s\ell}{a}\right)^4$$

$$B_i = \frac{s\ell}{a} + \frac{1}{3!}\left(\frac{s\ell}{a}\right)^3$$

$$\begin{bmatrix} A & B \\ C & D \end{bmatrix} = \begin{bmatrix} A_1 & B_1 \\ C_1 & D_1 \end{bmatrix}\begin{bmatrix} A_2 & B_2 \\ C_2 & D_2 \end{bmatrix}\cdots\begin{bmatrix} A_m & B_m \\ C_m & D_m \end{bmatrix}$$

c. Product Series Representation

The hyperbolic sines and cosines may be expanded into product series. (Ref. 3)

$$\operatorname{ch} z = \prod_{n=0}^{\infty} \left[1 + \frac{4 z^2}{(2n+1)^2 \pi^2} \right]$$

$$\operatorname{sh} z = z \prod_{n=1}^{\infty} \left[1 + \frac{z^2}{n^2 \pi^2} \right]$$

Letting $z^2 = s(s+c) \dfrac{\ell^2}{a^2}$

$$\operatorname{ch} z = \operatorname{ch}\left[\sqrt{s(s+c)}\left(\frac{\ell}{a}\right)\right] = \prod_{n=0}^{\infty} \left[1 + \frac{4s(s+c)}{(2n+1)^2 \pi^2}\left(\frac{\ell}{a}\right)^2 \right]$$

$$\sqrt{\frac{s+c}{s}} \operatorname{sh}\left[\sqrt{s(s+c)}\left(\frac{\ell}{a}\right)\right] = \left(\frac{s+c}{a}\right)\ell \prod_{n=1}^{\infty} \left[1 + \frac{s(s+c)}{n^2 \pi^2}\left(\frac{\ell}{a}\right)^2 \right]$$

$$\sqrt{\frac{s}{s+c}} \operatorname{sh}\left[\sqrt{s(s+c)}\left(\frac{\ell}{a}\right)\right] = \frac{s\ell}{a} \prod_{n=1}^{\infty} \left[1 + \frac{s(s+c)}{n^2 \pi^2}\left(\frac{\ell}{a}\right)^2 \right]$$

Letting $\omega_n = \dfrac{(2n+1)\pi a}{2\ell}$

$$\gamma_n = \frac{1}{(2n+1)\pi}\left(\frac{c\ell}{a}\right)$$

$$P_n = \frac{n \pi a}{\ell}$$

$$\xi_n = \frac{1}{2n\pi}\left(\frac{c\ell}{a}\right)$$

we obtain the following matrix equation for the transmission equations.

$$\begin{bmatrix} A & B \\ C & D \end{bmatrix} = \exp.\left\{-\frac{u_0}{a} \cdot \frac{s\ell}{a}\right\} \begin{bmatrix} A_1 & B_1 \\ C_1 & D_1 \end{bmatrix}$$

where

$$A_1 = \prod_{n=0}^{\infty} \left[1 + \frac{2\zeta_n s}{\omega_n} + \frac{s^2}{\omega_n^2} \right]$$

$$B_1 = (s+c)\,\frac{\ell}{a} \prod_{n=1}^{\infty} \left[1 + \frac{2\xi_n s}{P_n} + \frac{s^2}{P_n^2} \right]$$

$$C_1 = \frac{s\ell}{a} \prod_{n=1}^{\infty} \left[1 + \frac{2\xi_n s}{P_n} + \frac{s^2}{P_n^2} \right]$$

It is clear from looking at the damping terms $\zeta_n = \frac{1}{(2n+1)\pi}\left(\frac{c\ell}{a}\right)$ and $\xi_n = \frac{1}{2n\pi}\left(\frac{c\ell}{a}\right)$ that the damping coefficient is inversely proportional to the mode number.

One should, therefore, expect that the peaks which occur in the feedline transfer functions should be sharper at the higher frequencies. This in fact, is what happens for this Shuttle Orbiter feedline configuration (Figure 46).

Bode plots of the hyperbolic cosine have been obtained using from 2 to 7 roots and are shown in Figures 3 - 8. The product expansions by their very nature maintain the roots exactly, but the error in gain increases with increasing frequency.

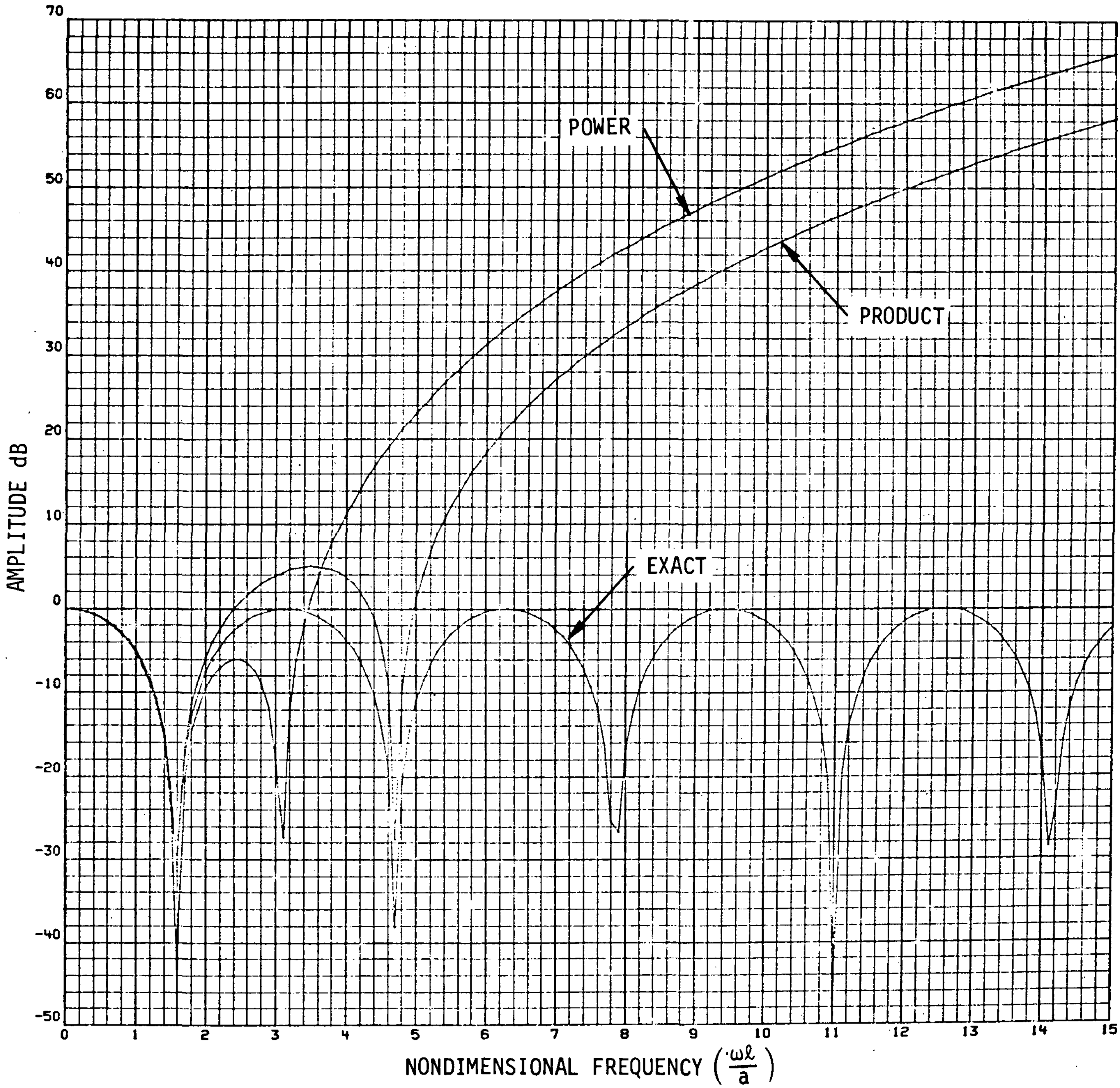

Figure 3 Power and Product Expansion Hyperbolic Cosine (4th Order)

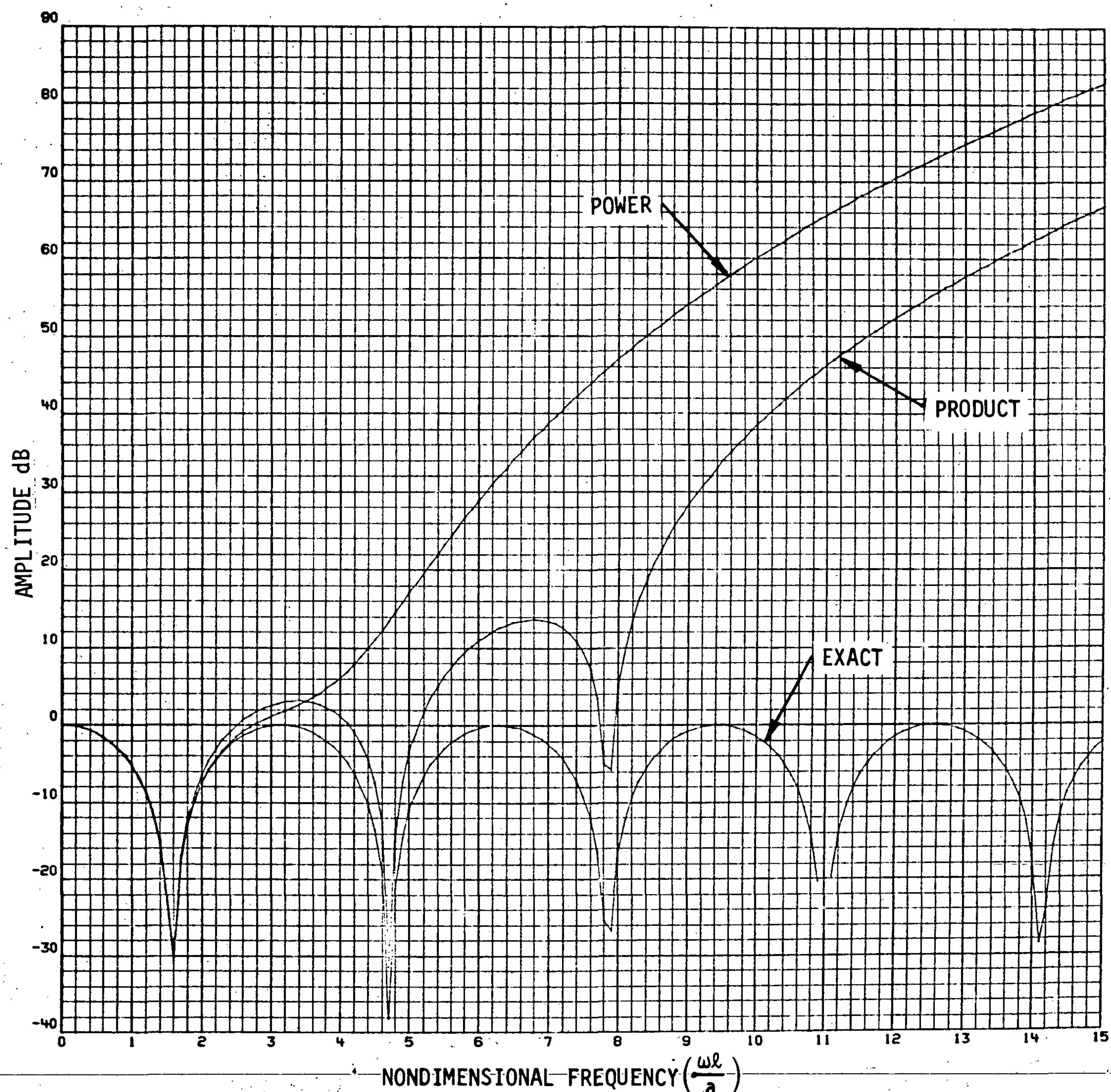

Figure 4 Power and Product Expansion
Hyperbolic Cosine (6th Order)

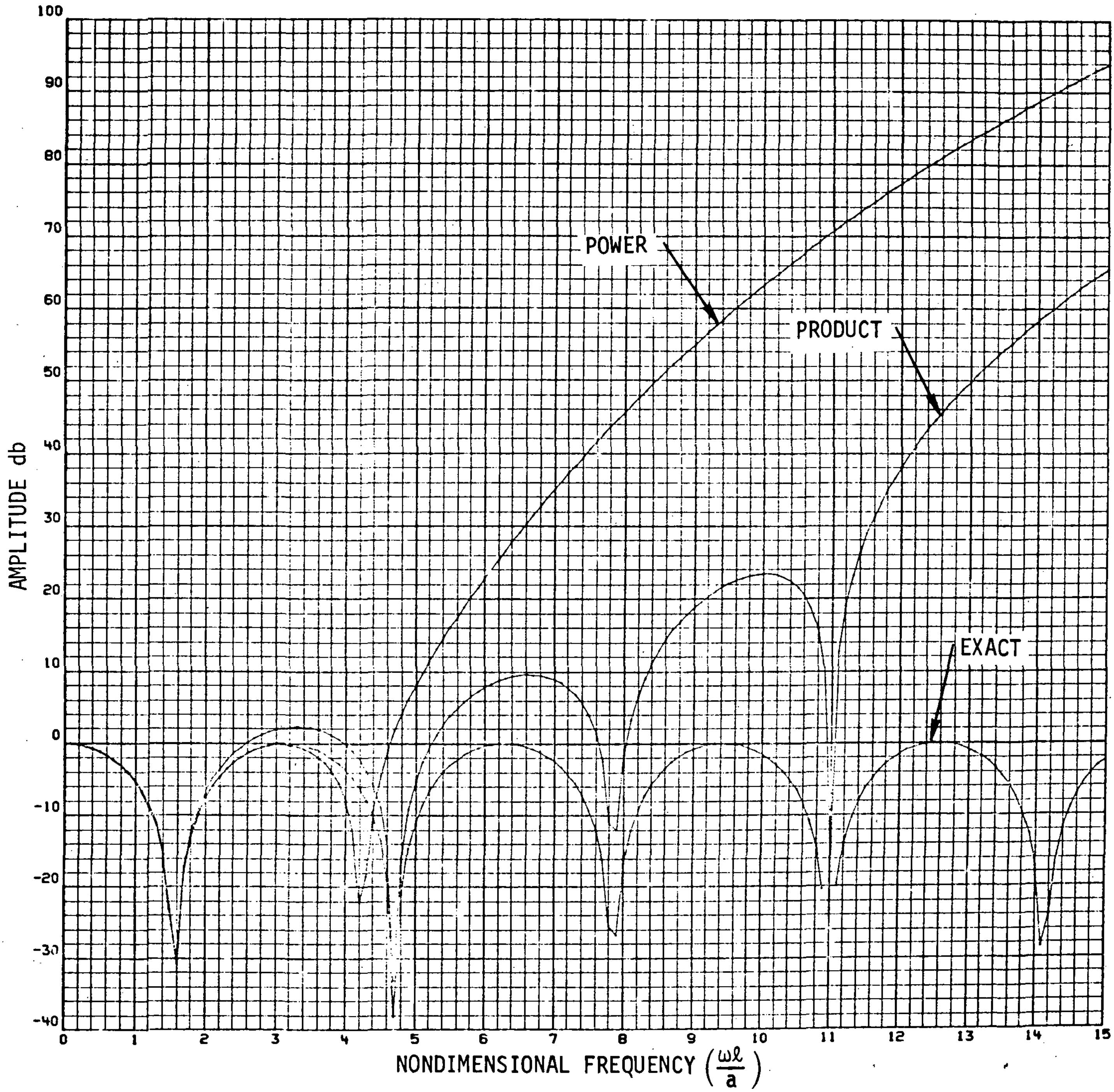

Figure 5 Power and Product Expansion
Hyperbolic Cosine (8th Order)

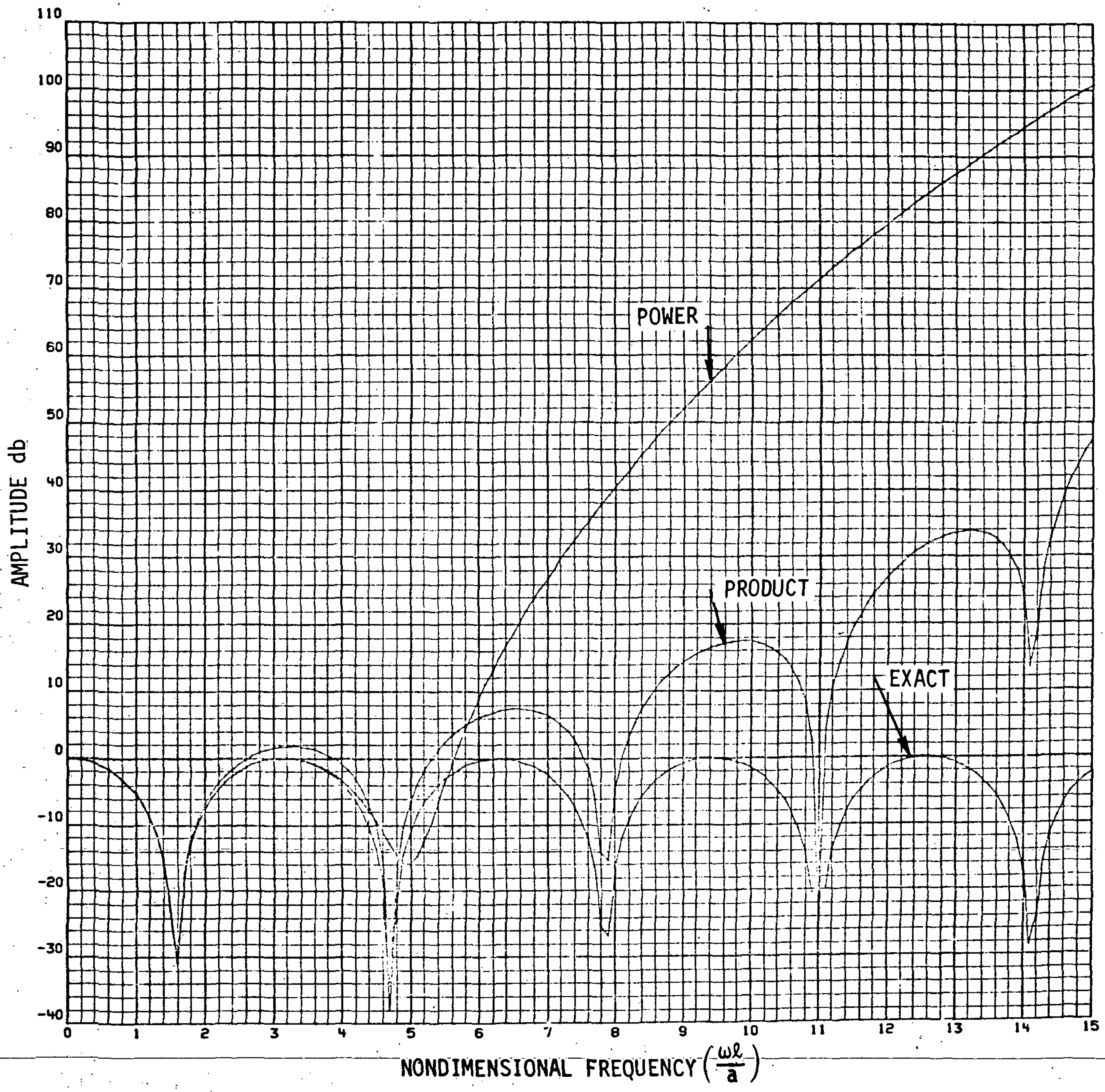

Figure 6 Power and Product Expansion
Hyperbolic Cosine (10th Order)

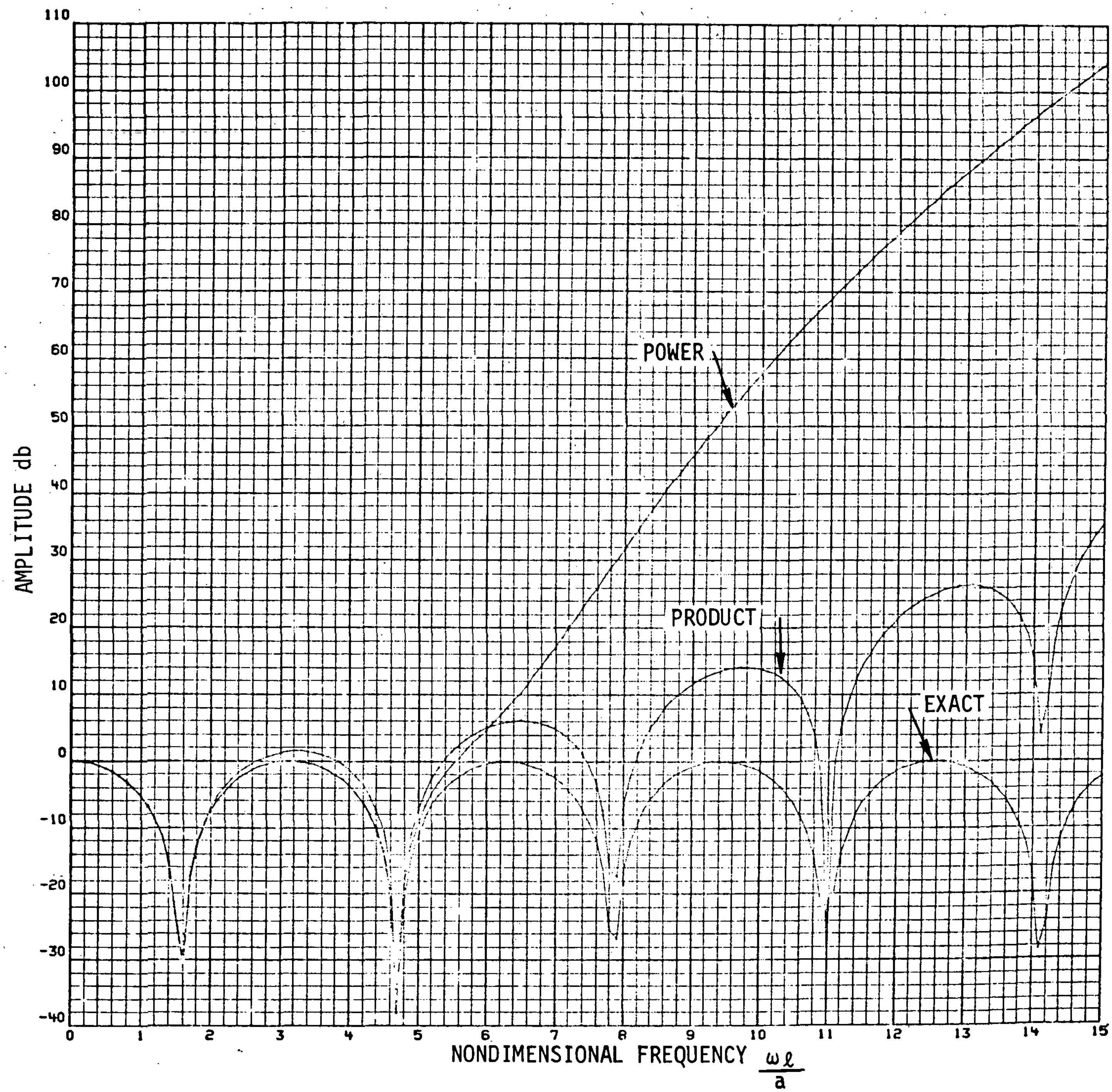

Figure 7 Power and Product Expansion
Hyperbolic Cosine (12th Order)

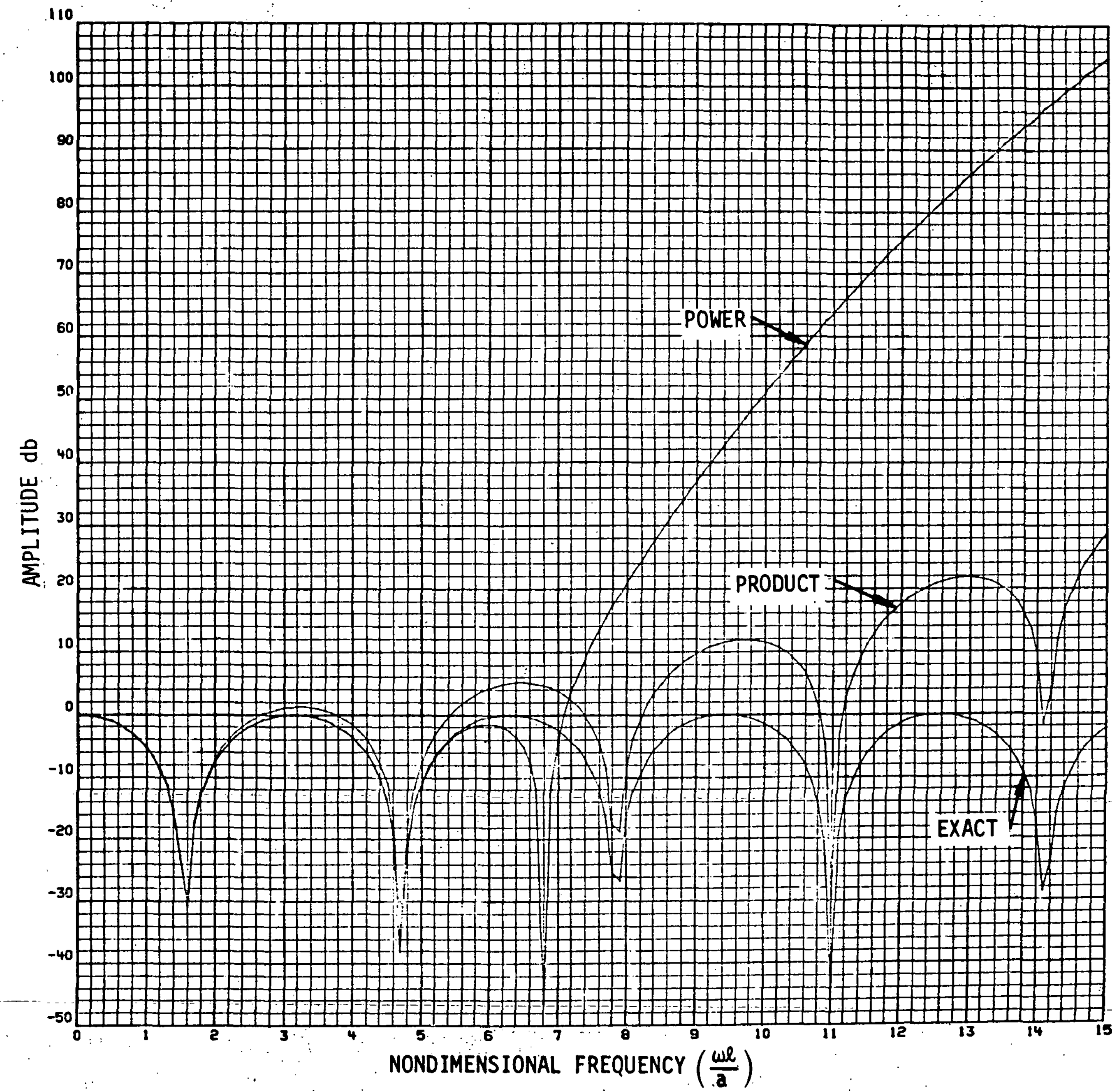

Figure 8 Power and Product Expansion Hyperbolic Cosine (14th Order)

2. Feedline Transfer Function For a Straight Line With Single Compliance Pump

The dynamic characteristics of a feedline are most readily summarized by means of the feedline transfer function. This transfer function is usually defined as the pump inlet pressure (P_S) divided by the tank bottom pressure (P_T). In order to investigate relative merits of lumped vs distributed damping, use will be made of a simplified feedline shown in Figure 9.

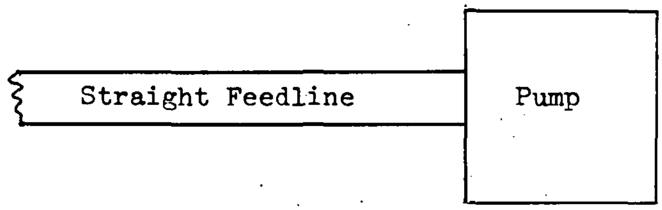

Figure 9. Simplified Feedline

The relationship between P_s and the P_T are given by the following equations:

$$P_T = A(s)\, P_s + B(s) \frac{a}{Ag} \dot{W}_s$$

$$\frac{P_s}{\dot{W}_s} = G(s) = \frac{k}{s}$$

where

$$A(s) = \exp.\left\{-\frac{u_o}{a} \cdot \frac{s\ell}{a}\right\} ch\left[\sqrt{s(s+c)}\left(\frac{\ell}{a}\right)\right]$$

$$B(s) = \exp.\left\{-\frac{u_o}{a} \cdot \frac{s\ell}{a}\right\} \sqrt{\frac{s+c}{s}}\; sh\left[\sqrt{s(s+c)}\left(\frac{\ell}{a}\right)\right]$$

$$\dot{W}_s = \rho g A U_s$$

Using the above relationship, the feedline transfer function becomes:

$$\frac{P_s}{P_t} = \frac{\exp.\left\{\frac{U_o}{a} \cdot \frac{s\ell}{a}\right\}}{ch\left[\sqrt{s(s+c)}\left(\frac{\ell}{a}\right)\right] + \Gamma\sqrt{s(s+c)}\left(\frac{\ell}{a}\right) sh\left[\sqrt{s(s+c)}\left(\frac{\ell}{a}\right)\right]}$$

where

$$\Gamma = \frac{a^2}{Ag\ell k}$$

When using the single compliance model the following constants were used.

$$\frac{U_0}{a} = 0$$

$$\frac{c\ell}{a} = .006$$

$$\Gamma = 0.208$$

$$\ell = 1200 \text{ IN.} \; (30.48 \text{ M.})$$

$$a = 20{,}000 \; \frac{\text{IN.}}{\text{SEC.}} \; \left(507 \; \frac{\text{M.}}{\text{SEC.}}\right)$$

The transmission parameters previously considered had the damping distributed along the line segment. An alternate procedure is to lump the damping at the ends of elemental sections of the feedline. The pressure loss due to damping in a section of the feedline is given by the following expression:

$$P_2 = - f \frac{\ell}{D} \left(\frac{\rho U^2}{2}\right)$$

$$\frac{1}{\sqrt{f}} = 2 \,\text{LOG}\left(N_R \sqrt{f}\right) - 0.8$$

The linear perturbation equations may be obtained by removing the steady state terms. The resulting equations for the perturbed values of pressure and velocity are given below:

$$\Delta P = - c \ell \rho u$$

$$c = \frac{f U_0}{D\left(1 + .866\sqrt{f}\right)}$$

In order to compare lumped with distributed damping, Bode plots of the feedline transfer function were obtained for an n-segmented line with lumped damping. These results were compared with the "exact" solution using distributed damping. Two typical runs using lumped damping for n = 1 and 5 are shown in Figures 11 and 12 and may be compared with the case of distributed damping shown in Figure 10. The results are seen to be identical except for the peak gains.

The effects of the length of elemental sections on the error have been shown graphically for the peak gains at the first and fifth peaks in Figures 13 and 14. A more informative curve may be obtained by plotting peak gains P_s/P_t vs nondimensional frequency Θ where $\Theta = \frac{\omega l}{n a}$. This curve (Figure 15) shows that in the frequency range of interest, the error is acceptable provided $\Theta < 1$ It should be noted that $\Theta \doteq 0$ corresponds to distributed damping.

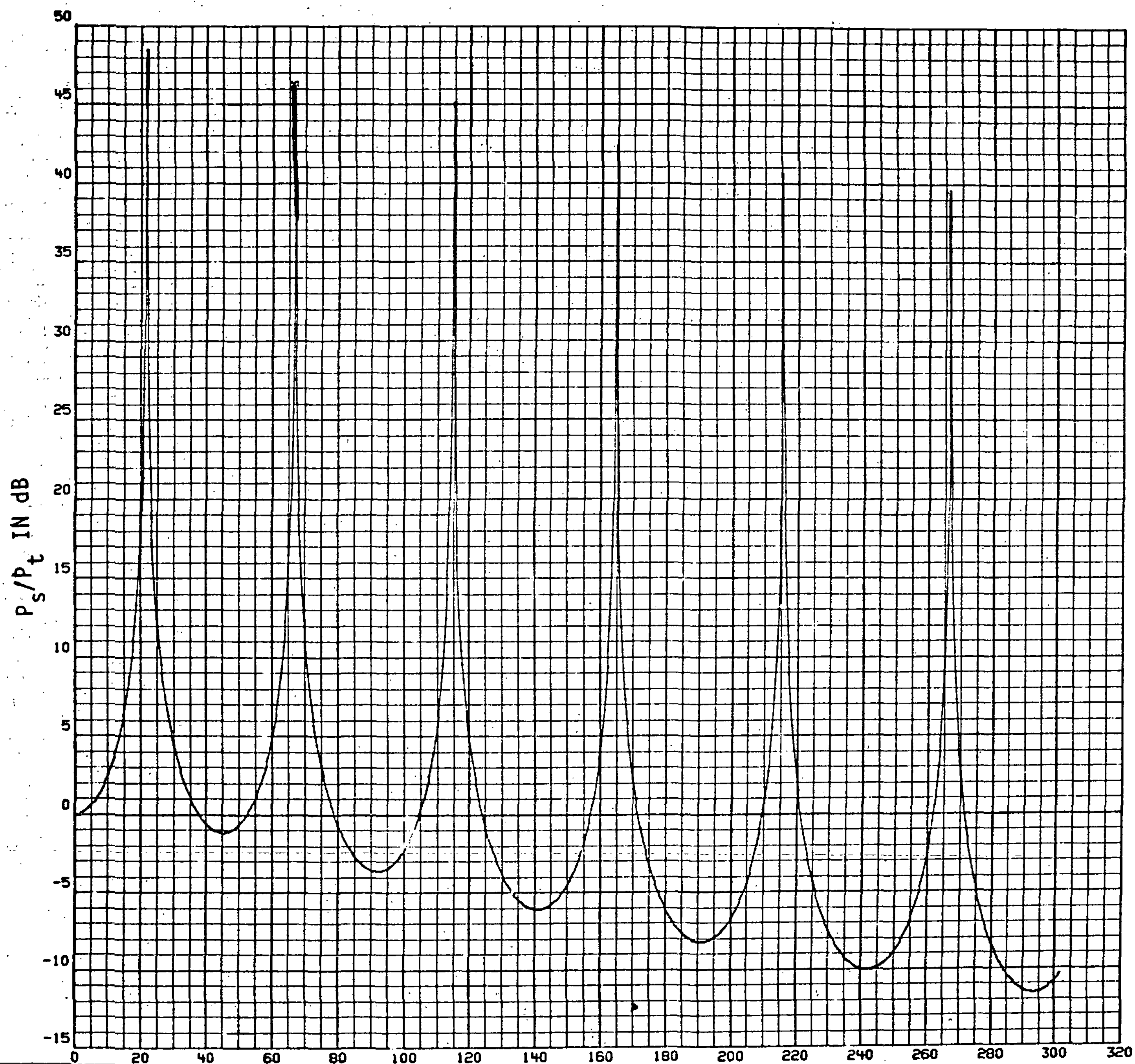

Figure 10 Straight Line with Single Compliance Pump "Exact" Solution

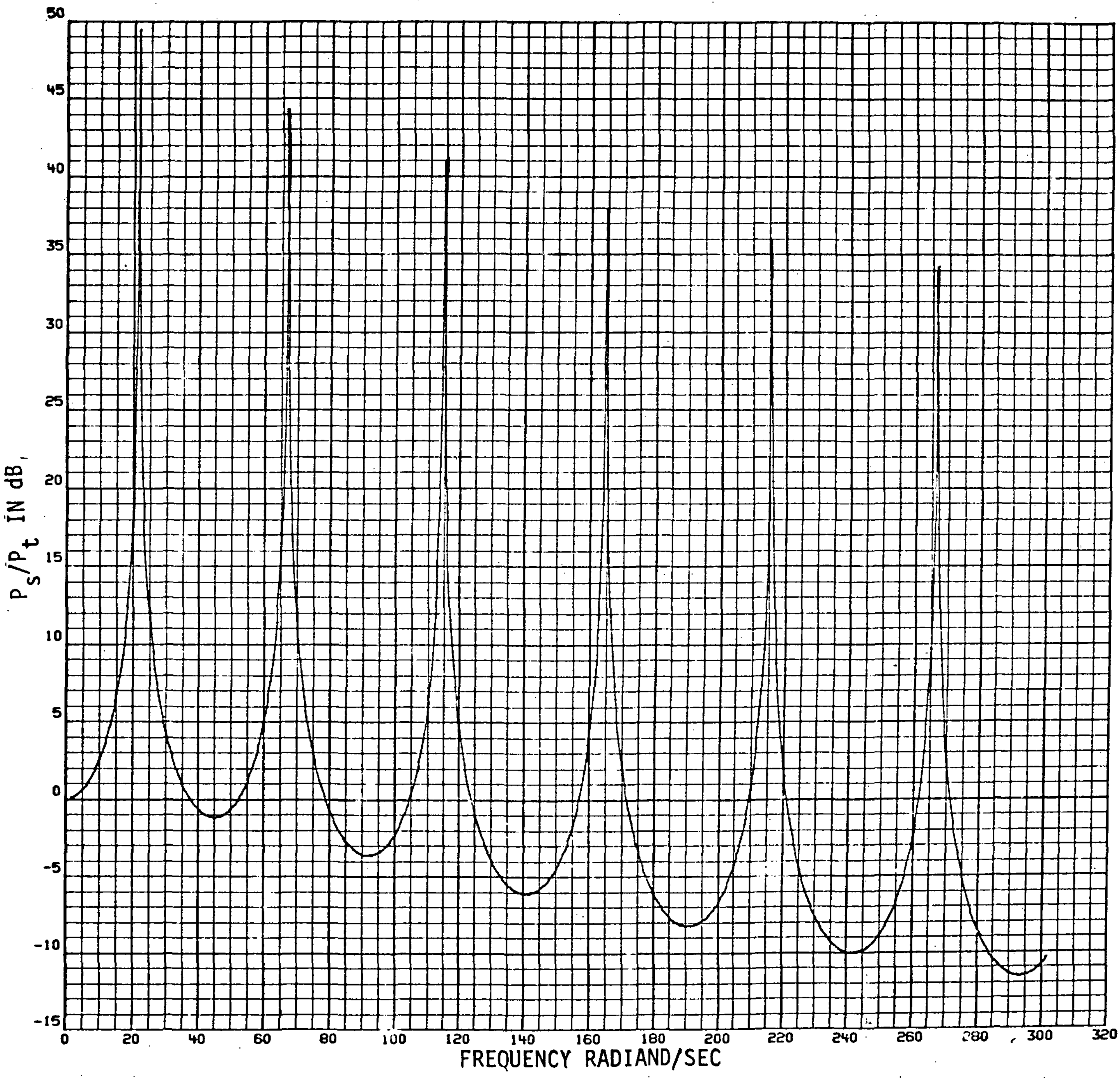

Figure 11 Straight Line with Single Compliance Pump Damping Lumped (One Segment)

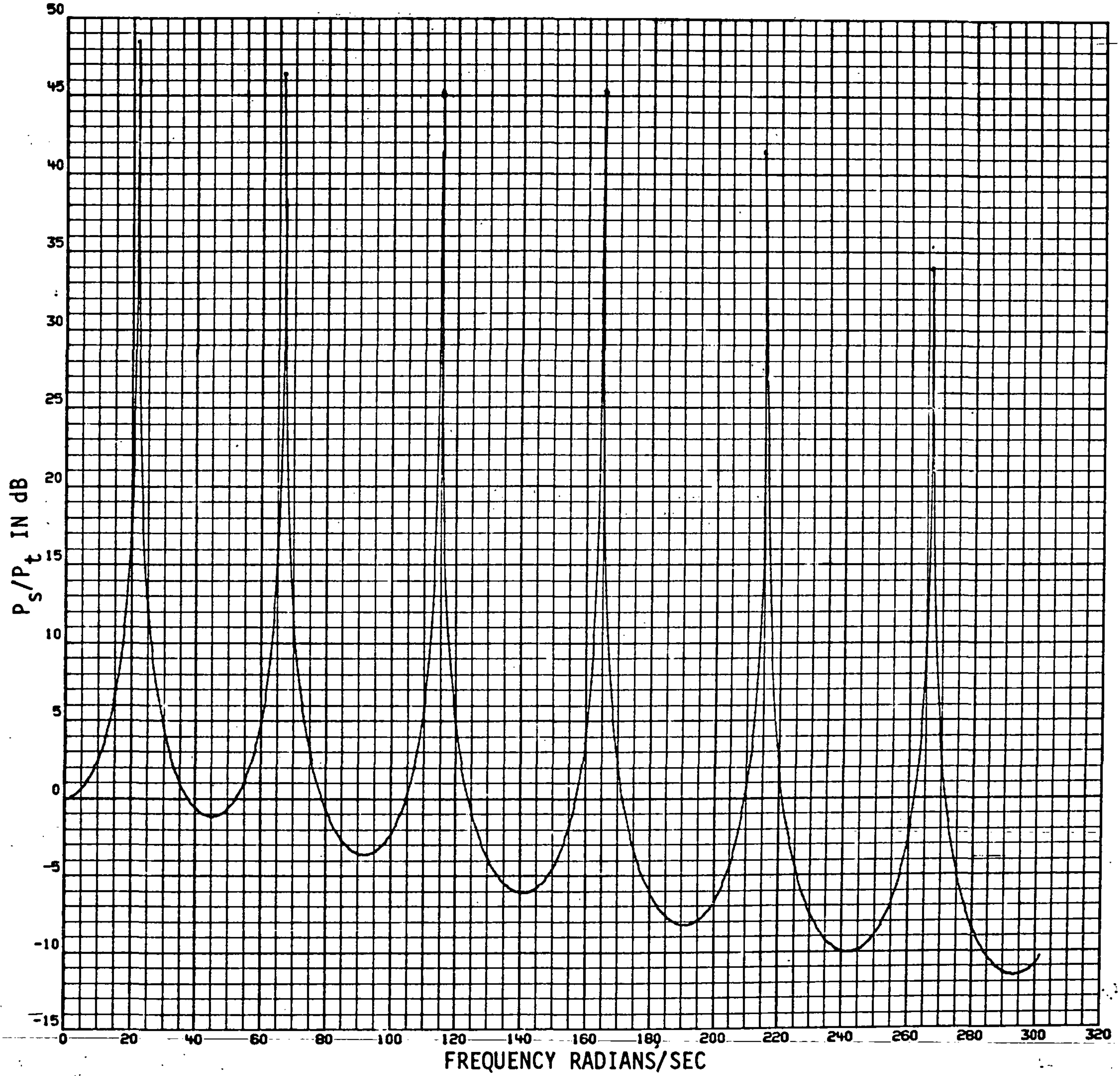

Figure 12 Straight Line with Single Compliance Pump
Damping Lumped (Five Segments)

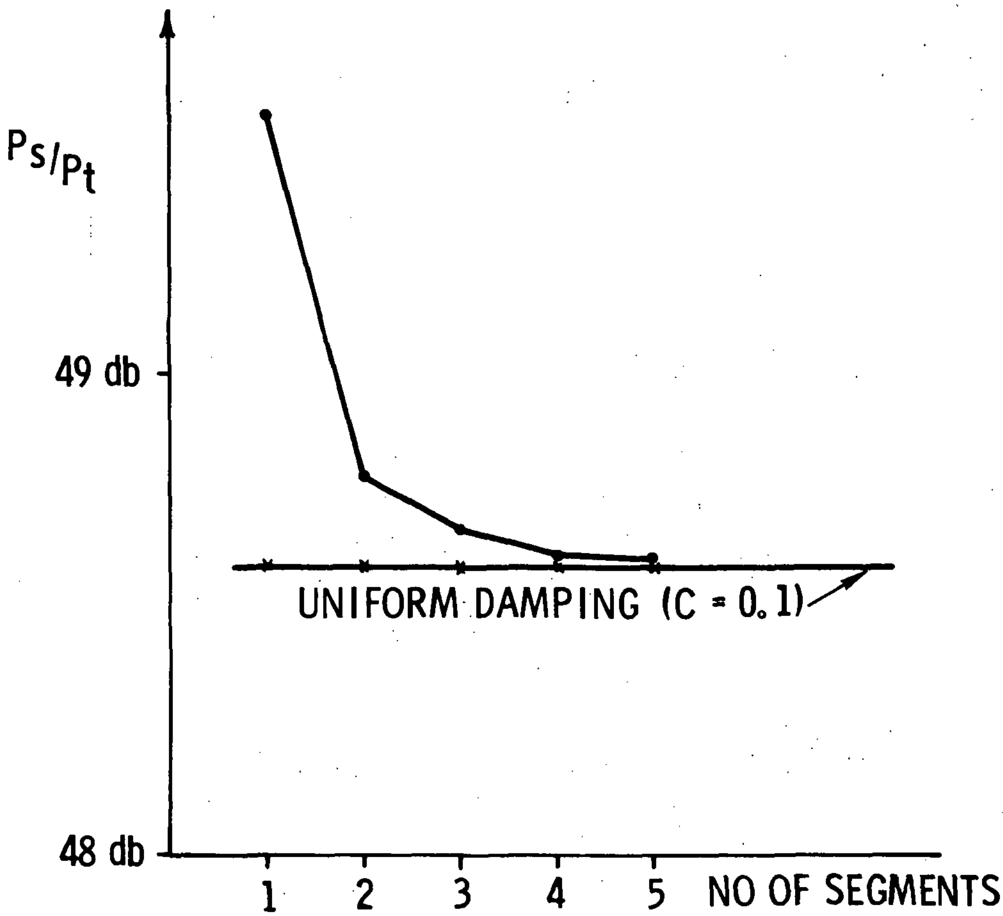

Figure 13 Peak Gain Vs No. of Segments at ω = 21.75 Rad/Sec

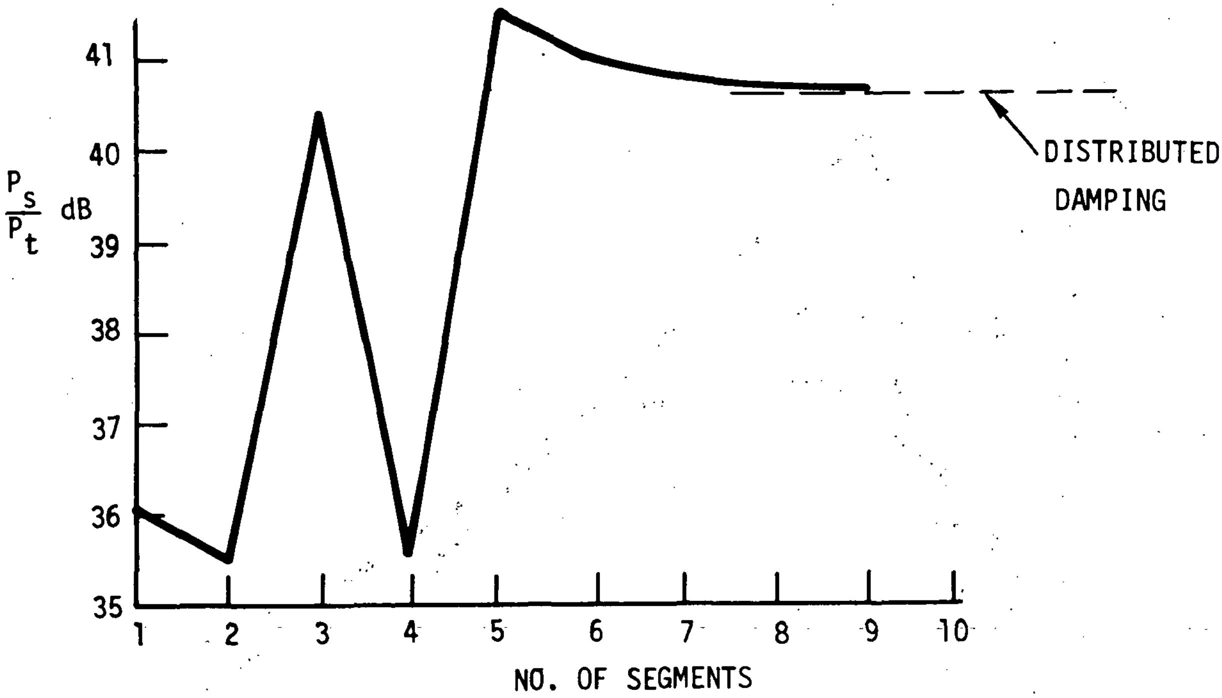

Figure 14 Peak Gain Vs No. of Segments at $\omega = 215$ Rad/Sec

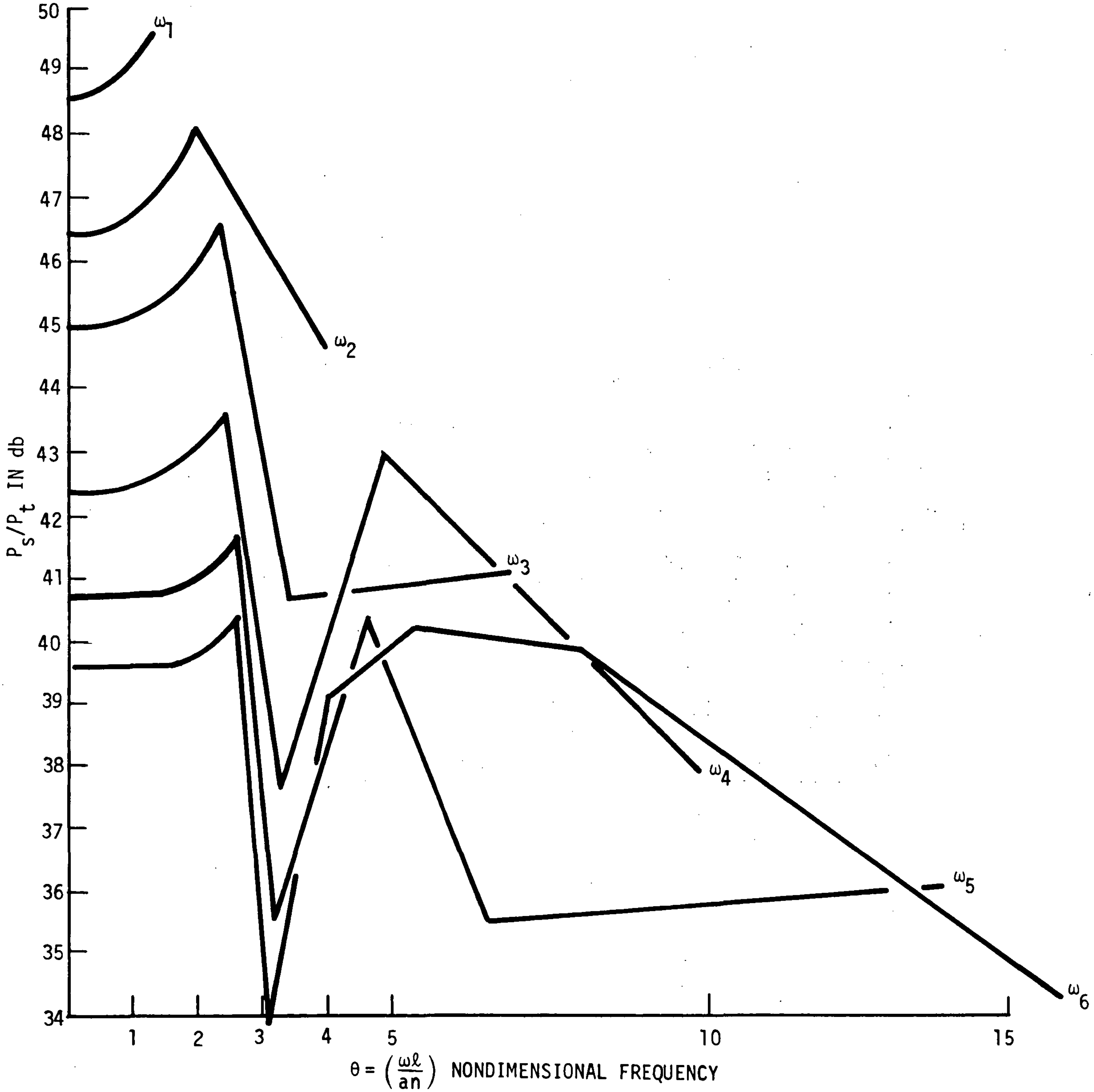

Figure 15 Peak Gain Vs. Nondimensional Frequency

3. Feedline Transfer Function of Straight Feedline with Double Compliance Pump

Prior to the analysis of the Shuttle Orbiter feedline, a simplified feedline consisting of a straight 1200 in. (30.48 m) line with a double compliance pump will be considered. Because of the lack of bends in the line, the only damping is that due to the shear stresses already considered when determining the transmission parameters. Current state of the art is to obtain the dynamic pump characteristics experimentally in terms of the pump termination impedance or the pump inlet pressure (P_s) divided by the flow rate ($\dot{W}_s$). For use in this simplified line as well as the Shuttle Orbiter feedline, use will be made of the pump termination impedance obtained from tests on the J-2 engine in lieu of more precise information on the Shuttle engines.

The relationship between the pump inlet pressure (P_s) and the tank bottom pressure (P_T) are given by the following equations:

$$P_T = A(s)\,P_s + \frac{a}{Ag}\,B(s)\,\dot{W}_s$$

$$\frac{P_s}{\dot{W}_s} = G(s)$$

where

$$G = K\,h(s)$$

$$h(s) = \frac{1 + \frac{2\zeta_0 s}{2\pi f_0} + \frac{s^2}{(2\pi f_0)^2}}{\left(1+\frac{s}{2\pi f_1}\right)\left(1+\frac{2\zeta_2 s}{2\pi f_2}+\frac{s^2}{(2\pi f_2)^2}\right)}$$

$\zeta_0 = .233$ $\qquad f_0 = 13.64$ Hz.

$\zeta_2 = .145$ $\qquad f_1 = 2.64$ Hz.

$K = 3.58\ \frac{\text{SEC}}{\text{IN.}^2}\left(5.44\times10^4\ \frac{1}{\text{M SEC}}\right)$ $\qquad f_2 = 19.71$ Hz.

The feedline transfer function may now be obtained in terms of the feedline transmission parameters and the pump characteristics.

$$\frac{P_s}{P_t} = \frac{\exp.\left\{\frac{U_o}{a}\cdot\frac{s\ell}{a}\right\}}{ch\left[\sqrt{s(s+c)}\left(\frac{\ell}{a}\right)\right]+\left(\frac{\mu}{h(s)}\sqrt{\frac{s+c}{s}}\right)sh\left[\sqrt{s(s+c)}\left(\frac{\ell}{a}\right)\right]}$$

where

$$\mu = \frac{a}{KAg} = 0.058$$

$$\ell = 1200 \text{ IN. } (30.48 \text{ M.})$$

$$a = 20{,}000 \frac{\text{IN.}}{\text{SEC.}} \left(507 \frac{\text{M.}}{\text{SEC.}}\right)$$

$$A = 250 \text{ IN.}^2 \quad (.161 \text{ M}^2)$$

$$\frac{c\ell}{a} = 0.006$$

These numbers have been chosen so that they are representative of the Shuttle Orbiter.

In order to evaluate the method of expanding the transmission parameters by power and product series, it was necessary to obtain an "exact" Bode plot by using the transcendental functions which appear in the transmission parameters. These results are shown in Figures 16 and 17. The Bode plots using the power and product series representation are shown in Figures 18 - 29 and Figures 30 - 41, respectively. Results have been obtained using polynomial approximations correct to the 4th, 8th, 12th, 16th, 20th, and 40th order in $\frac{s\ell}{a}$. The results show that the power series approximations are in fairly good agreement provided the nondimensional frequency $\frac{\omega\ell}{na} < 1$ where $\frac{\ell}{n}$ is the length of the elemental segment. For frequencies above this value, the gains and to a larger extent the phase, begin to vary from the "exact" solution. The product series solutions of the same order have about the same accuracy as the power series results up to the 8th order. The higher order solutions, however, are not as satisfactory. The gain curve tends to slope downward. This can be explained by looking at the product series expansions of the hyperbolic cosine curves given in Figures 3 - 8. The product expansion of the hyperbolic cosine (as well as the hyperbolic sine, not shown) have errors which increase the gain at the higher frequencies. Since these terms appear in the denominator of the transfer function P_S/P_T they have the effect of reducing the gain at higher frequencies.

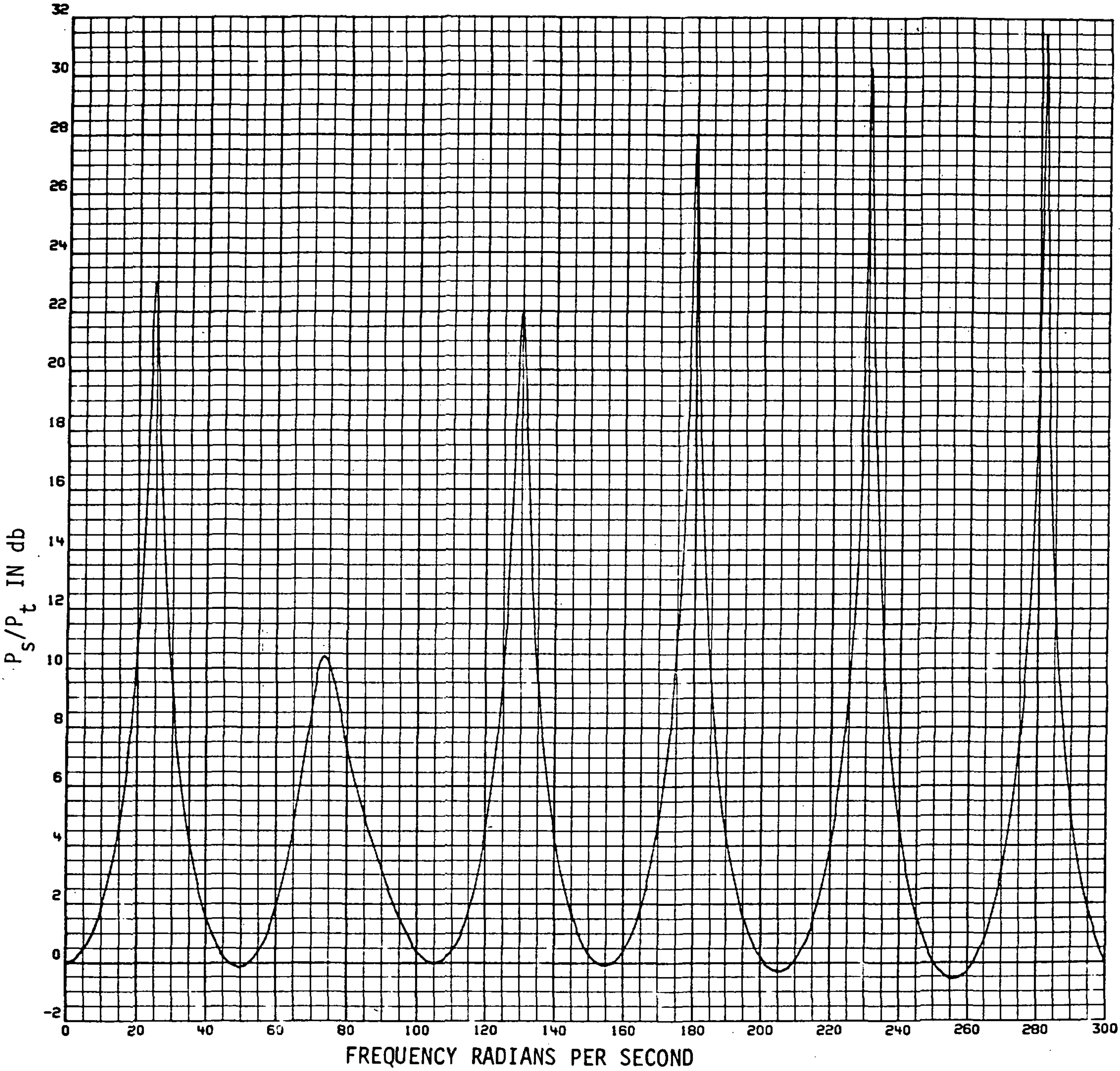

Figure 16 Straight Line with Double Compliance Pump "Exact" Solution

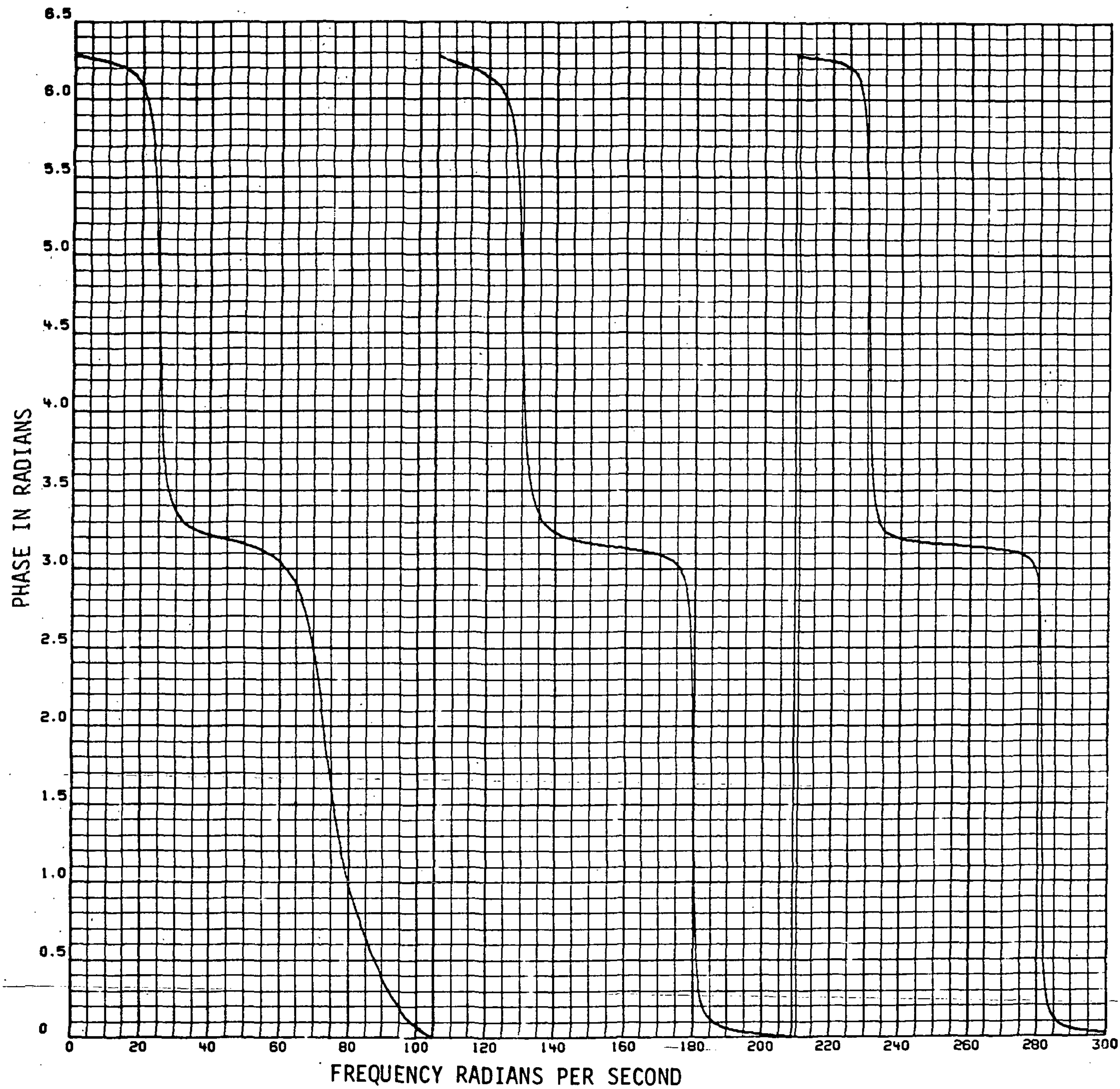

Figure 17 Straight Line with Double Compliance Pump
"Exact" Solution

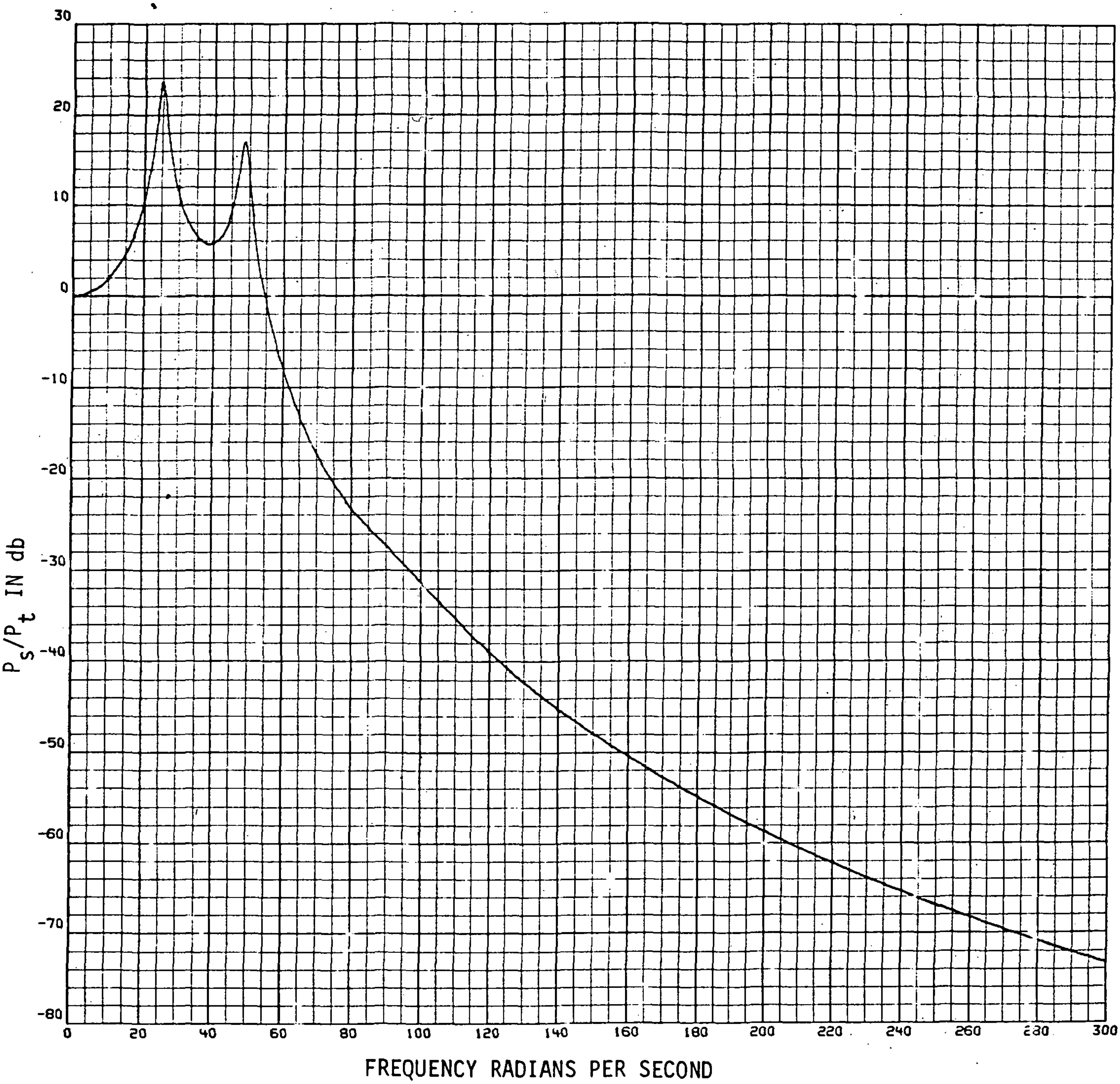

Figure 18 Straight Line with Double Compliance Pump Power Series (4th Order)

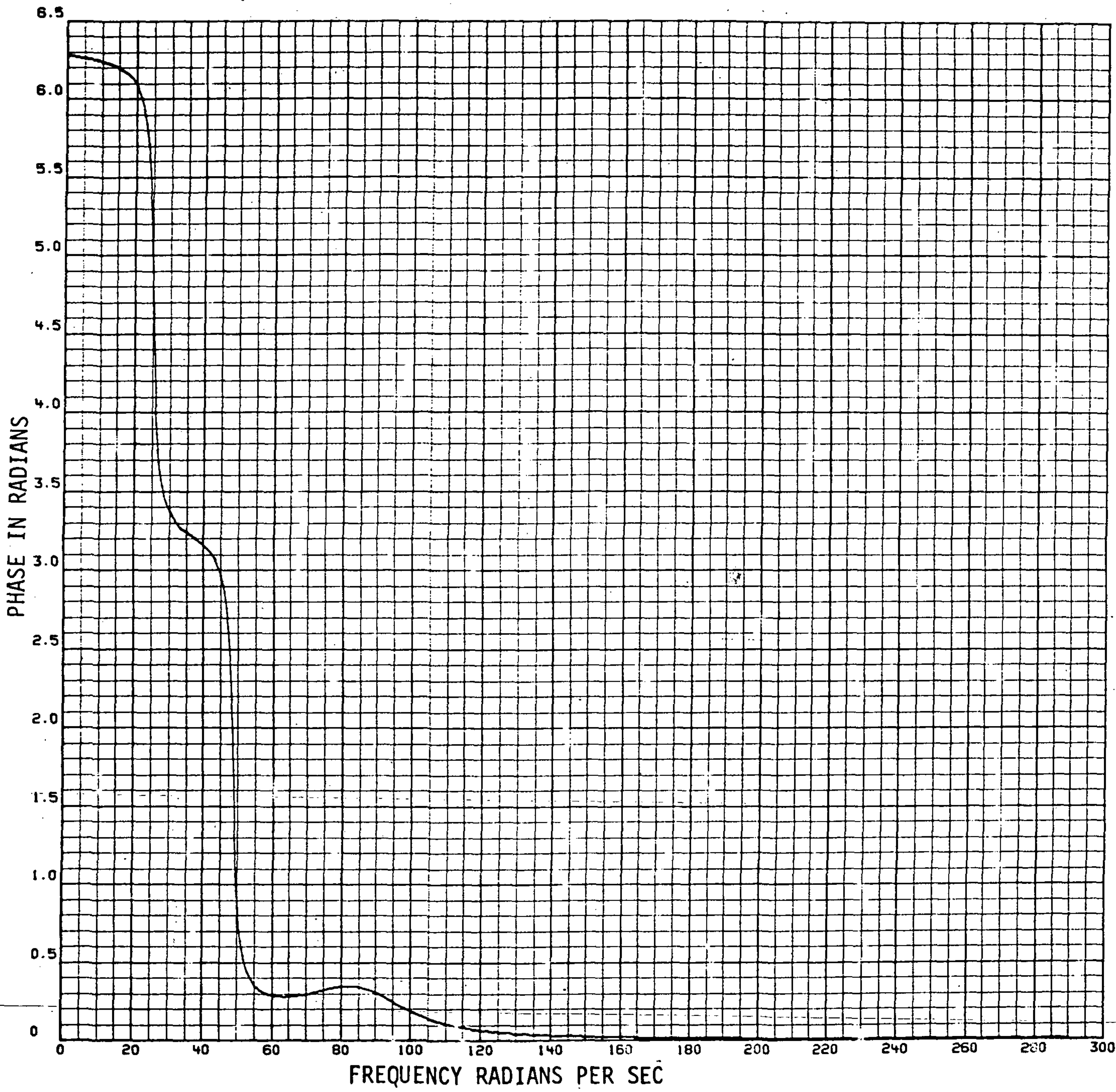

Figure 19 Straight Line with Double Compliance Pump Power Series (4th Order)

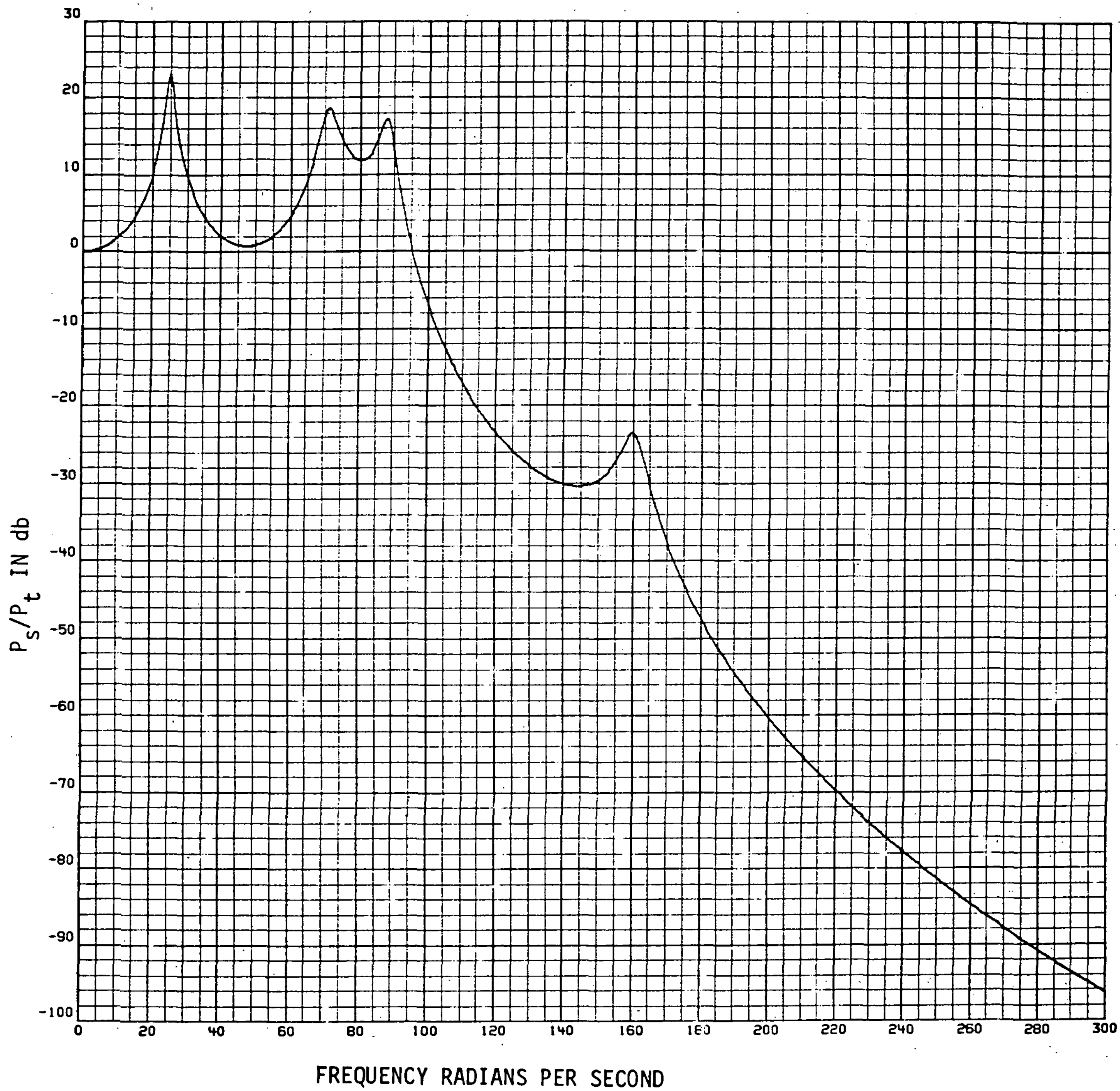

Figure 20 Straight Line with Double Compliance Pump Power Series (8th Order)

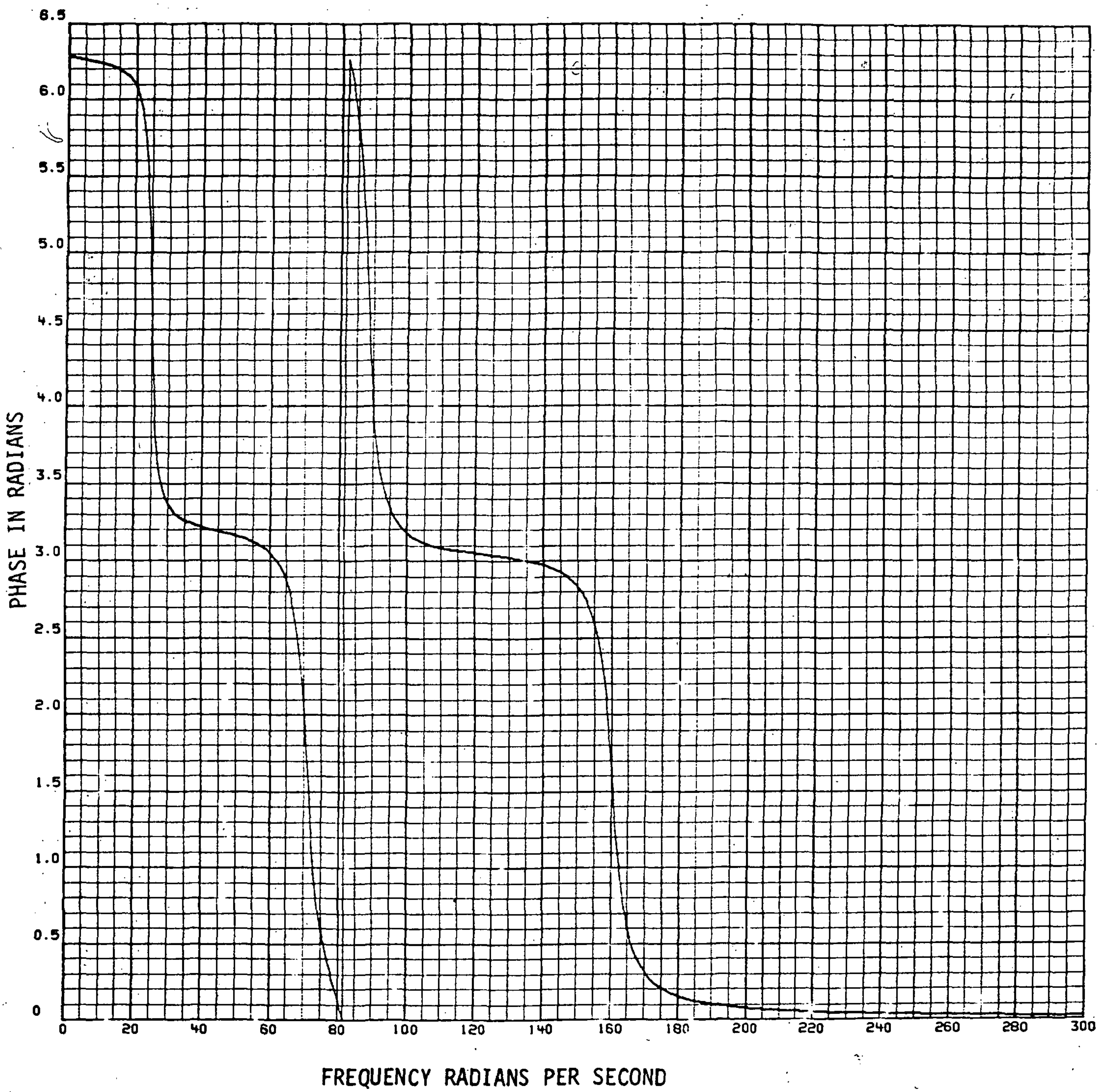

Figure 21 Straight Line with Double Compliance Pump Power Series (8th Order)

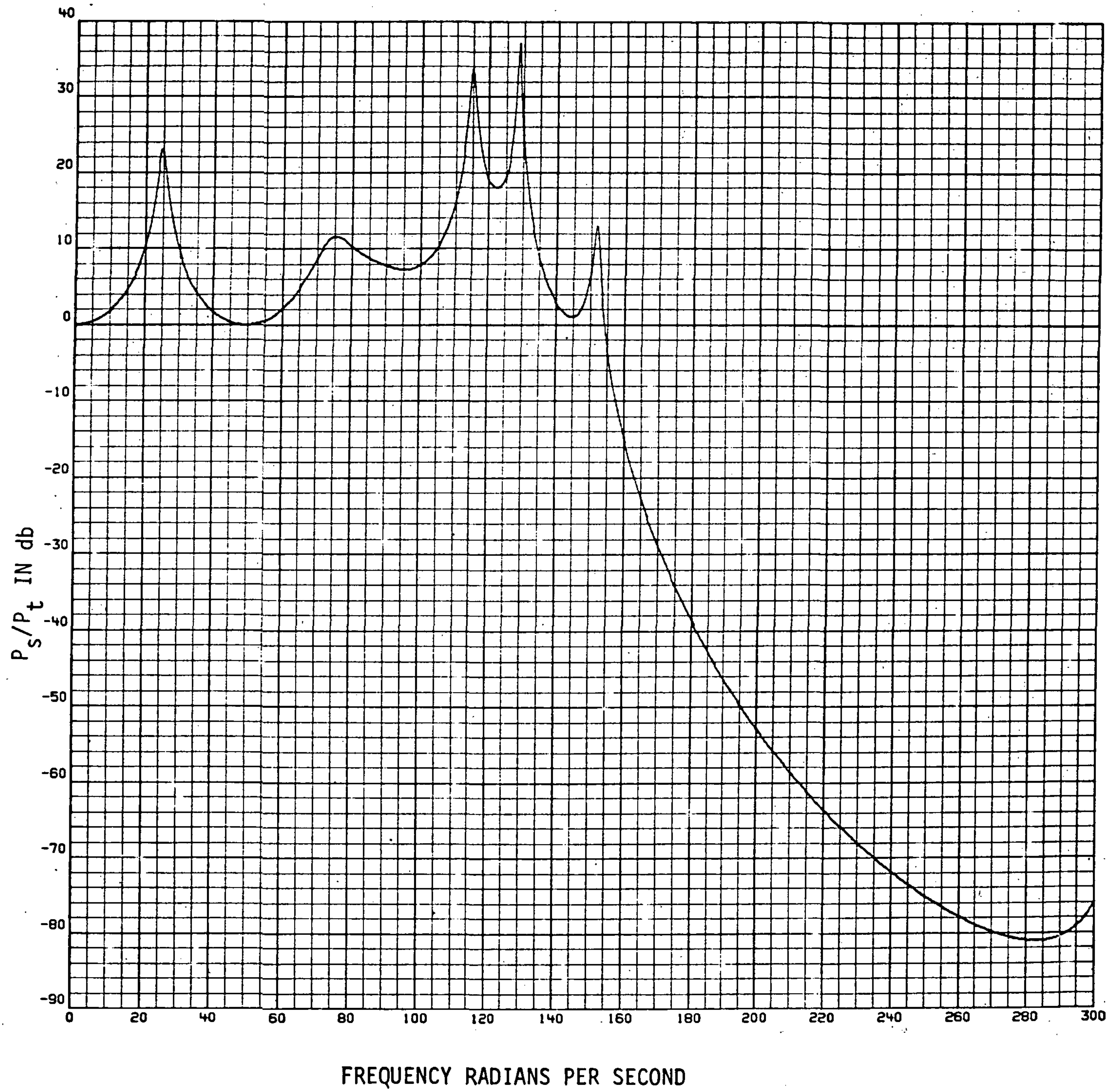

Figure 22 Straight Line with Double Compliance Pump Power Series (12th Order)

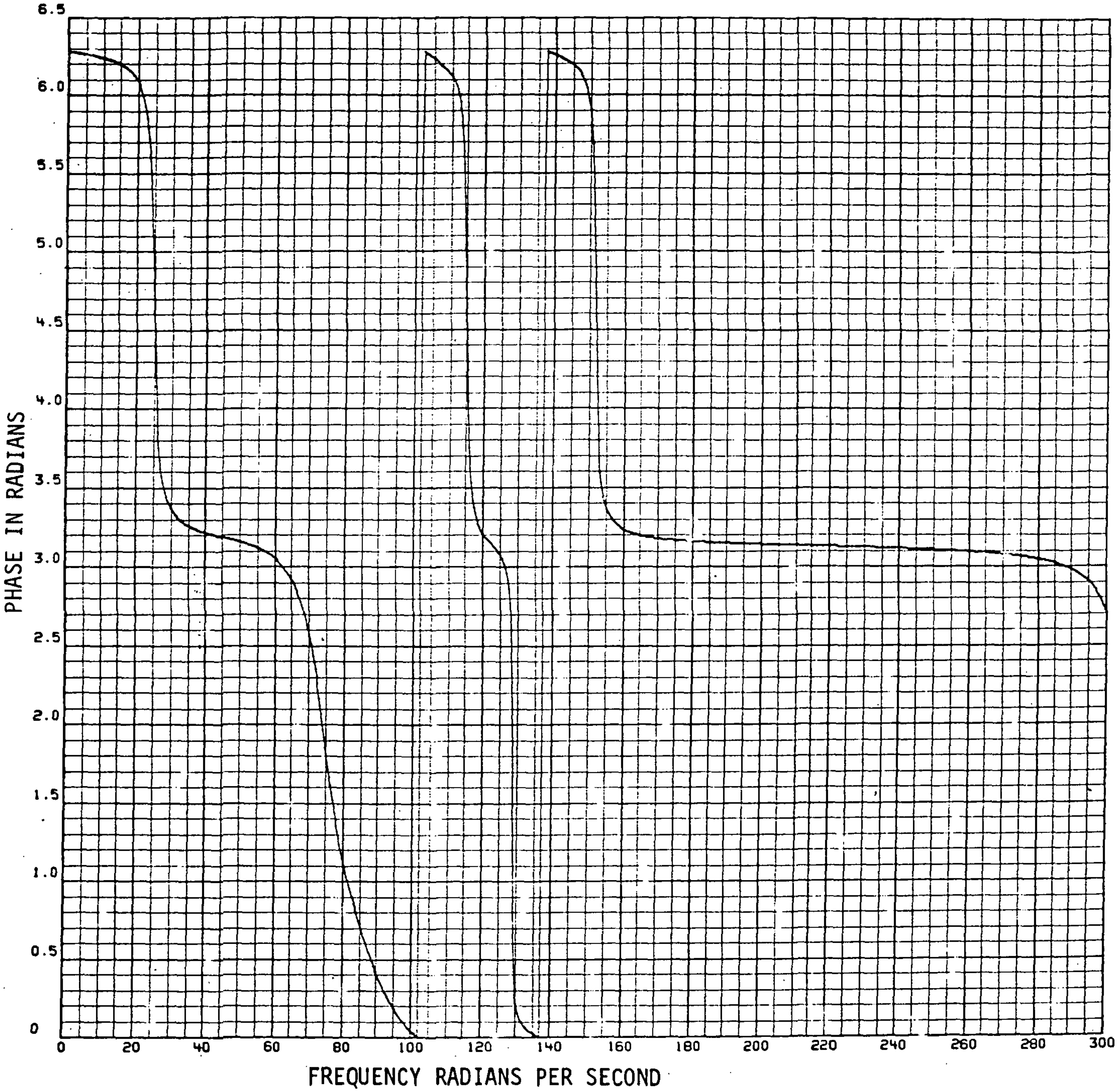

Figure 23 Straight Line with Double Compliance Pump
Power Series (12th Order)

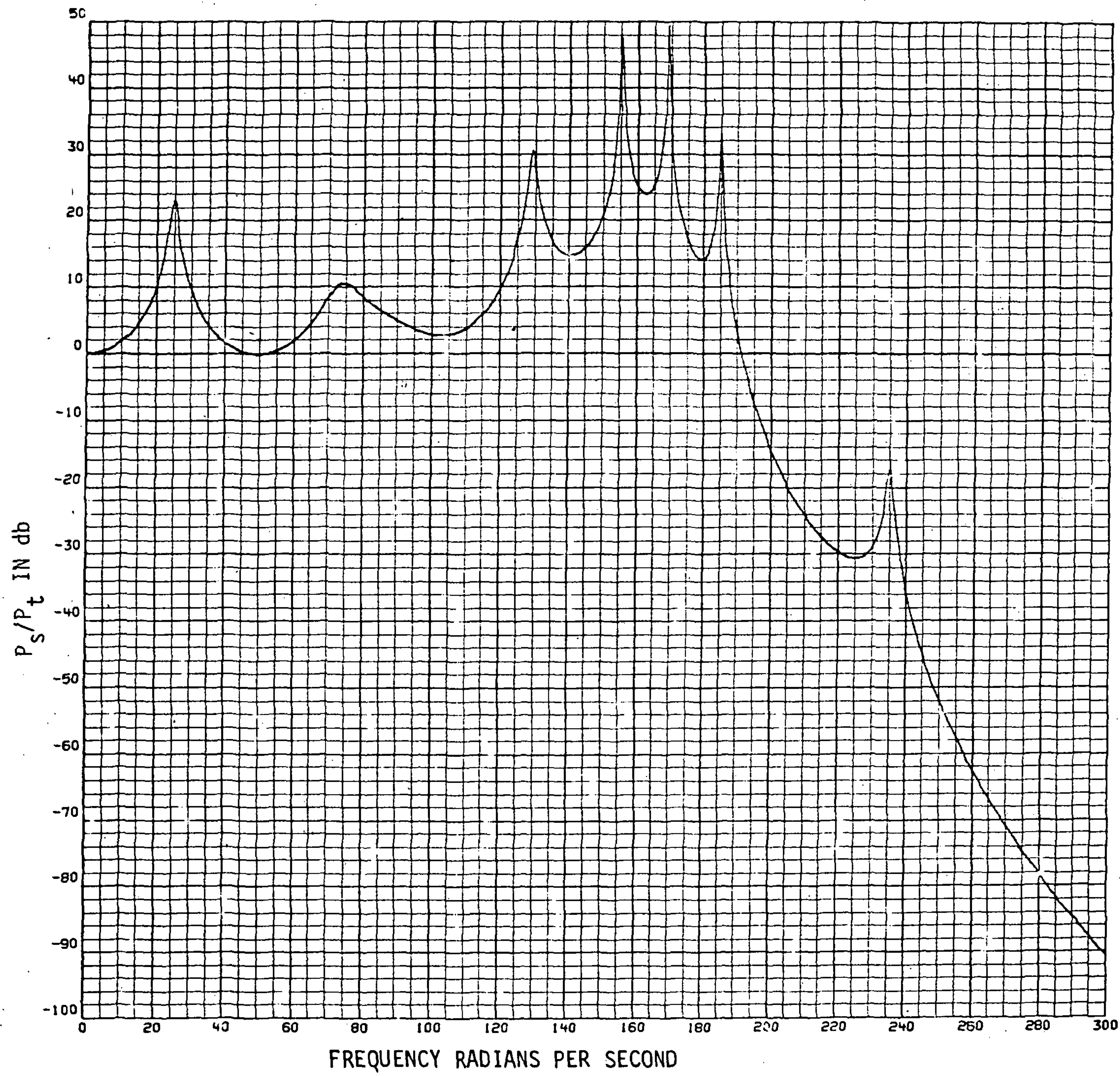

Figure 24 Straight Line with Double Compliance Pump Power Series (16th Order)

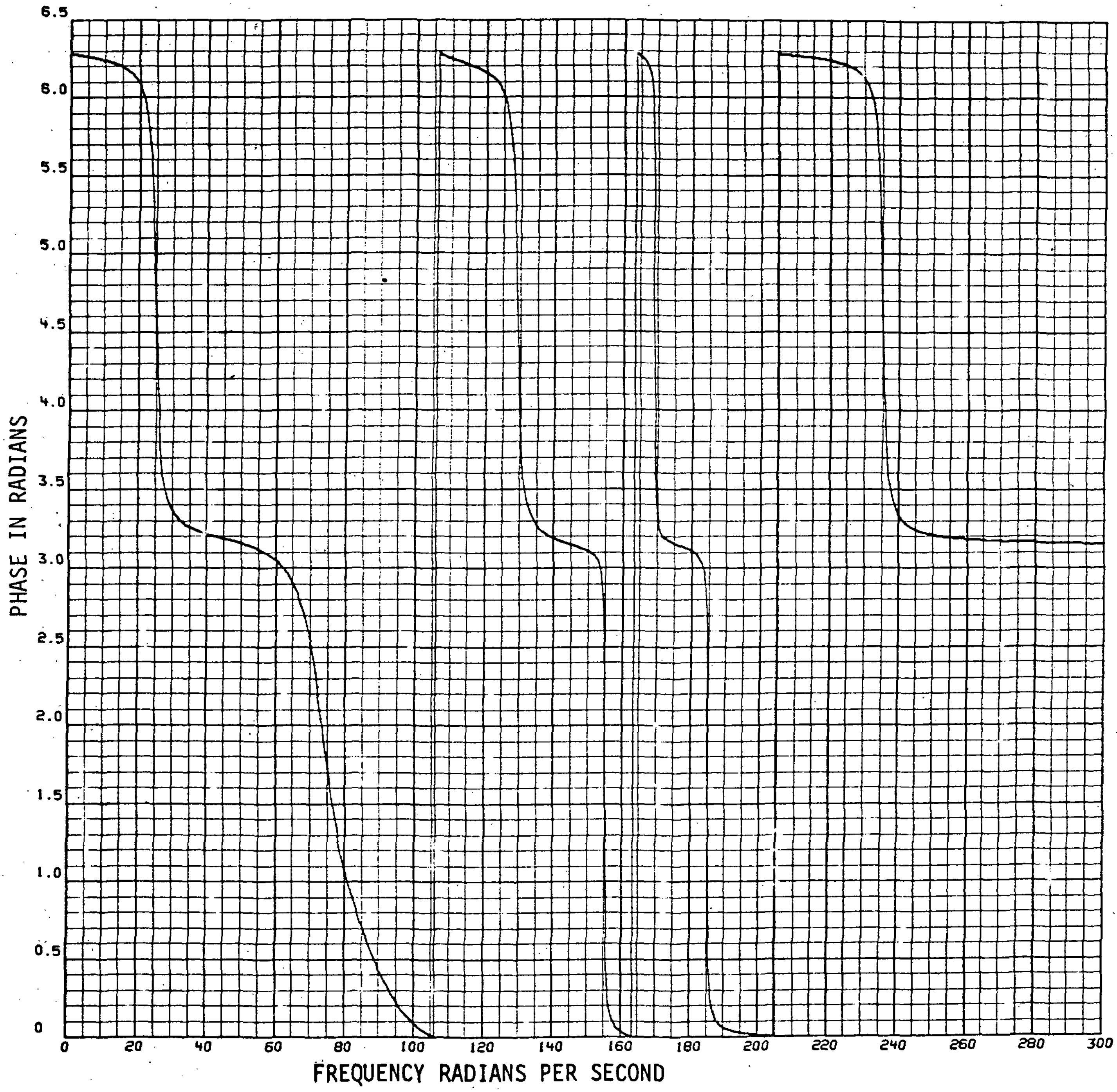

Figure 25 Straight Line with Double Compliance Pump
Power Series (16th Order)

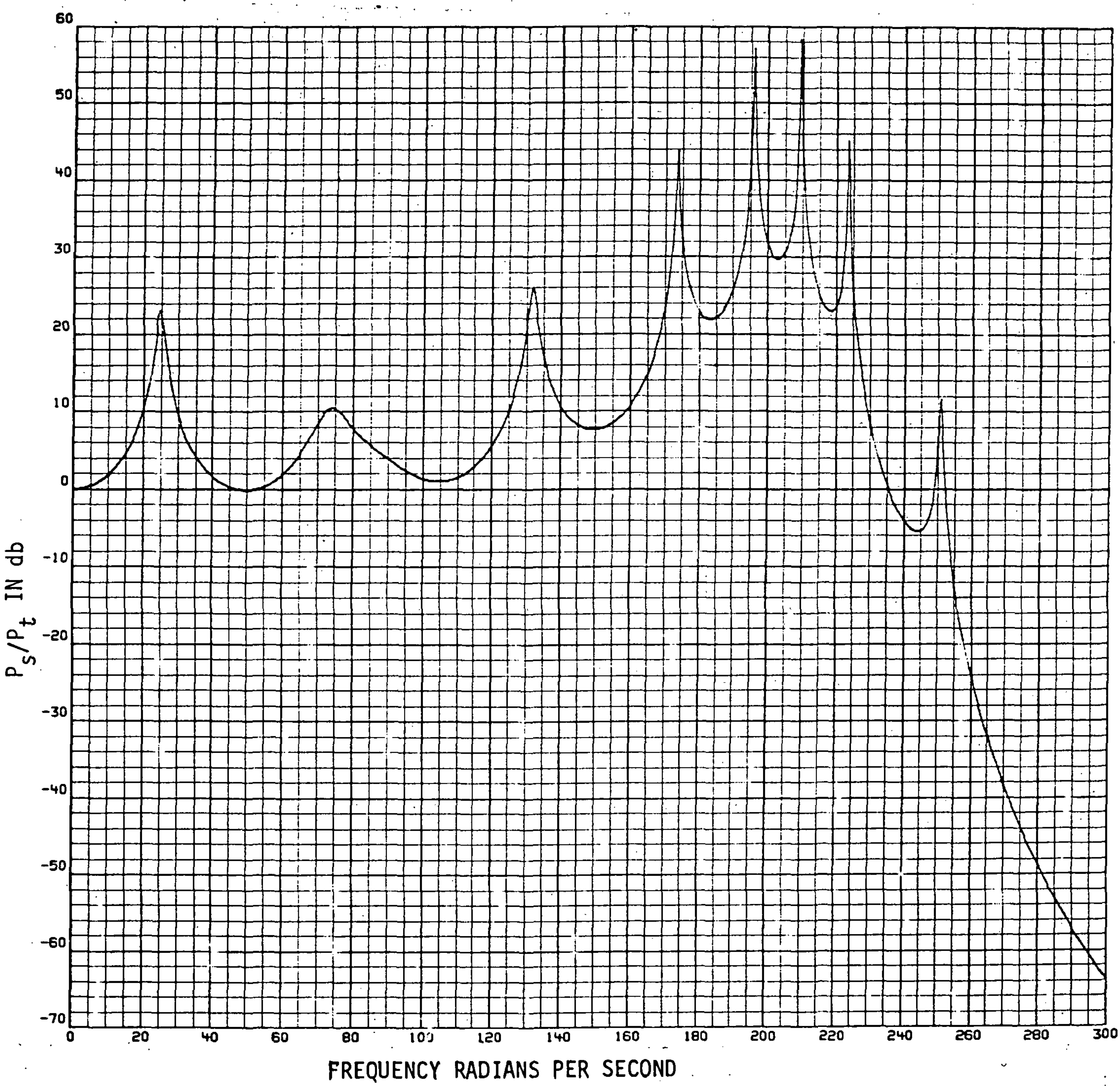

Figure 26 Straight Line with Double Compliance Pump Power Series (20th Order)

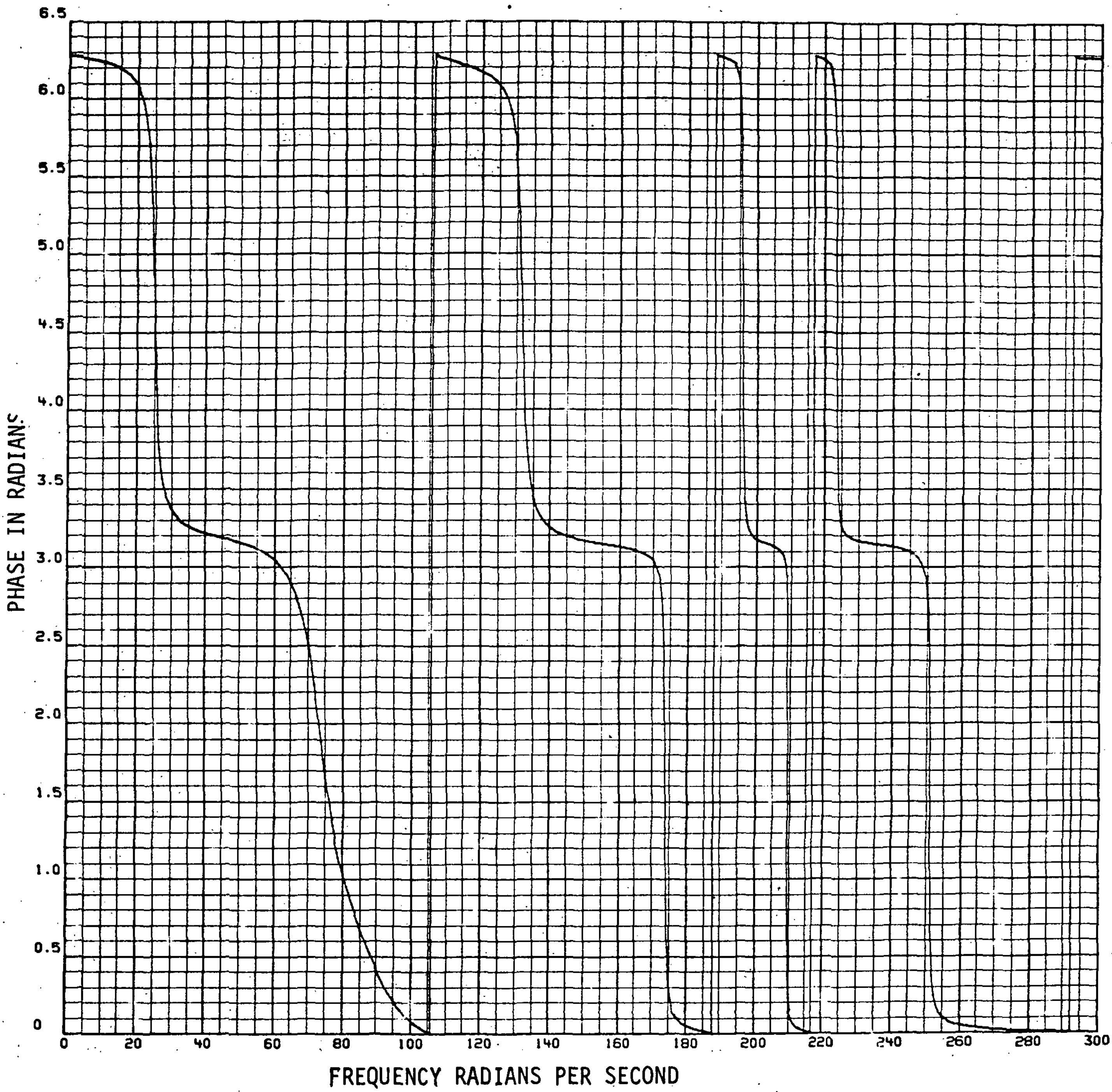

Figure 27 Straight Line with Double Compliance Pump Power Series (20th Order)

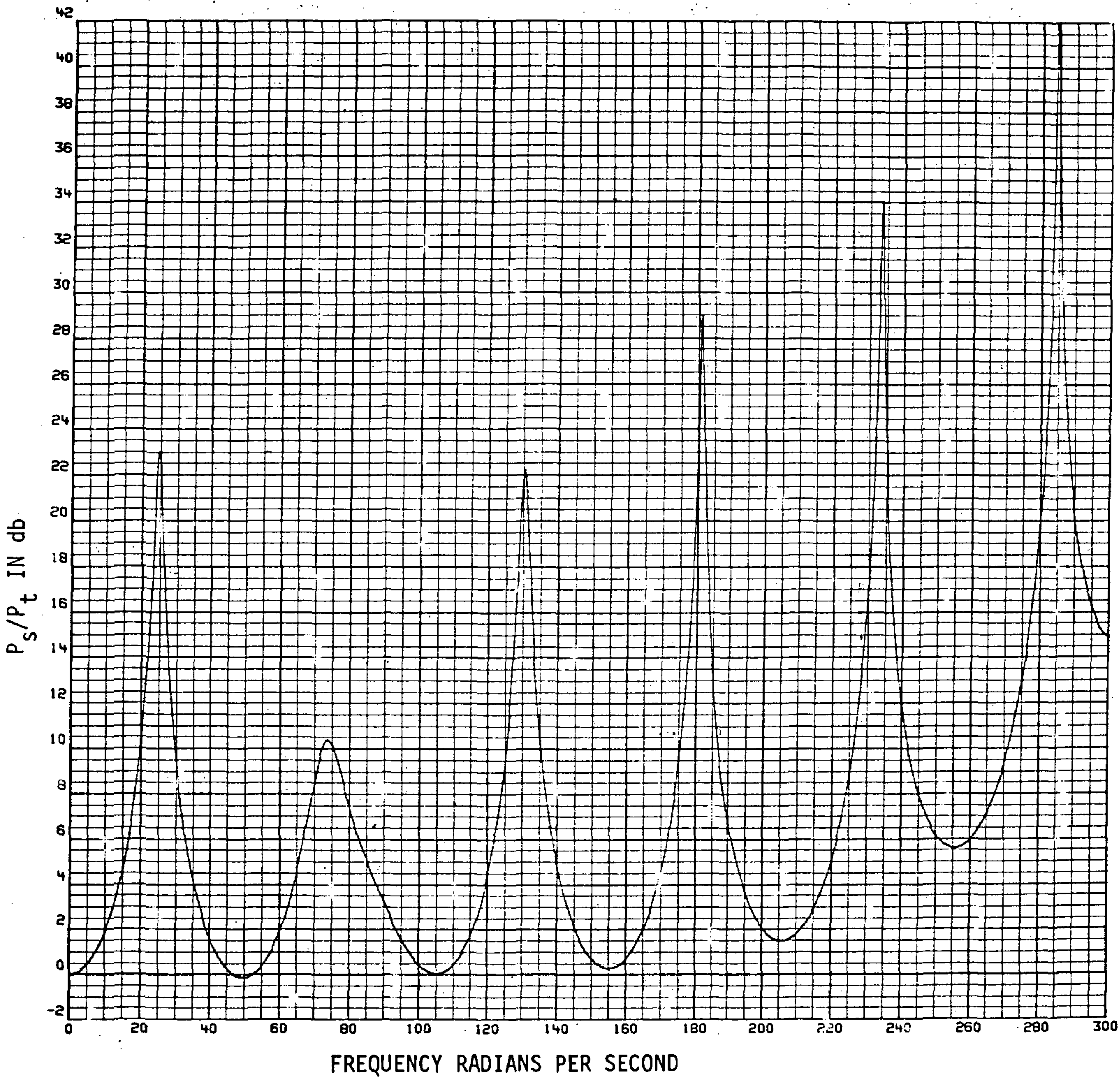

Figure 28 Straight Line with Double Compliance Pump Power Series (40th Order)

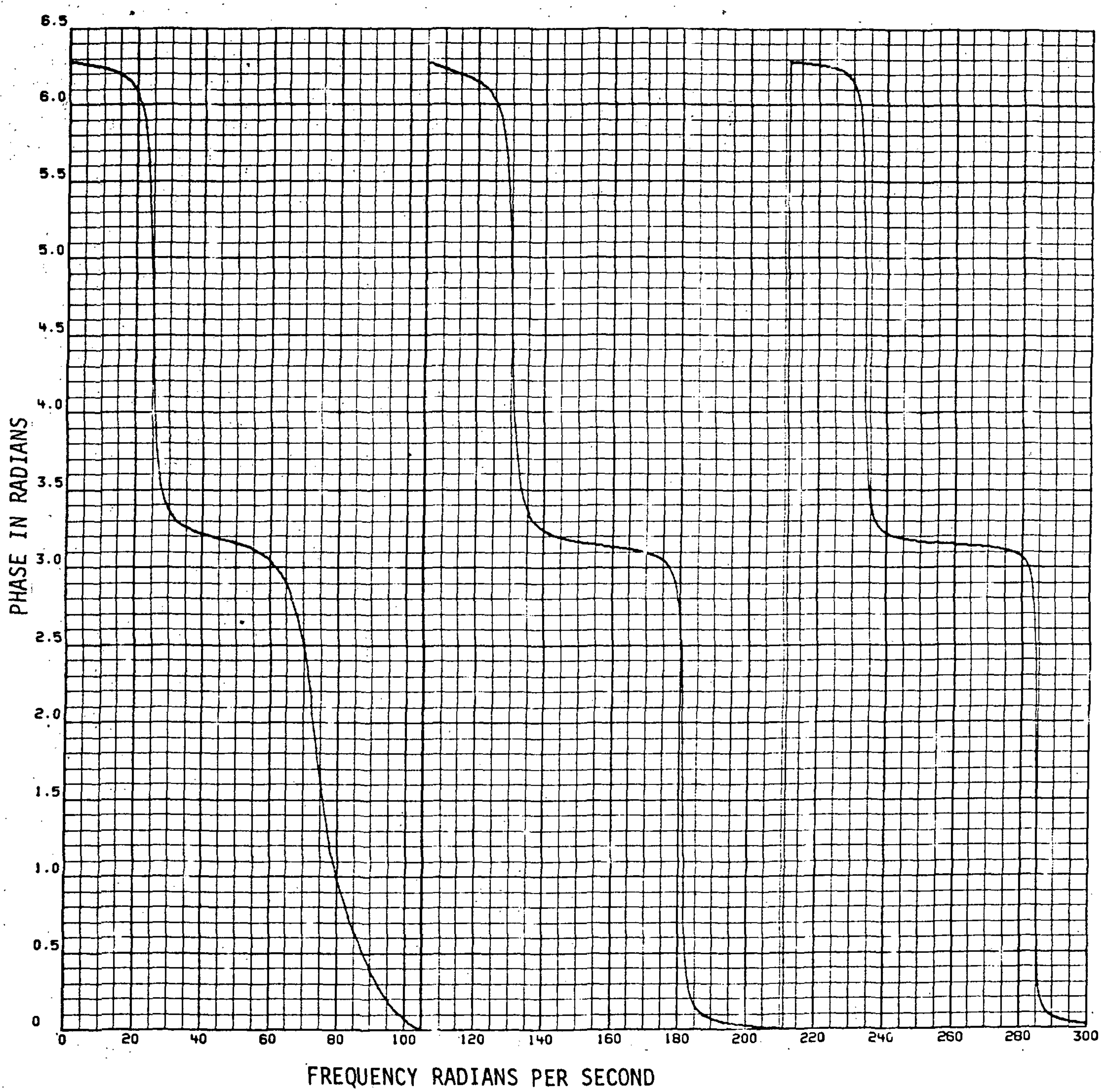

Figure 29 Straight Line with Double Compliance Pump Power Series (40th Order)

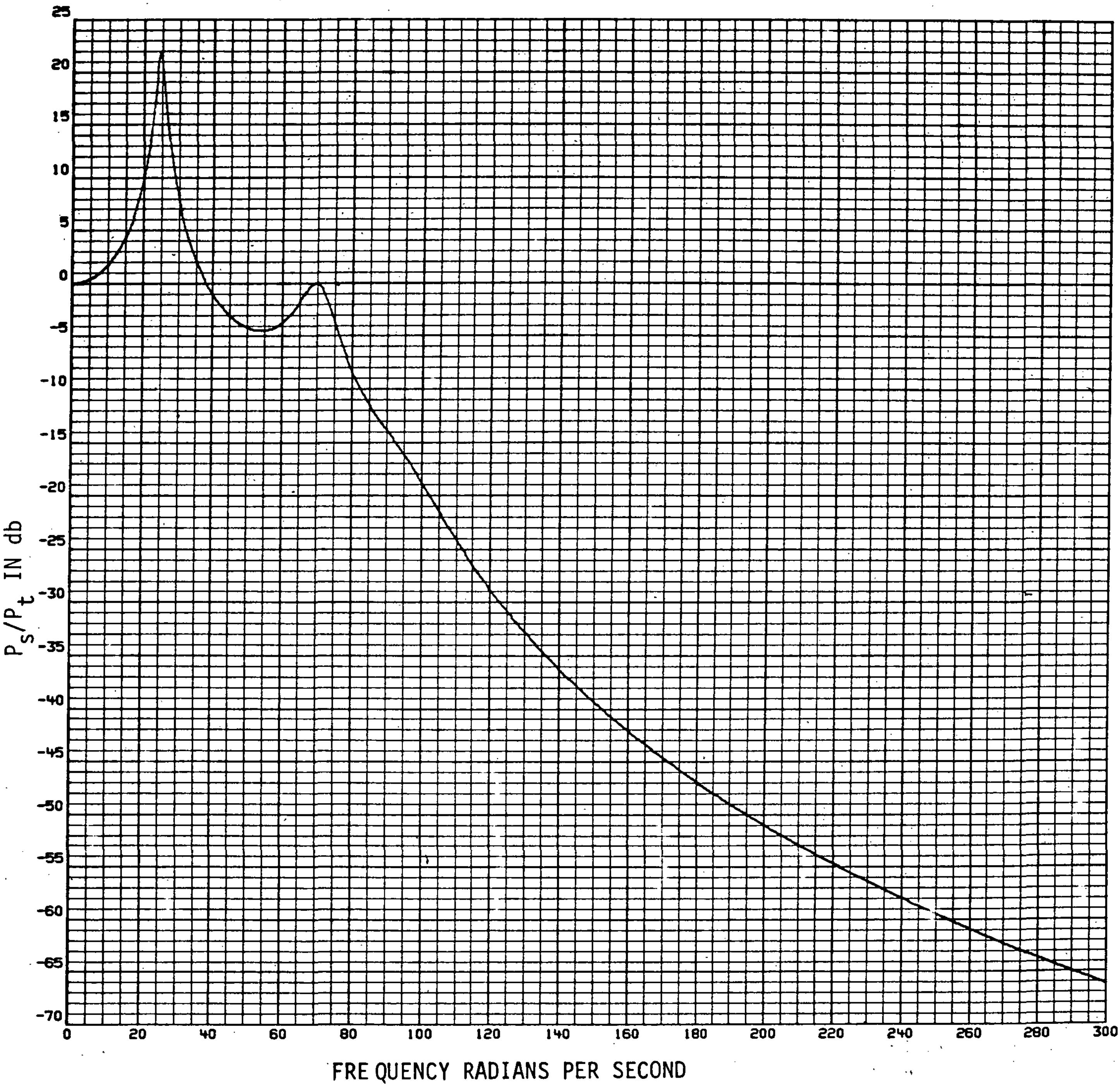

Figure 30 Straight Line with Double Compliance Pump Product Series (4th Order)

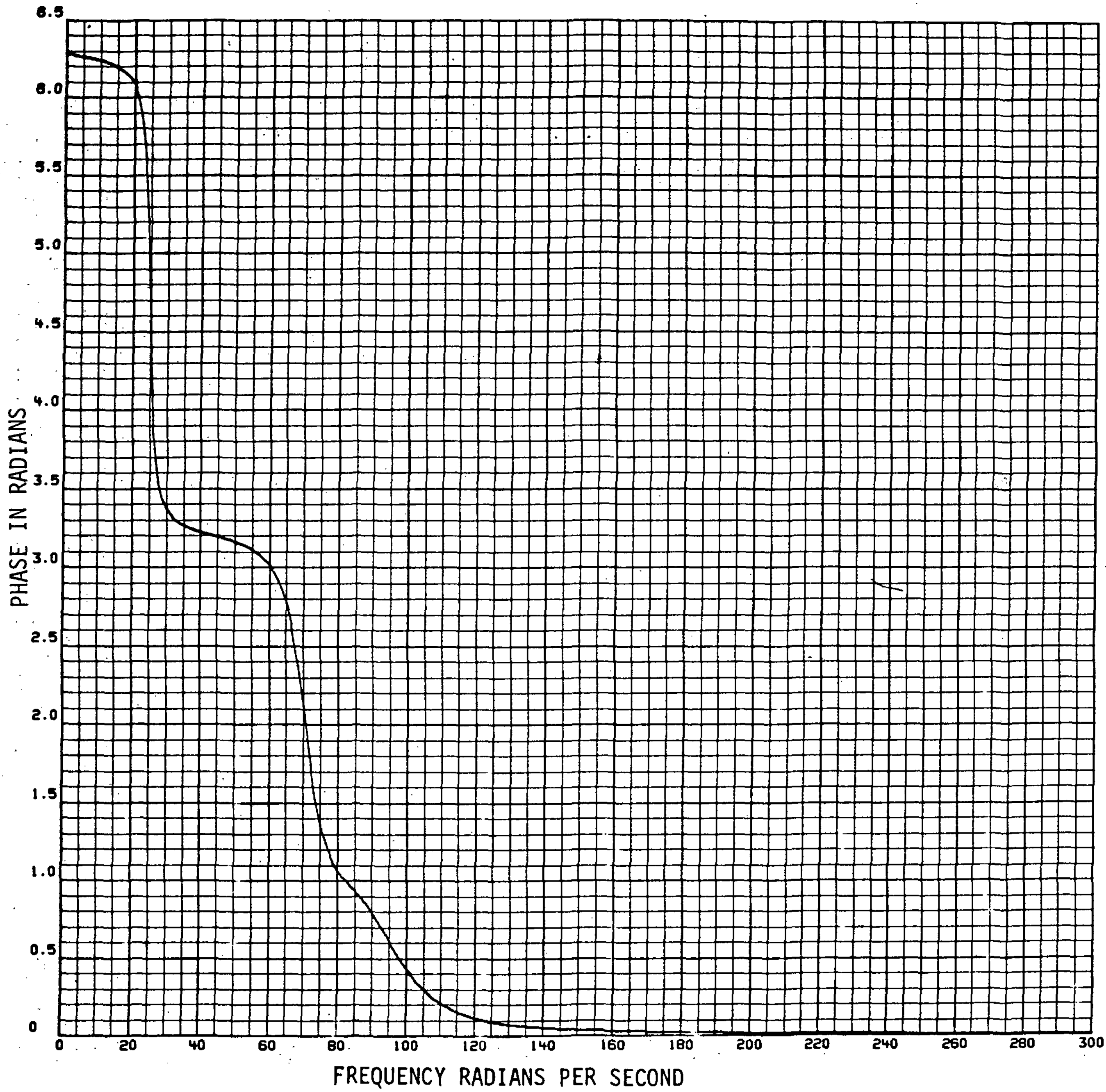

Figure 31 Straight Line with Double Compliance Pump Product Series (4th Order)

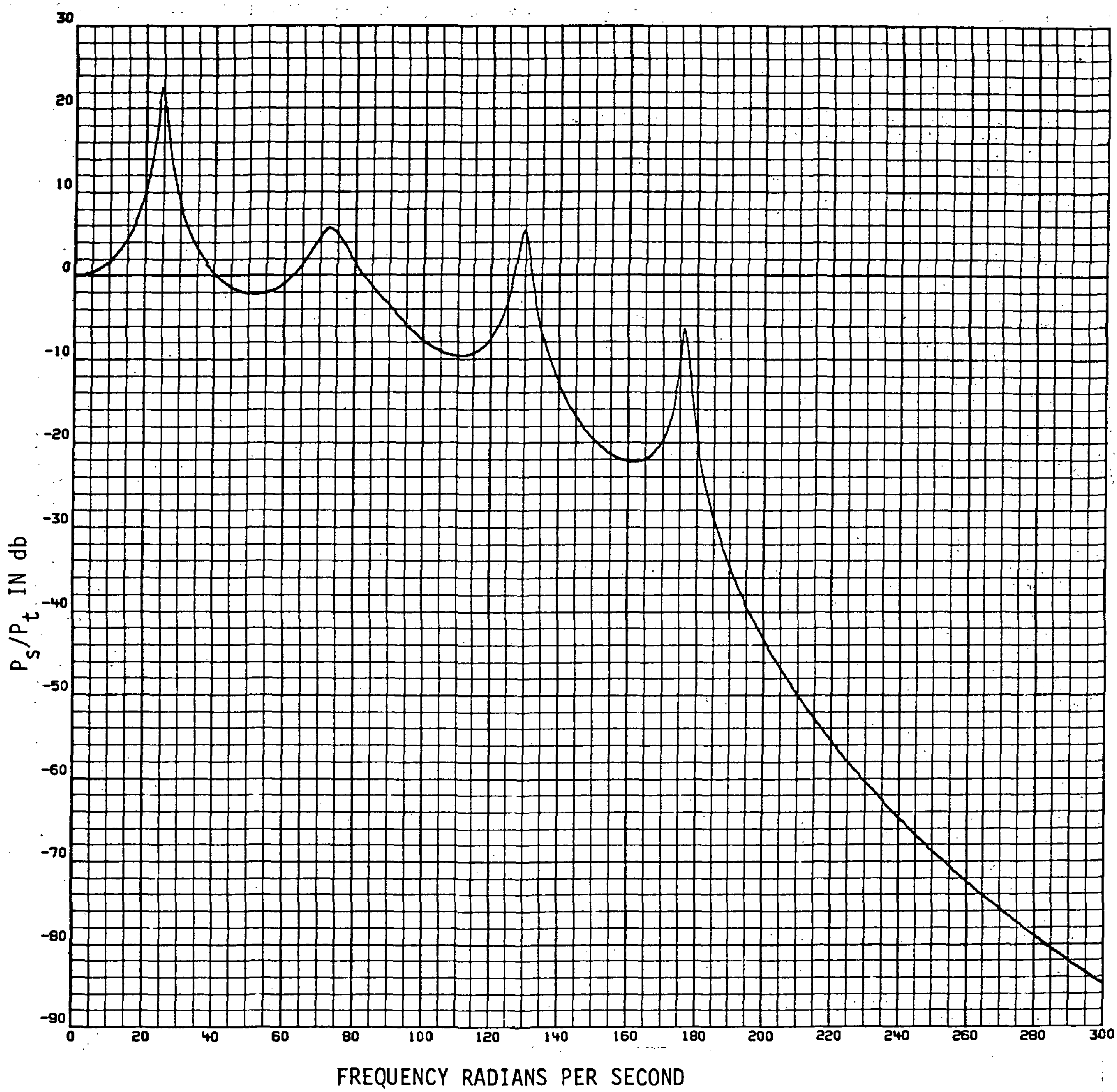

Figure 32 Straight Line with Double Compliance Pump Product Series (8th Order)

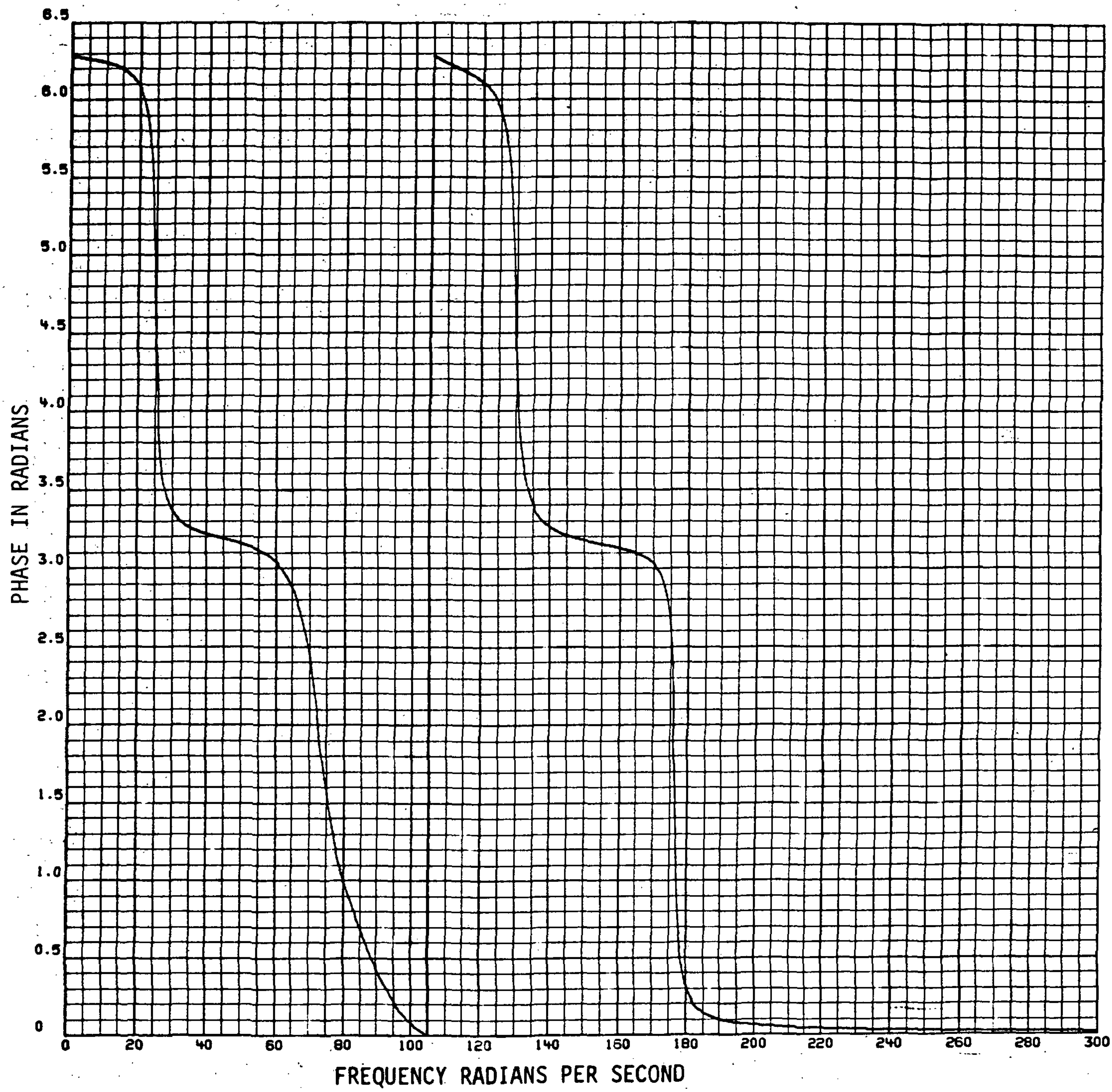

Figure 33 Straight Line with Double Compliance Pump Product Series (8th Order)

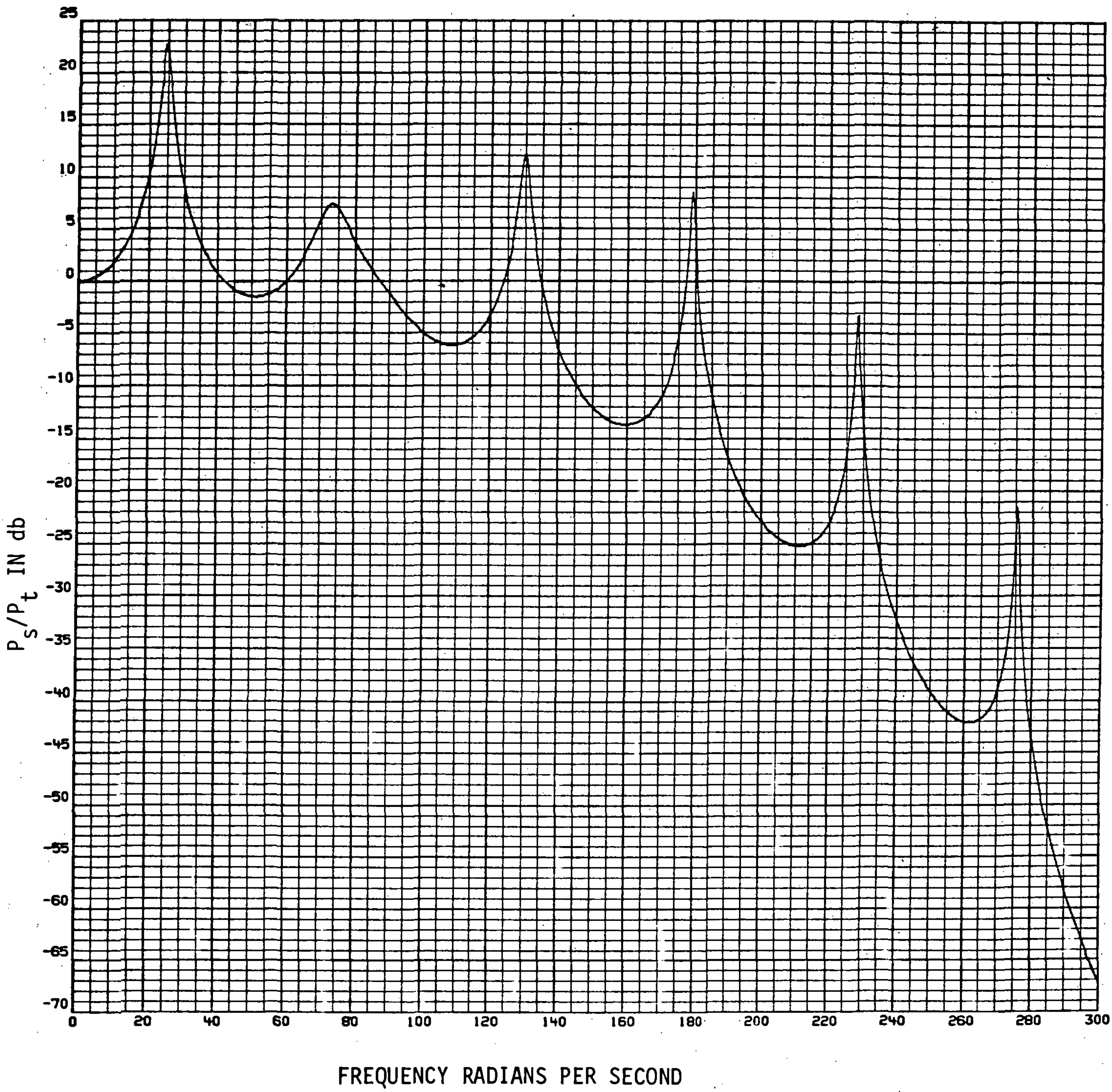

Figure 34 Straight Line with Double Compliance Pump Product Series (12th Order)

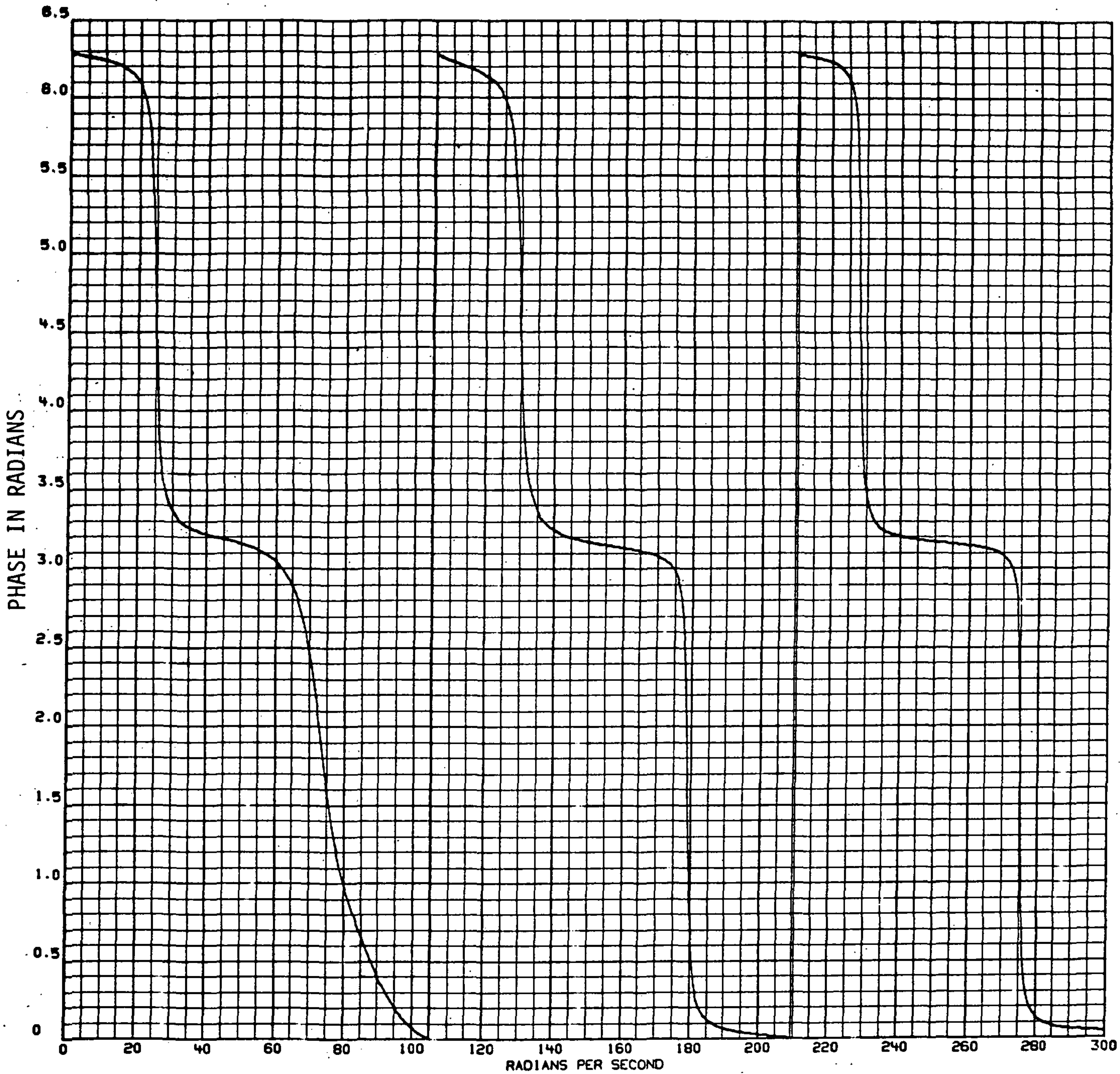

FREQUENCY RADIANS PER SECOND

Figure 35 Straight Line with Double Compliance Pump Product Series (12th Order)

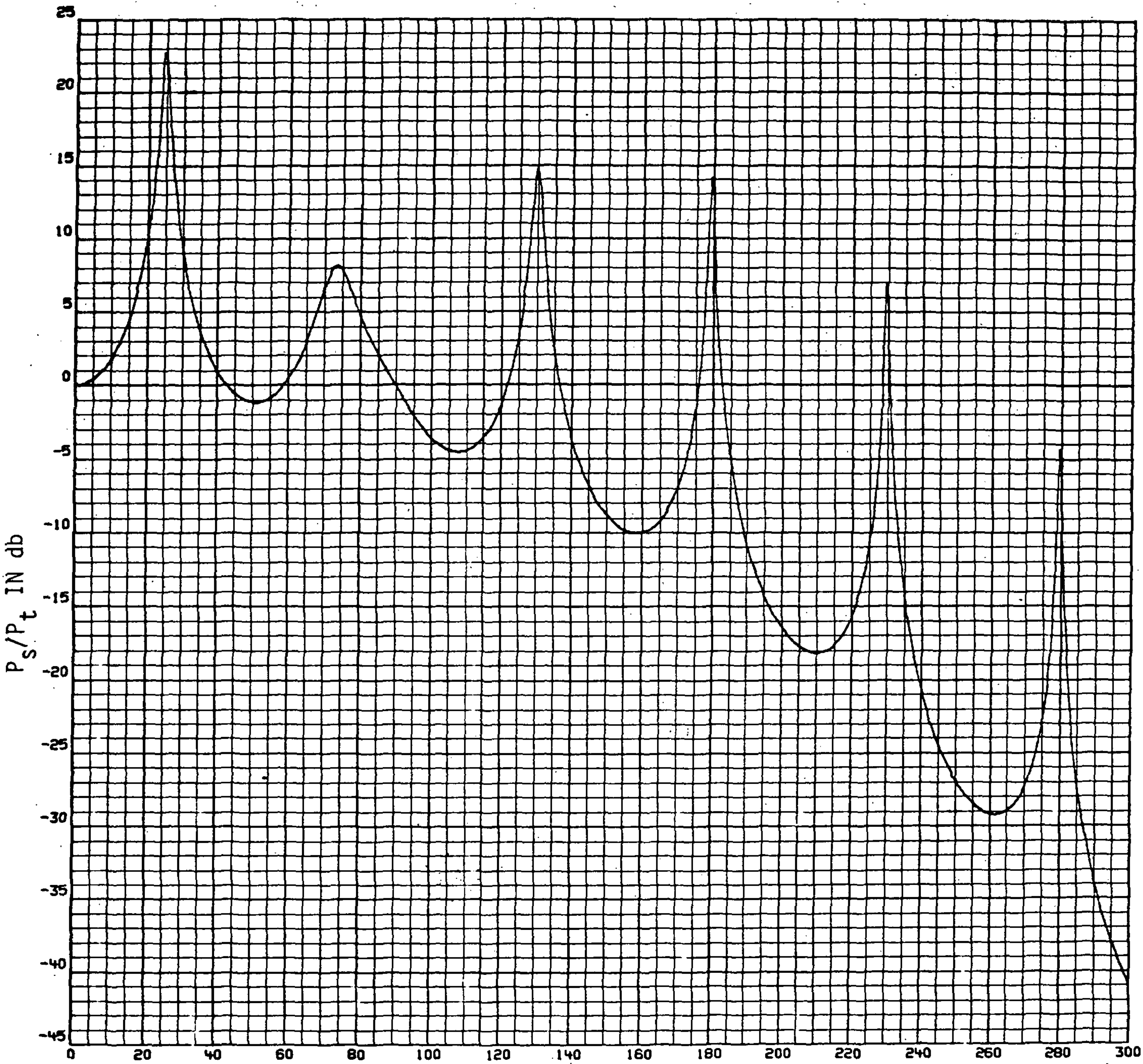

Figure 36 Straight Line with Double Compliance Pump Product Series (16th Order)

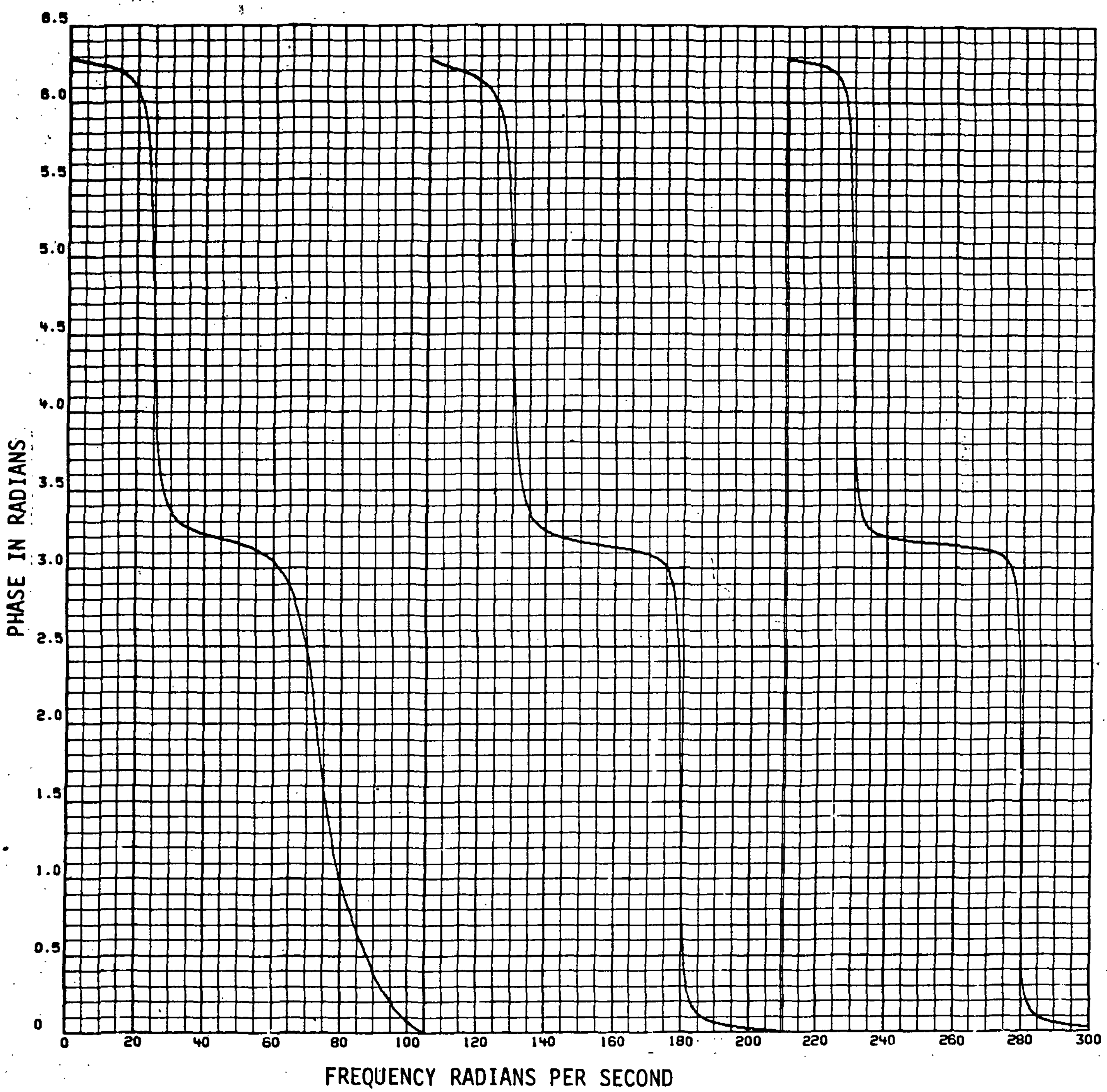

Figure 37 Straight Line with Double Compliance Pump Product Series (16th Order)

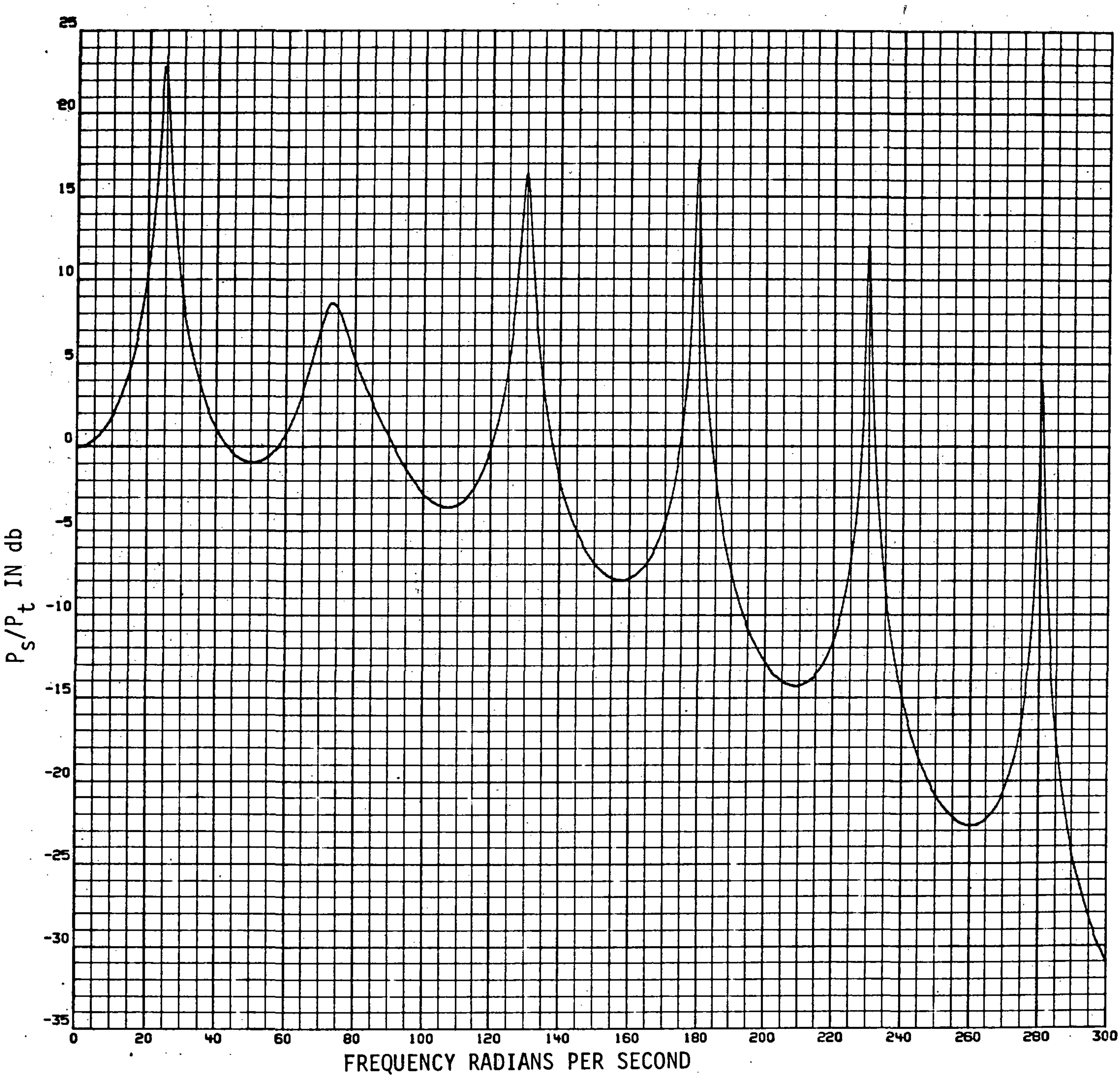

Figure 38 Straight Line with Double Compliance Pump Product Series (20th Order)

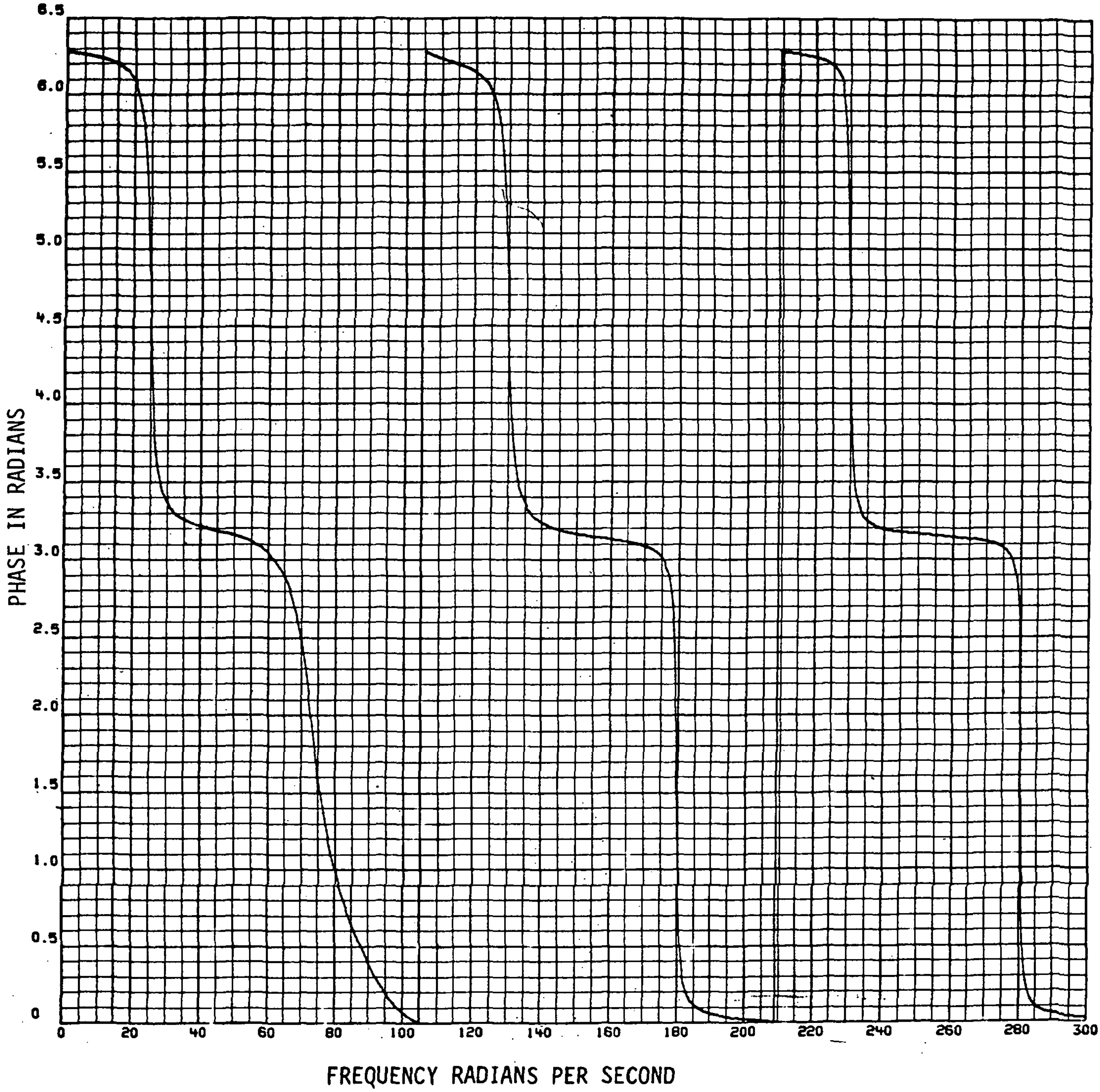

Figure 39 Straight Line with Double Compliance Pump Product Series (20th Order)

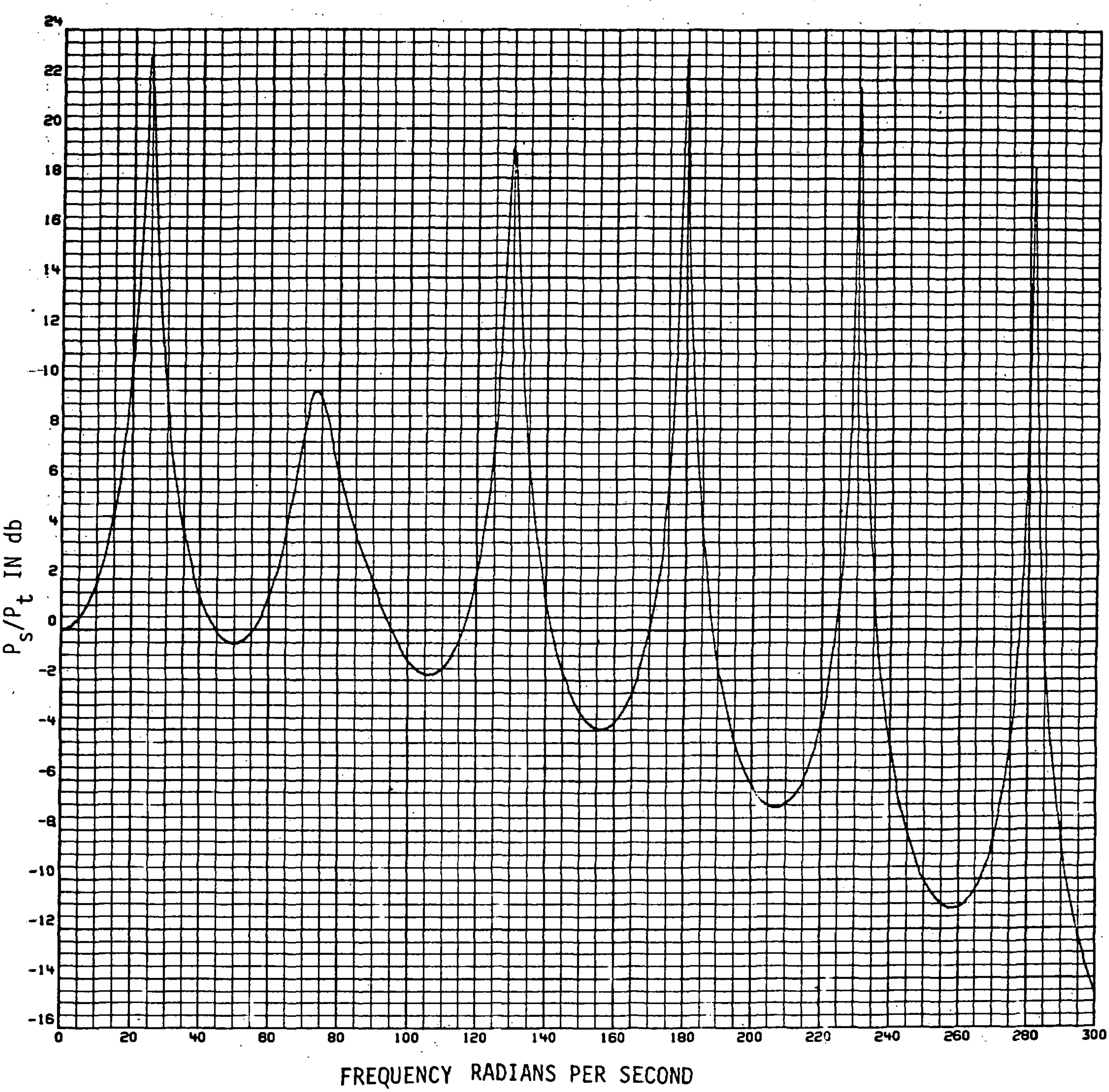

Figure 40 Straight Line with Double Compliance Pump Product Series (40th Order)

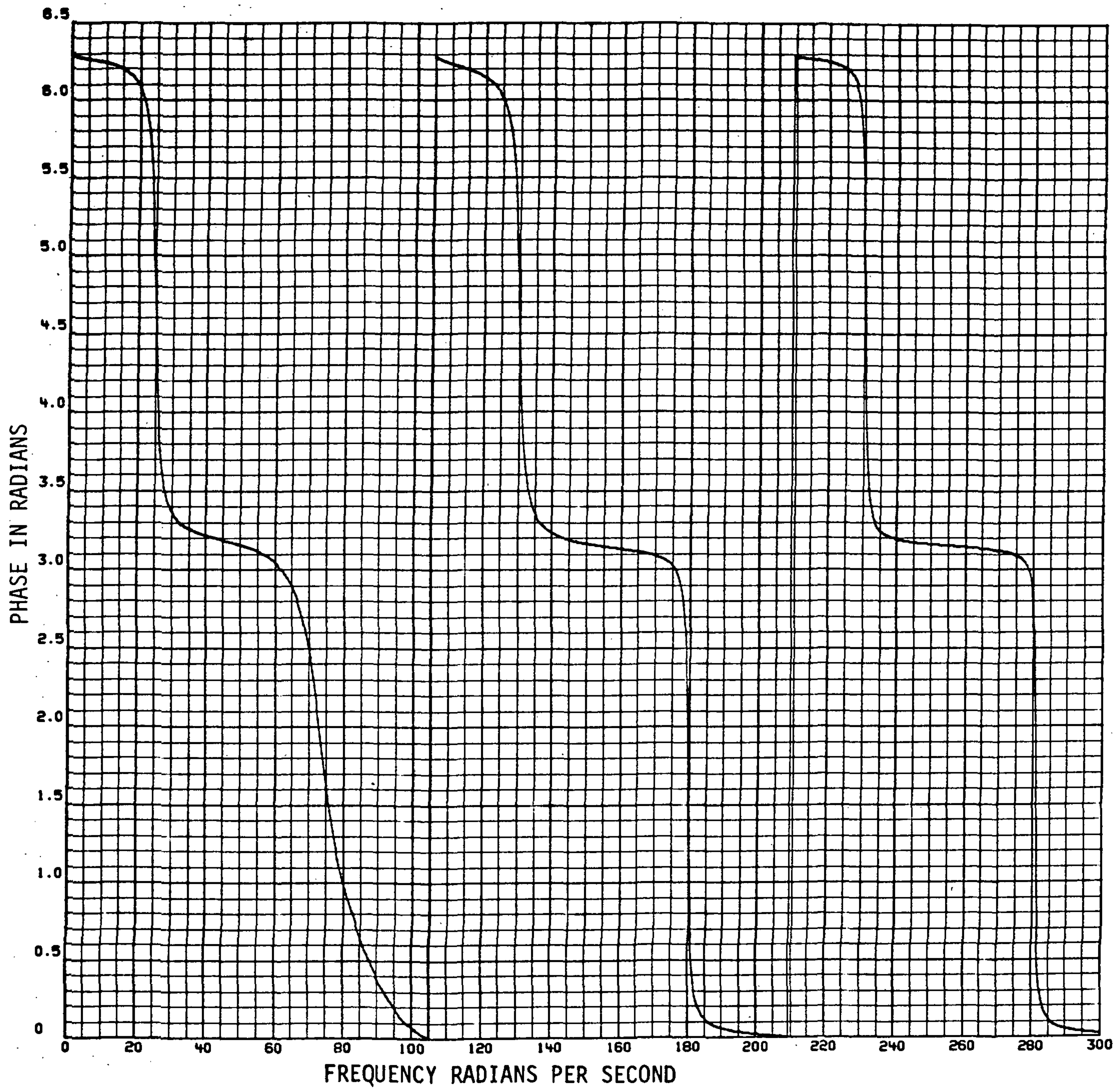

Figure 41 Straight Line with Double Compliance Pump Product Series (40th Order)

IV. SHUTTLE ORBITER FEEDLINE

1. Modeling

The Orbiter LO_2 System (Figures 42 - 44) has been modeled using power series, product series and the "exact" transcendental equations for the transmission parameters. In each of these methods, the damping due to bends, changes in cross-section, inlet losses, etc., were lumped at their respective locations. The damping due to these causes is lumped at locations A through I shown in Figure 45. The losses due to a bend in the line, entrance losses, etc., as given by the following formula.

$$\Delta P = \frac{1}{2} K \rho U^2$$

Removing the steady state terms, we obtain the following expression for the losses due to the perturbed flow.

$$\Delta P = K \rho U_o U$$

In terms of flow rate, this equation becomes

$$\Delta P = R \dot{W}$$

where

$$R = 2 P_o / \dot{W}_o$$

$$P_o = \text{steady state head loss}$$

The losses which occur at sections A - I are given in Table 1. The feedline may be conveniently subdivided into three main sections which have different properties. Additional information required for determining the feedline transfer function is summarized in Table 2.

The damping due to the shear stresses distributed along the line are lumped at the ends of the elemental sections when using the power series. This damping is handled directly when using the product series expansion.

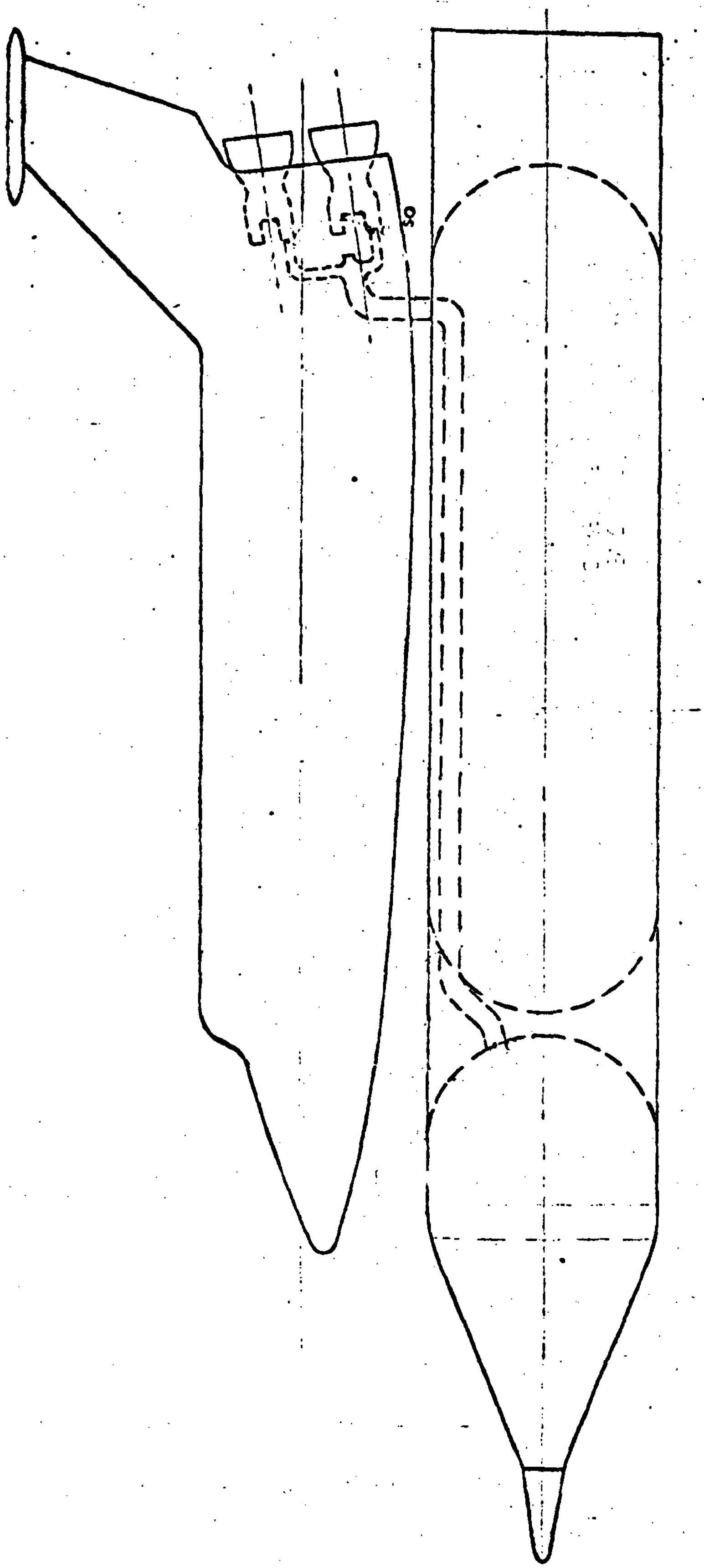

Figure 42 Shuttle Orbiter LOX Feedline

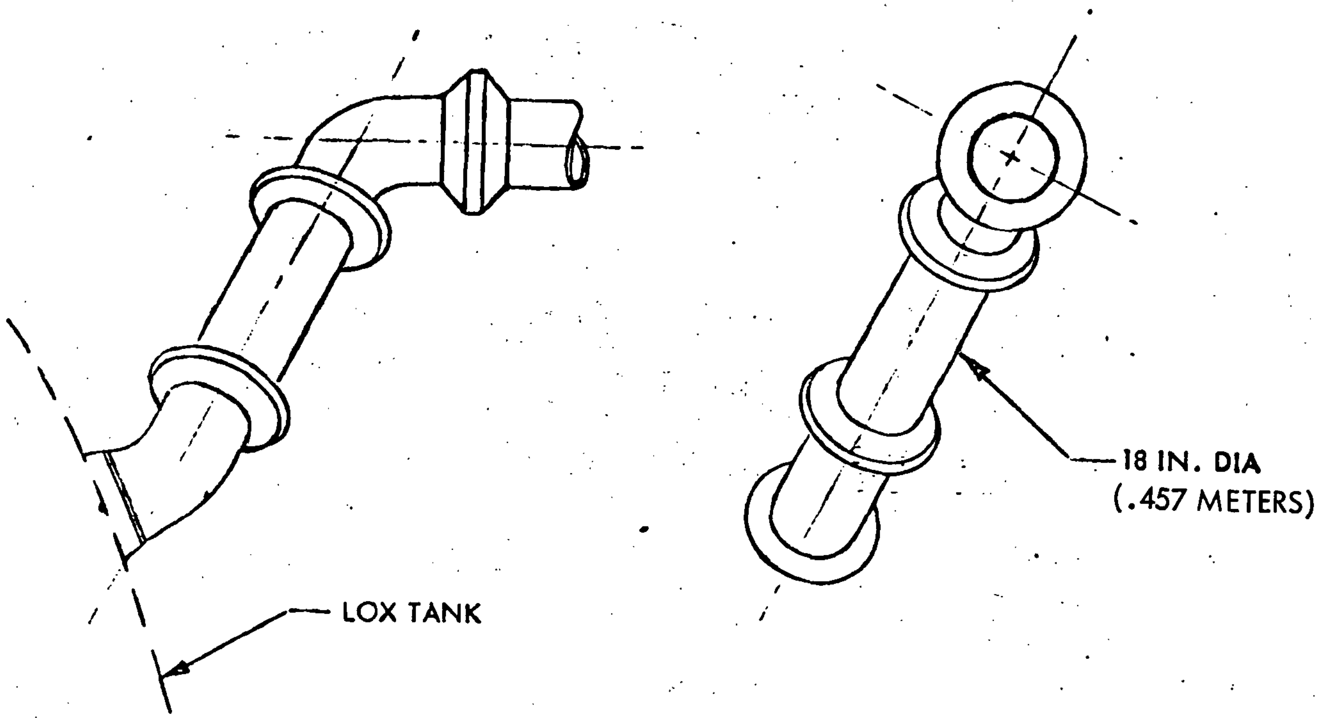

Figure 43 Shuttle Orbiter - LOX Feedline - Forward End

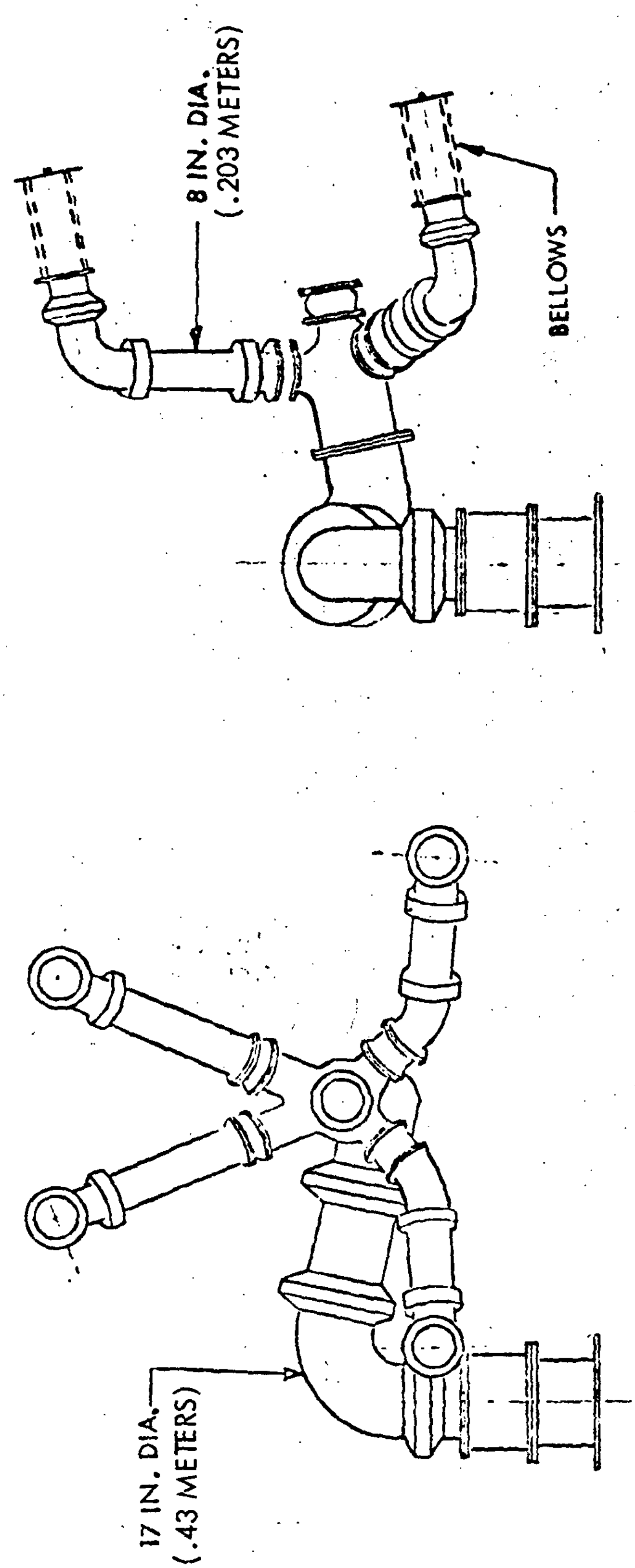

Figure 44 Shuttle Orbiter - LOX Feedline - Aft End

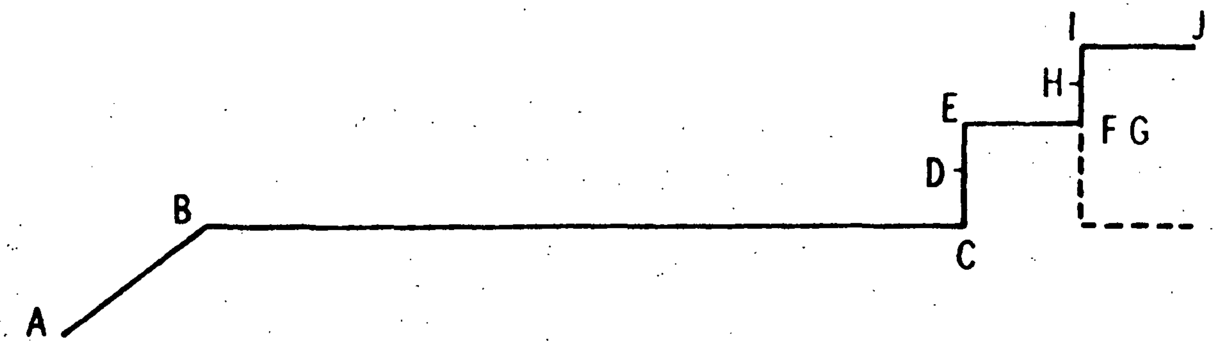

LINE	LENGTH INCHES	LENGTH METERS	MATERIAL	DIA INCHES	DIA METERS
A B	120	(3.05)	ALUMINUM	18	(4.57×10^{-1})
B C	850	(21.6)	ALUMINUM	18	"
C D	60	(1.52)	ALUMINUM	18	"
D E	60	(1.52)	STEEL	17	(4.3×10^{-1})
E F	90	(2.29)	STEEL	17	"
F G	62	(1.58)	STEEL	17	"
G H H I	75	(1.90)	STEEL	8	(2.03×10^{-1})
I J	62	(1.58)	STEEL	8	"

Figure 45 Feedline Geometry

Table 1 Damping Data

			FLOW RATE ($\dot{W}$)		PRESSURE (P_o)		DAMPING	(R)
LOCATION	DESCRIPTION	K	(LB/SEC)	KG/SEC	(PSI)	$\left(\frac{NEWTONS}{M^2}\right)$	$\left(\frac{SEC}{IN.^2}\right)$	$\frac{1}{M\ SEC}$
A	ENTRANCE LOSS	.5	2080	941	1.06	7.29×10^3	1.02×10^{-3}	15.4
B	90° BEND	.16	2080	941	.32	2.2×10^3	$.307 \times 10^{-3}$	4.69
C	90° BEND	.16	2080	941	.32	2.2×10^3	$.307 \times 10^{-3}$	4.69
D	DISCONNECT	.6	2080	941	1.60	11×10^3	1.54×10^{-3}	23.4
E	90° BEND	.16	2080	941	.42	2.9×10^3	$.402 \times 10^{-3}$	6.15
F	90° BEND	.16	2080	941	.42	2.9×10^3	$.402 \times 10^{-3}$	6.15
G	MANIFOLD	.5	520	235	1.67	11.5×10^3	6.42×10^{-3}	97.8
H	PREVALVE	.6	520	235	2.0	13.7×10^3	7.65×10^{-3} *	116
I	90° BEND	.16	520	235	.53	3.64×10^3	2.03×10^{-3} *	31

* THE DAMPING AT H&I HAVE BEEN COMBINED IN THE MODEL

Table 2 Feedline Data

LOCATION	AD	DF	FG
PIPE MATERIAL	ALUMINUM	STEEL	STEEL
DIAMETER	18 INCHES (4.57×10^{-1} M)	17 INCHES (4.3×10^{-1} M)	8 INCHES (2.03×10^{-1}M)
PIPE THICKNESS (t)	.075 INCHES (1.91×10^{-3} M)	.05 INCHES (1.27×10^{-3} M)	.04 INCHES (1.02×10^{-3} M)
LOX MASS DENSITY (ρ)	2.2 SLUGS/FT^3 (1.13×10^3 KG/M^3)	2.2 SLUGS/FT^3 (1.13×10^3 KG/M^3)	2.2 SLUGS/FT^3 (1.13×10^3 KG/M^3)
ACOUSTIC SPEED (a)	1570 FT/SEC (478 M/SEC)	1960 FT/SEC (597 M/SEC)	2240 FT/SEC (682 M/SEC)
STEADY STATE FLUID VEL. (U_o)	16.2 FT/SEC (4.95 M/SEC)	18.7 FT/SEC (5.8 M/SEC)	20.9 FT/SEC (6.38 M/SEC)
REYNOLDS NO. (N_R)	11.7×10^6	12.5×10^6	6.5×10^6
DARCY WEISBACH CONSTANT (f)	.008	.008	.0086
DAMPING COEFFICIENT C	.08 1/SEC	.1 1/SEC	.252 1/SEC

2. Numerical Results

Bode plots of the feedline transfer function have been obtained using the "exact" transcendental functions for the transmission parameters. The results are given in Figures 46 and 47. This has been used as a basis for comparing the numerical results when using the power and product series expansions. Results have been obtained for 60th, 120th, 180th, and 240th order expressions for the orbiter feedline and are given in Figures 48 through 63. A comparison chart showing the peak gains for each of these approximations is shown in Table 3.

The NR stability program will allow the use of 60th order approximation to the line. The higher order results show the improvement to be expected as the order is increased. For the Shuttle Orbiter configuration, it is clear that the power series representation is preferable to the product series approximation for the transmission parameters. This is due in part to having to subdivide the line for the inclusion of lumped damping due to bends and changes in the cross-section of the line.

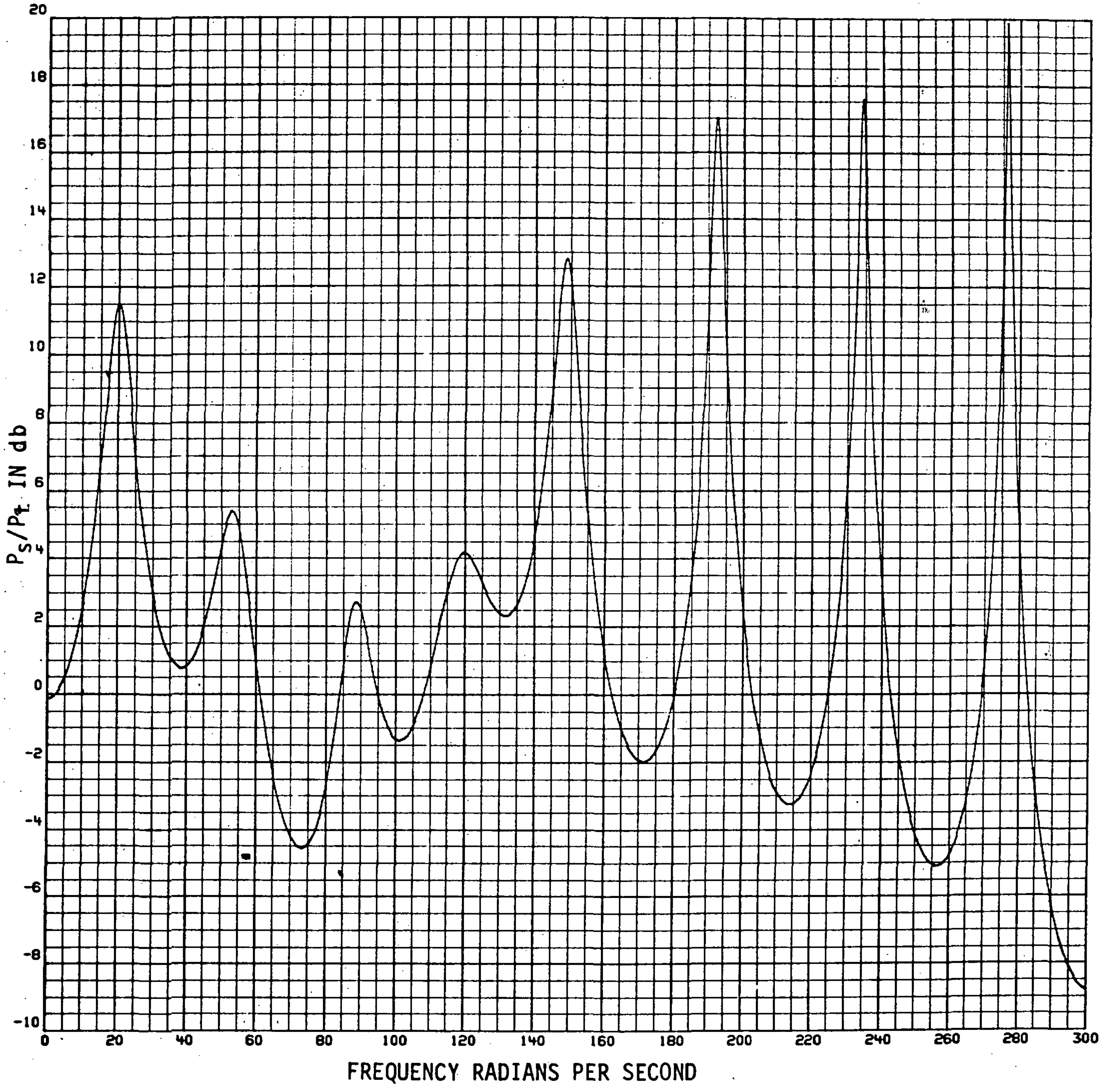

Figure 46 Shuttle Orbiter Feedline "Exact" Solution

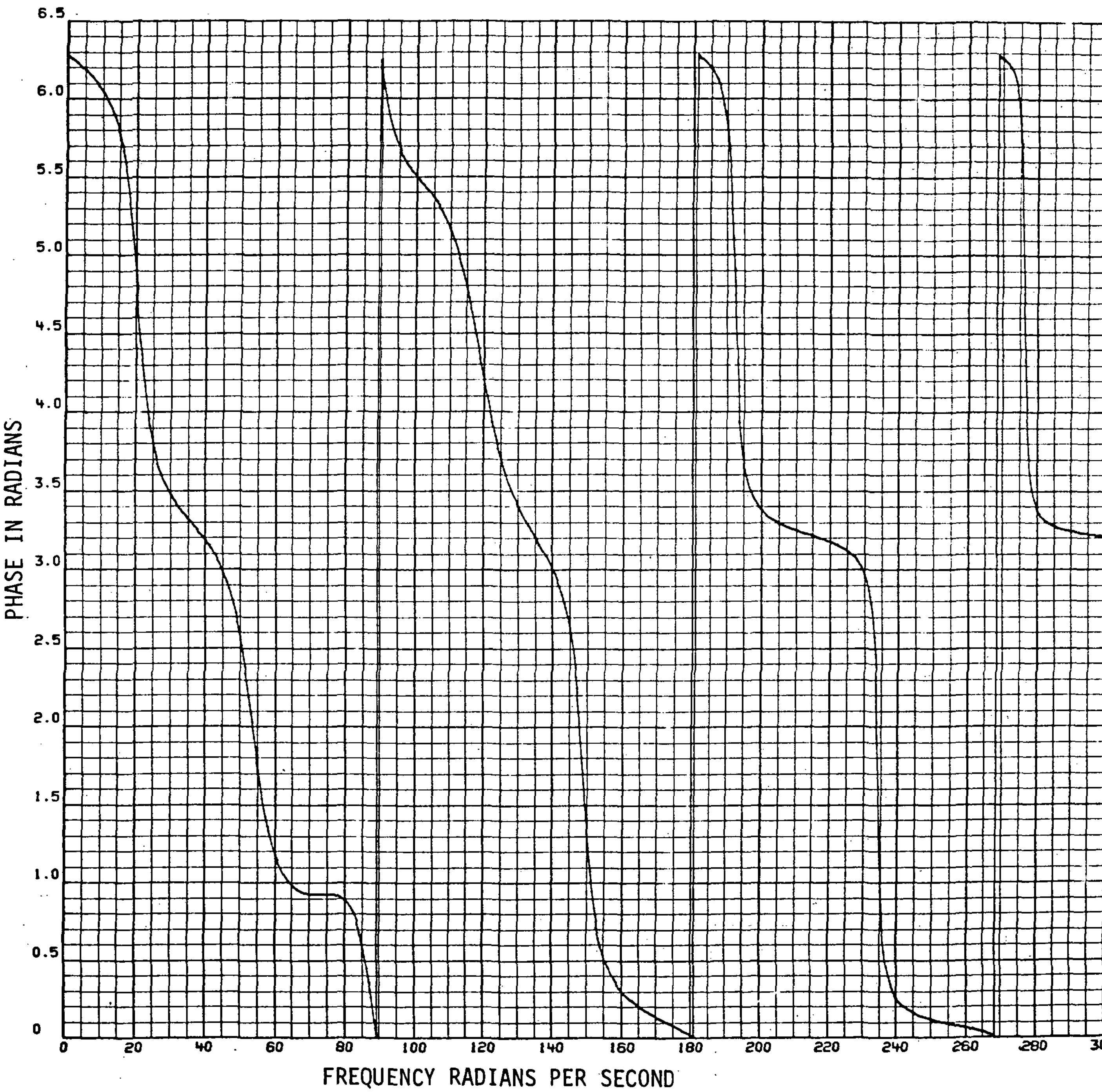

Figure 47 Shuttle Orbiter Feedline "Exact" Solution

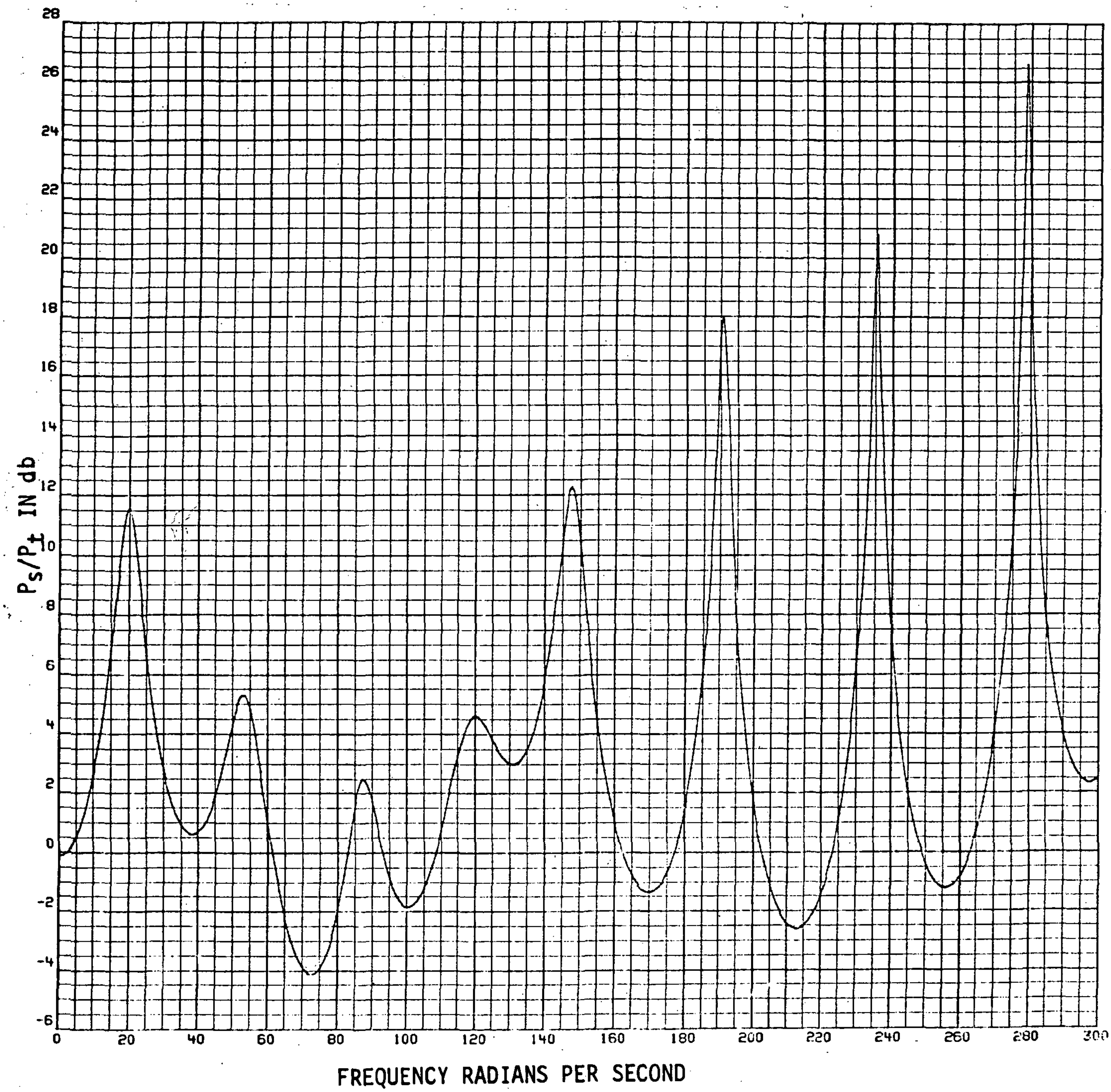

Figure 48 Shuttle Orbiter Feedline Power (60th Order)

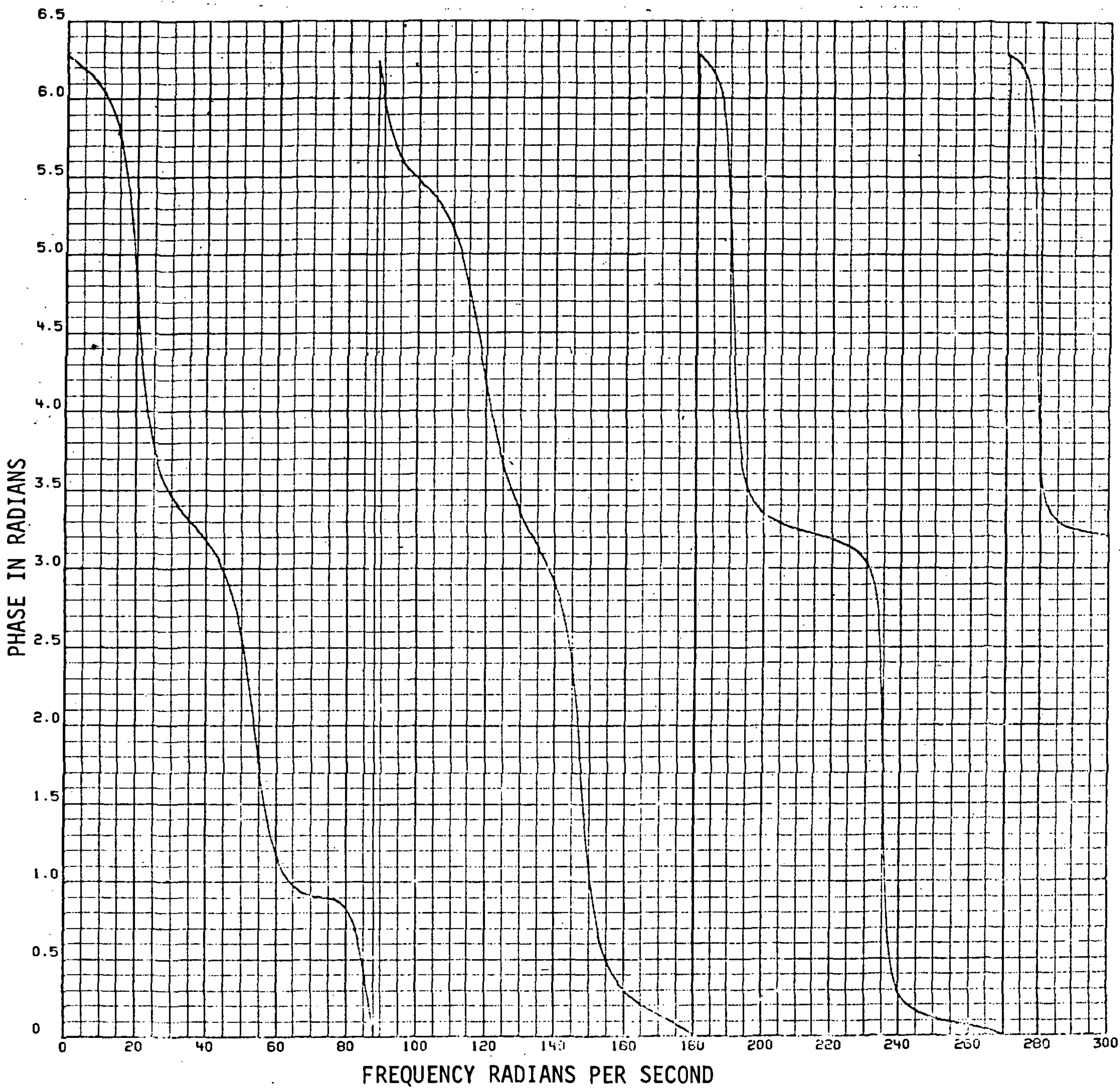

Figure 49 Shuttle Orbiter Feedline Power (60th Order)

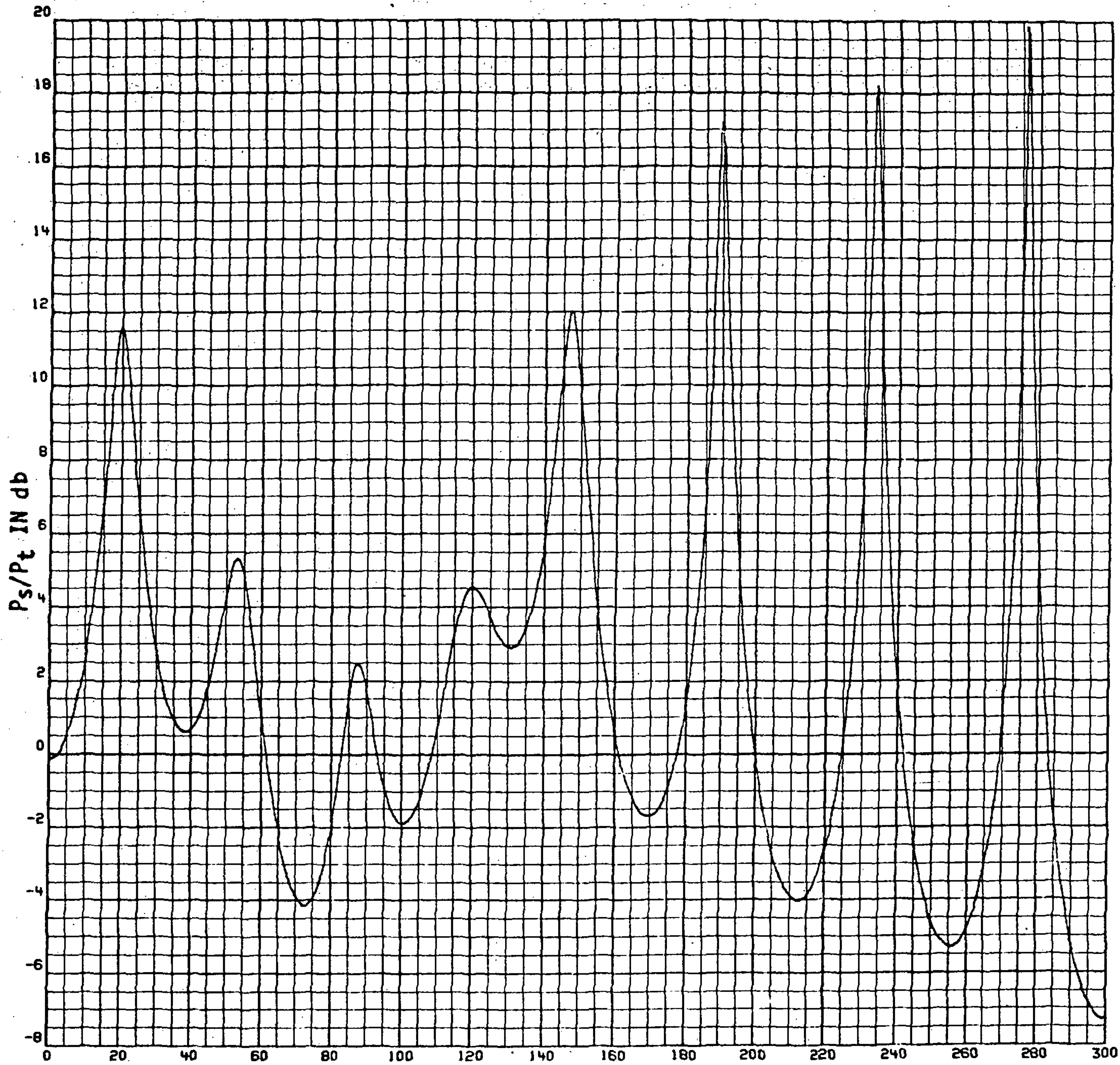

Figure 50 Shuttle Orbiter Feedline Power Series (120th Order)

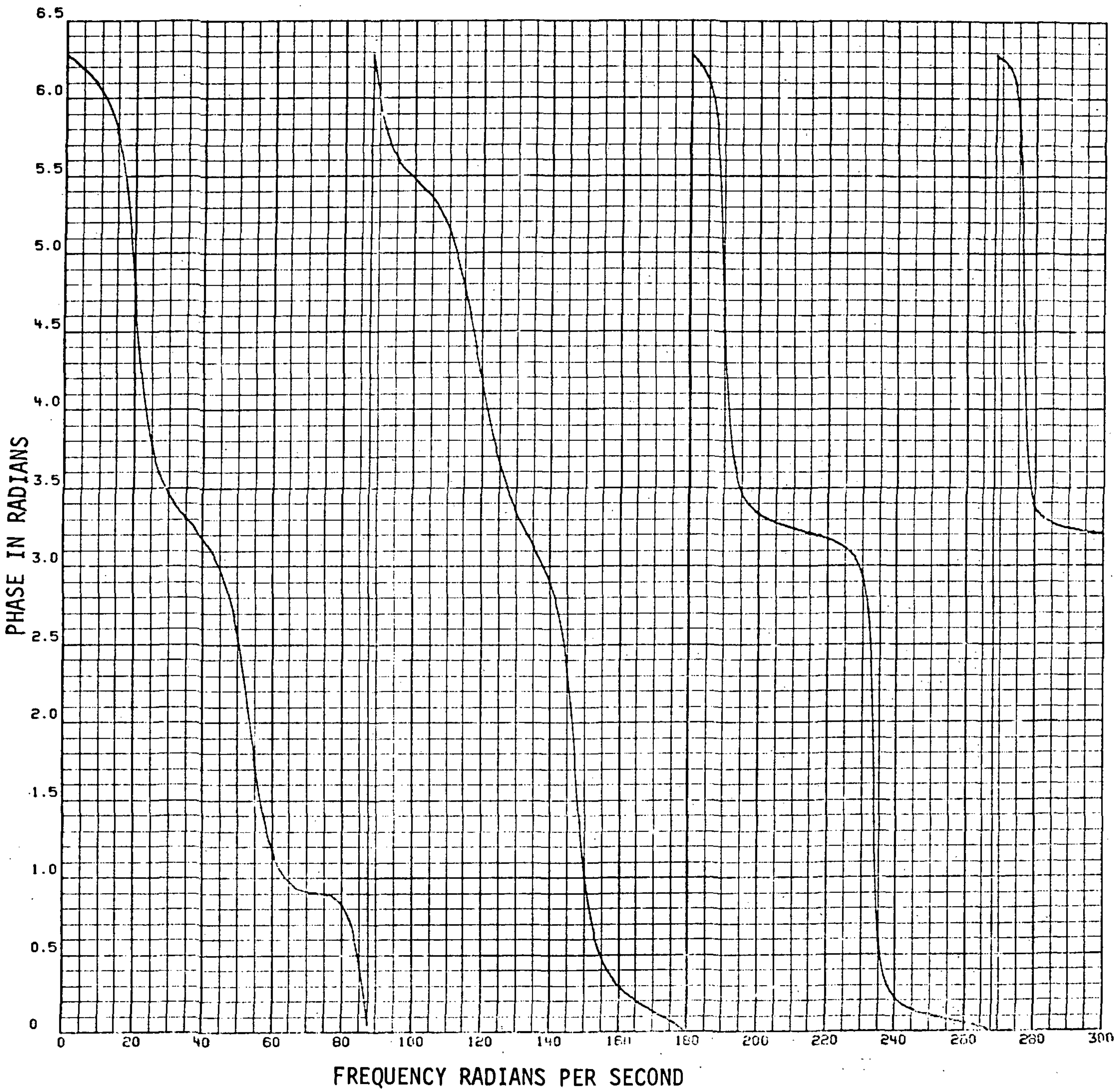

Figure 51 Shuttle Orbiter Feedline
Power Series (120th Order)

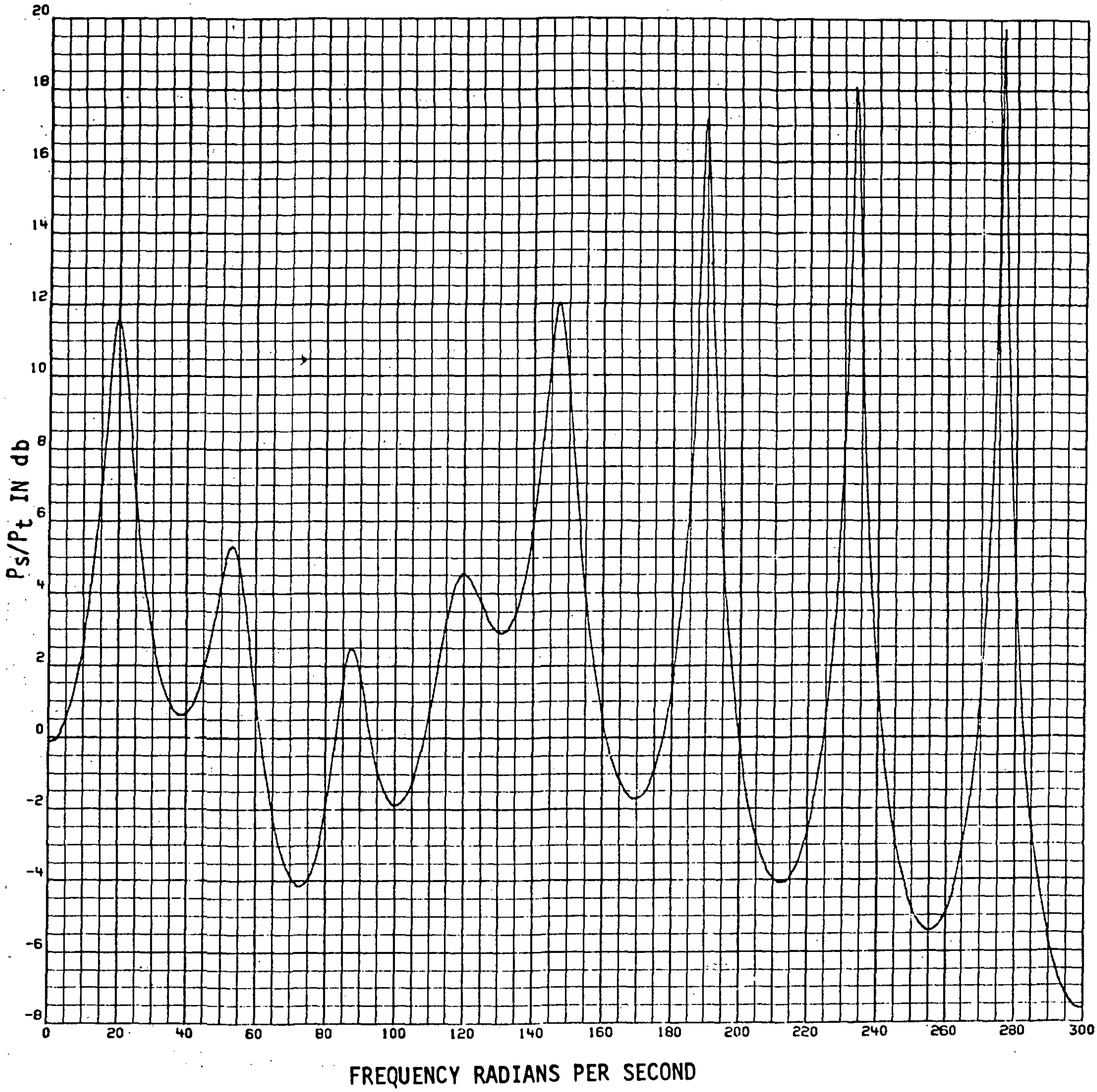

Figure 52 Shuttle Orbiter Feedline Power Series (180th Order)

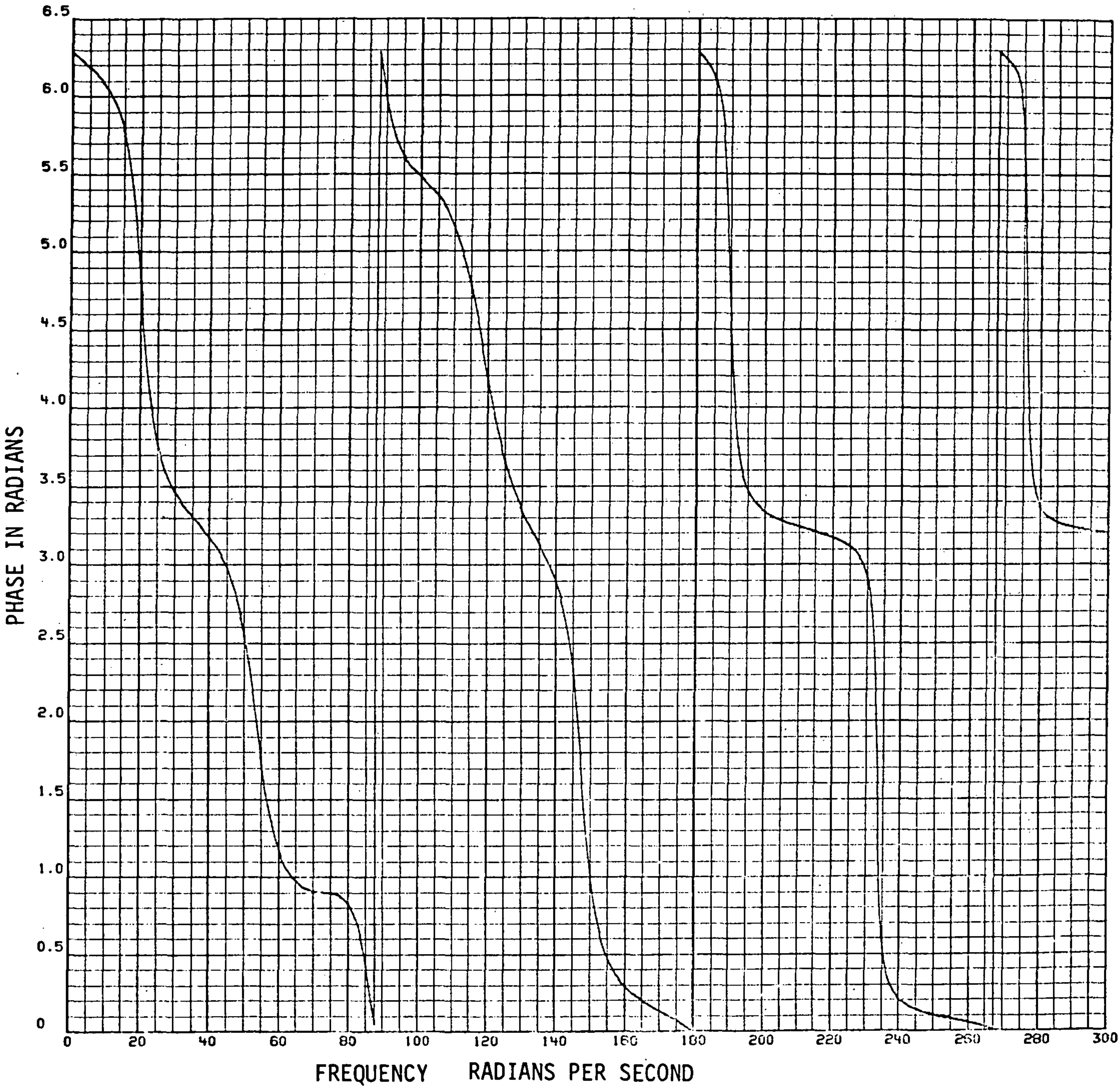

Figure 53 Shuttle Orbiter Feedline
Power Series (180th Order)

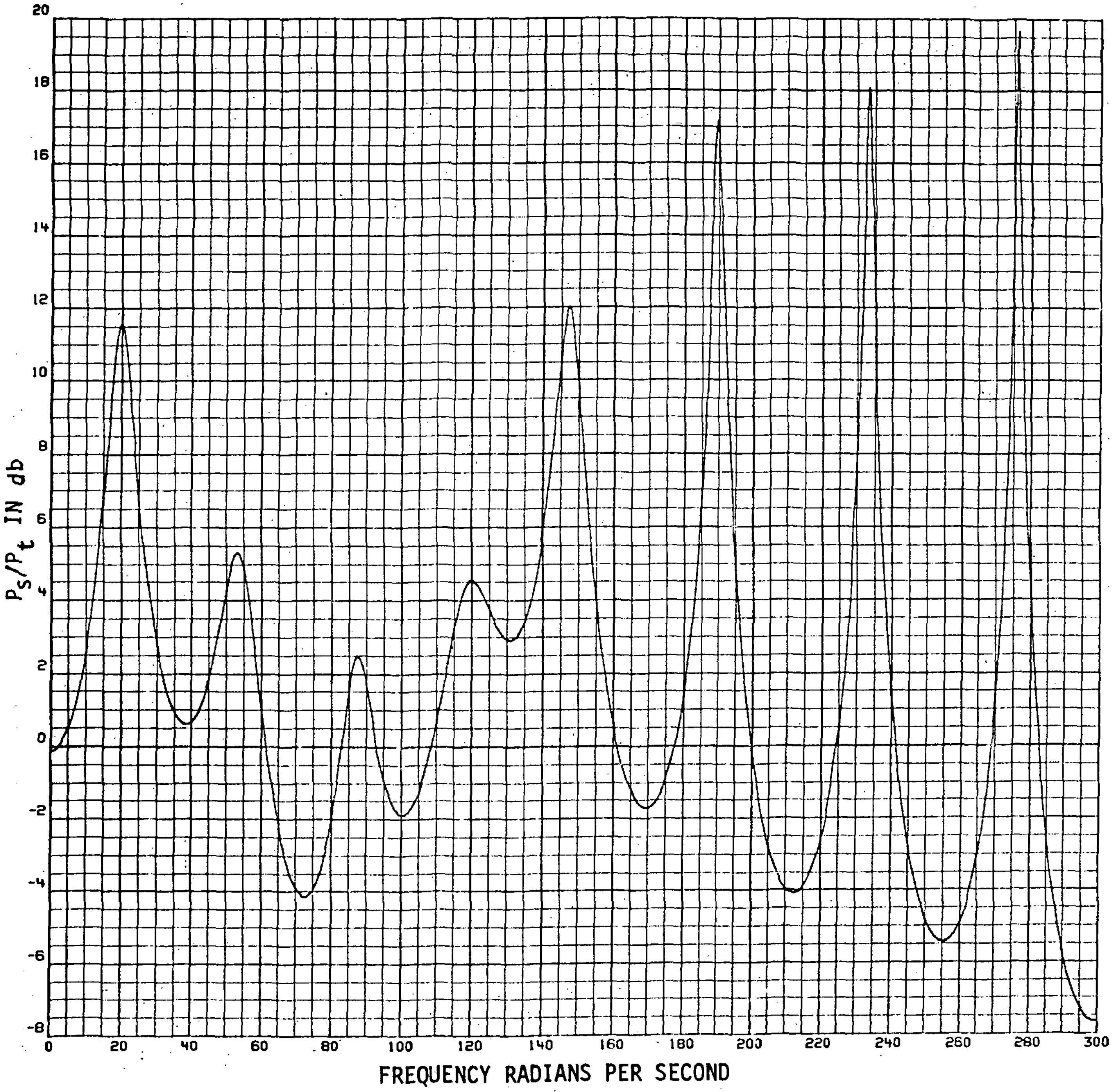

Figure 54 Shuttle Orbiter Feedline Power Series (240th Order)

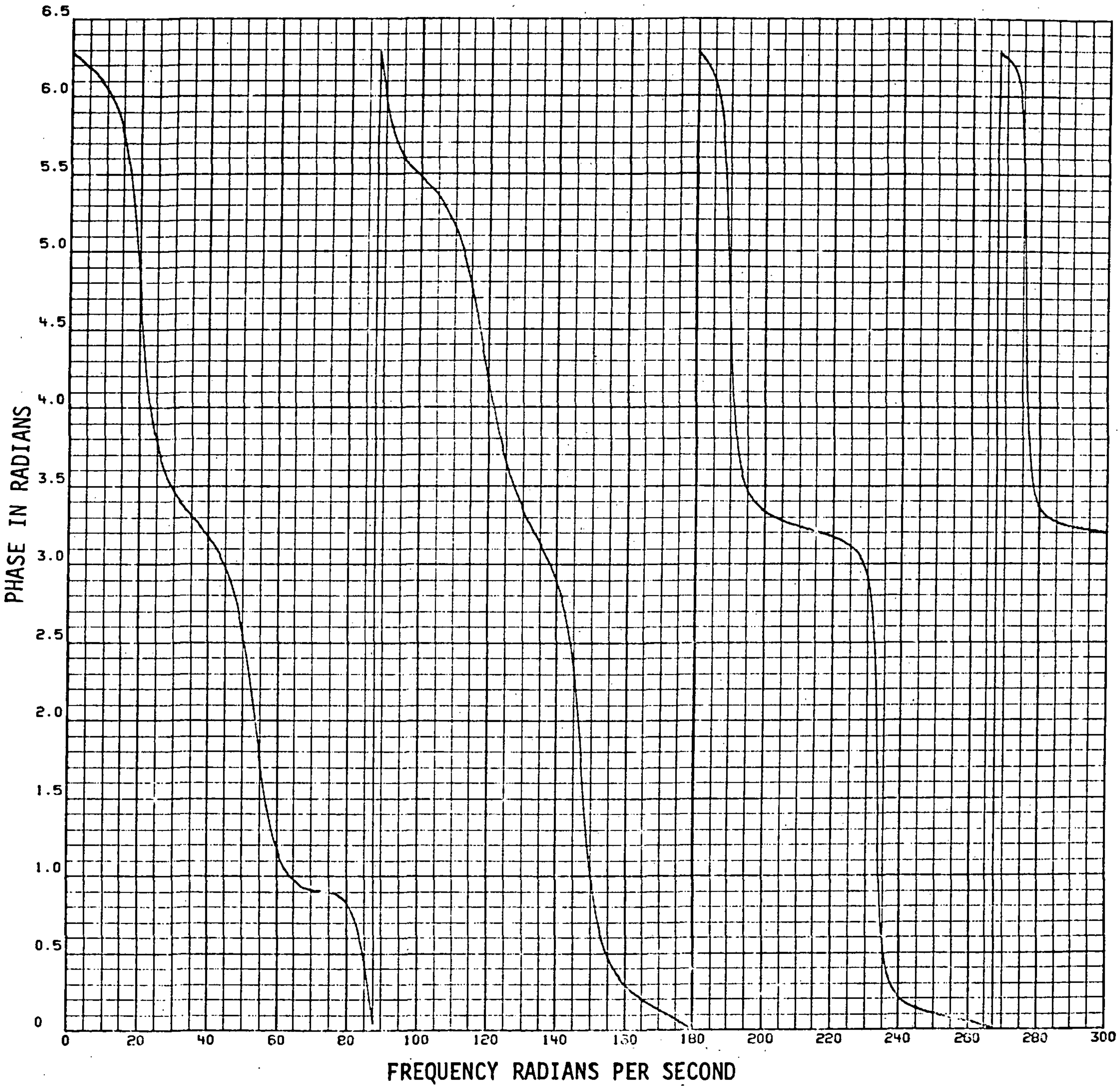

Figure 55 Shuttle Orbiter Feedline Power Series (240th Order)

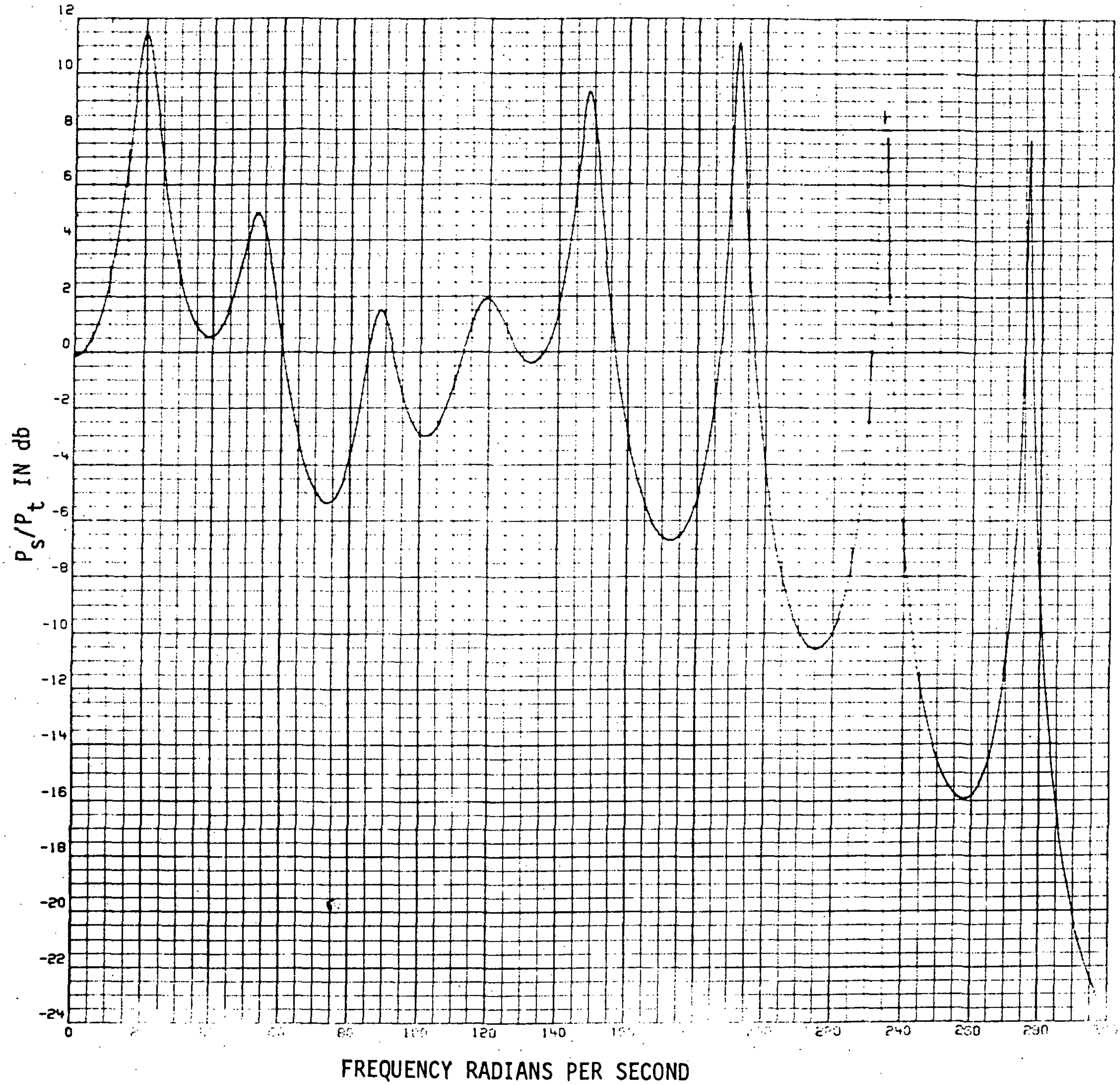

Figure 56 Shuttle Orbiter Feedline Product (60th Order)

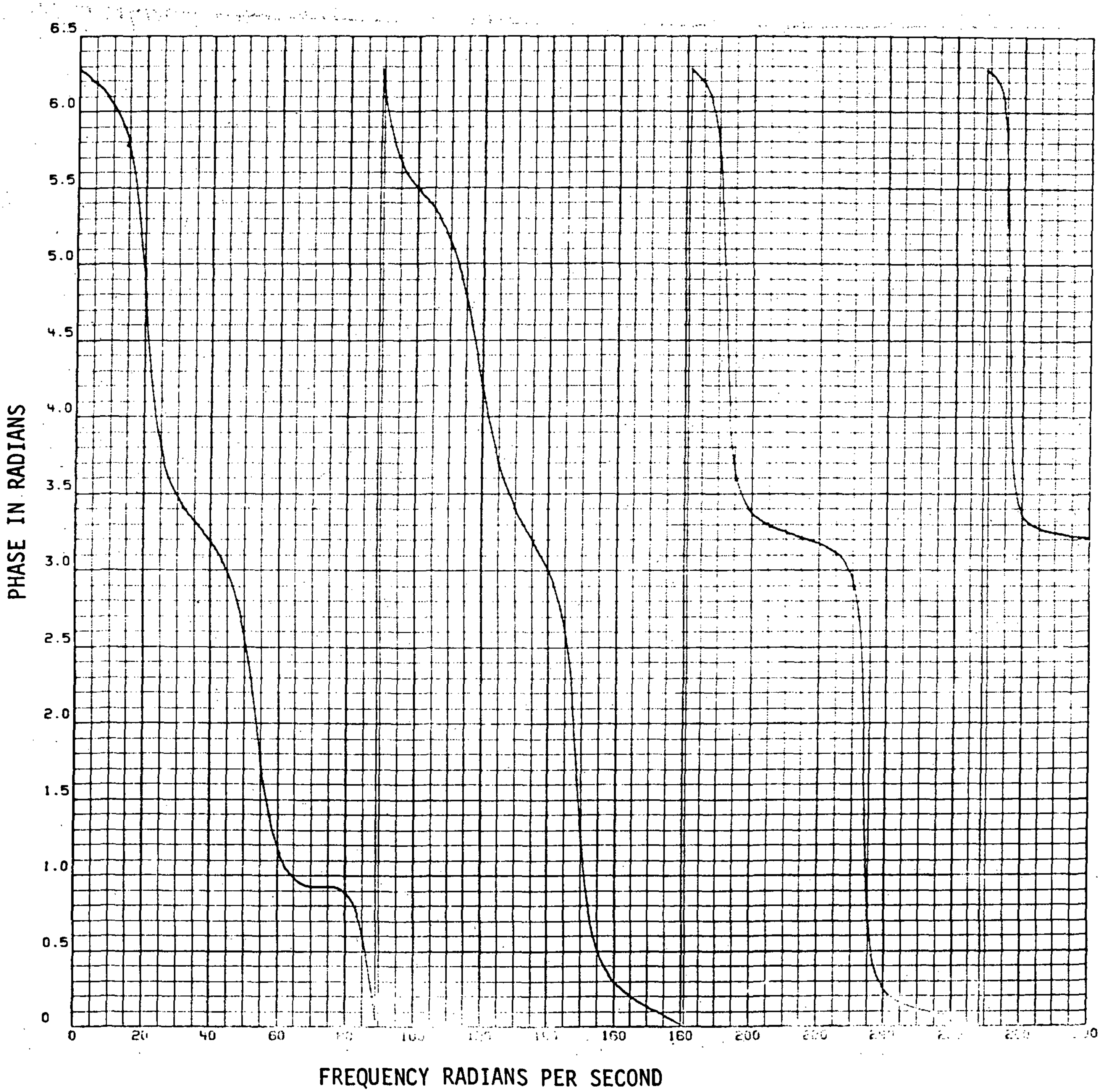

Figure 57 Shuttle Orbiter Feedline
Product (60th Order)

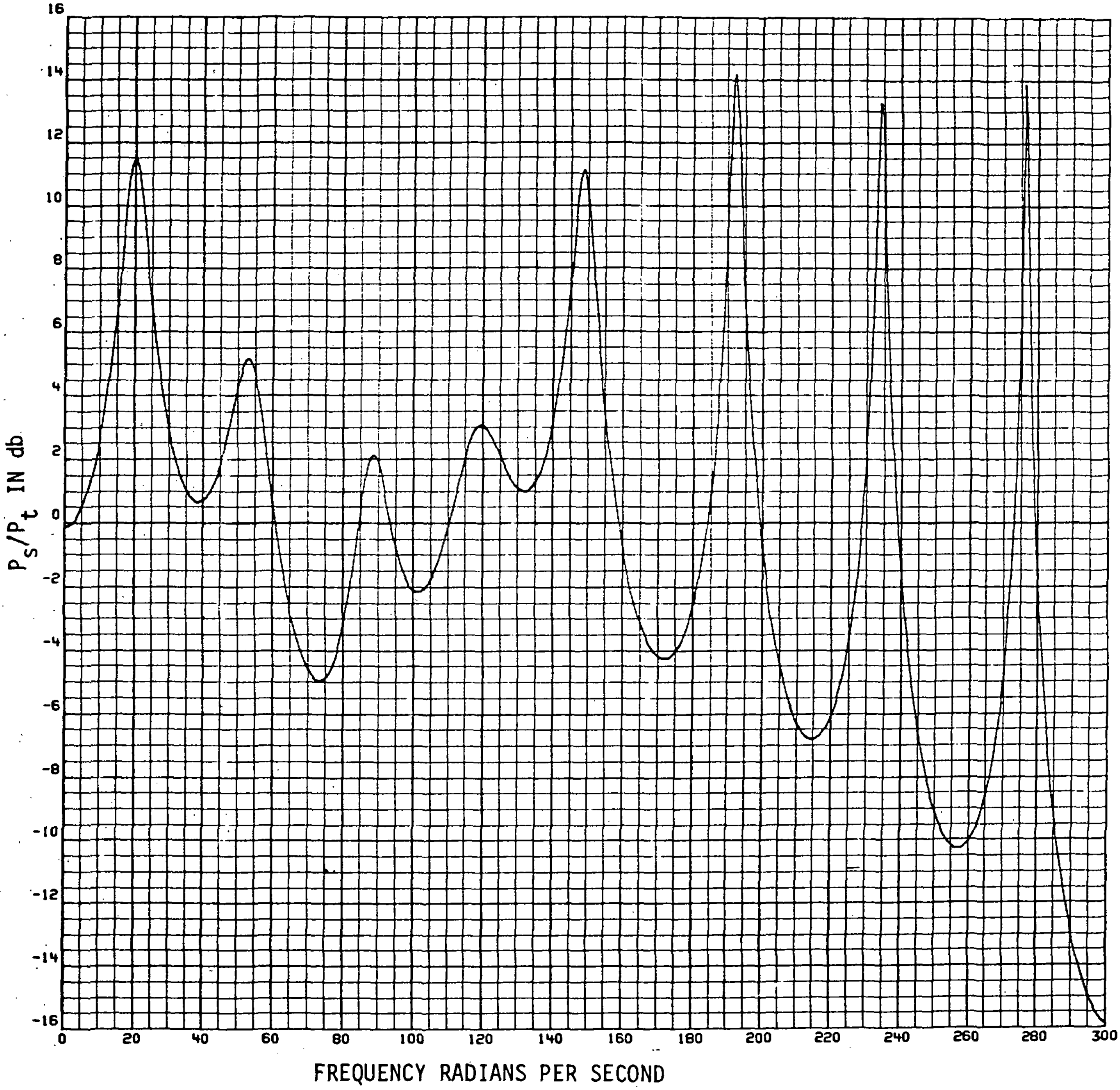

Figure 58 Shuttle Orbiter Feedline Product Series (120th Order)

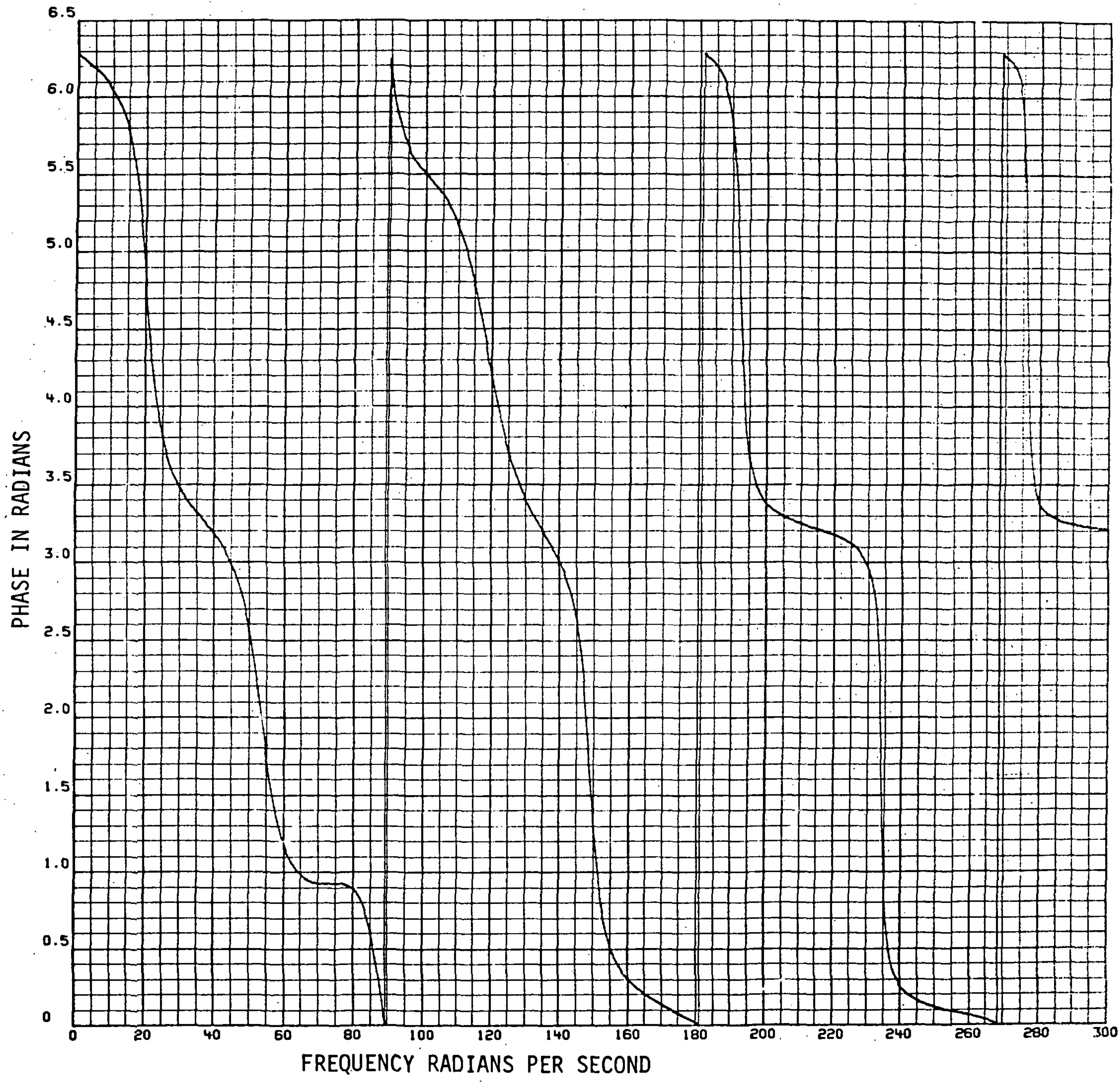

Figure 59 Shuttle Orbiter Feedline Product Series (120th Order)

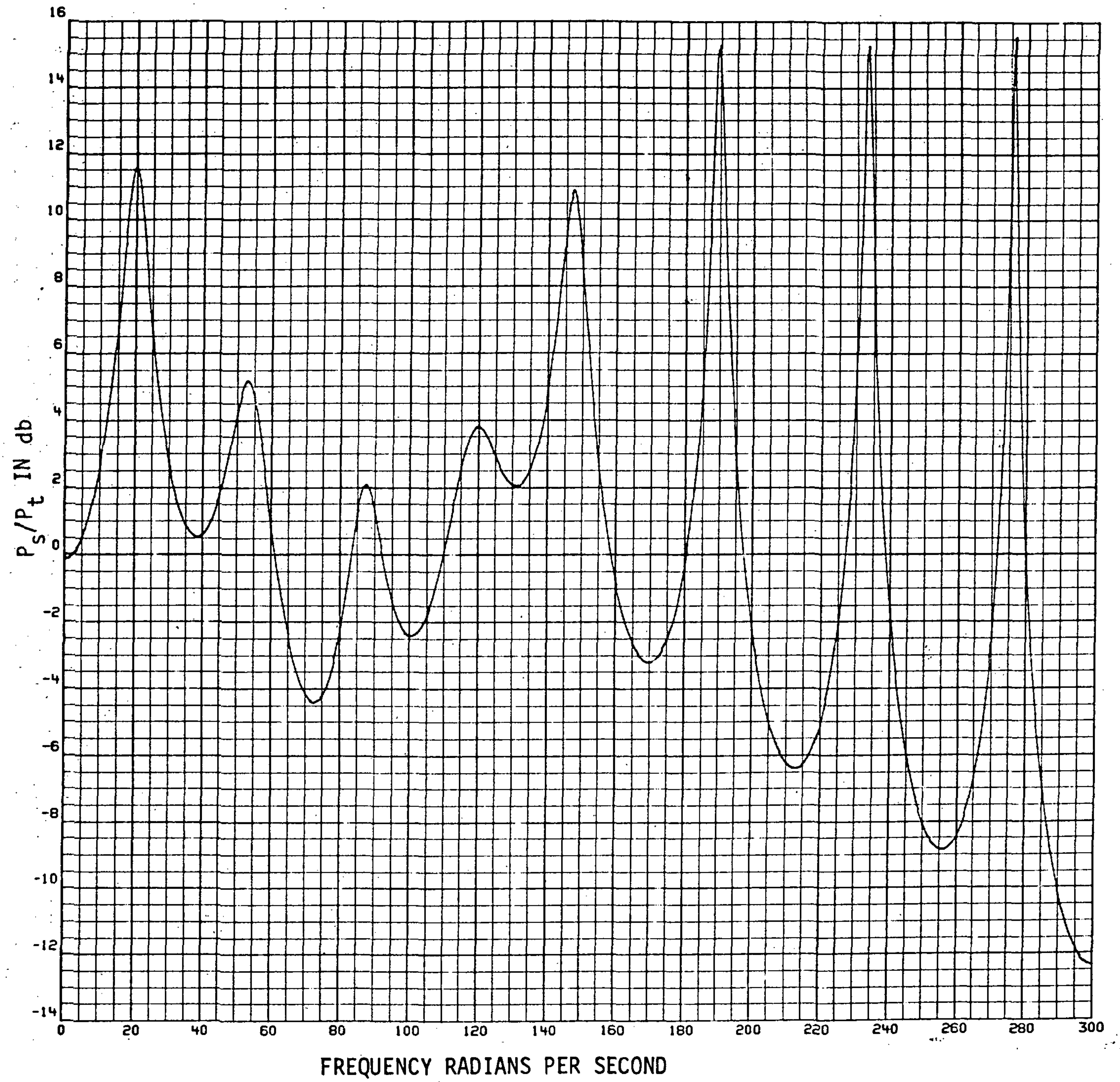

Figure 60 Shuttle Orbiter Feedline
Product Series (180th Order)

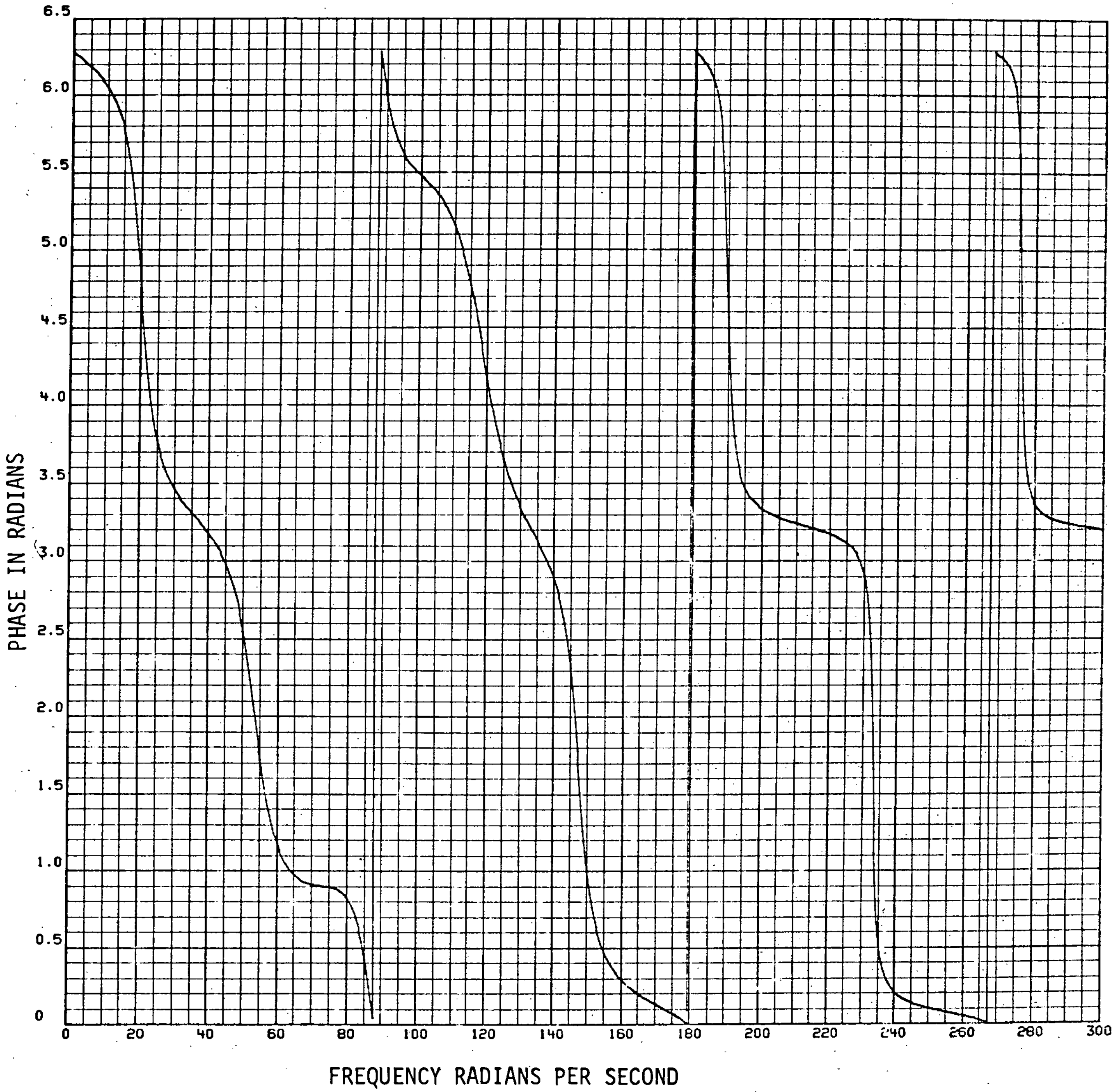

Figure 61 Shuttle Orbiter Feedline Product Series (180th Order)

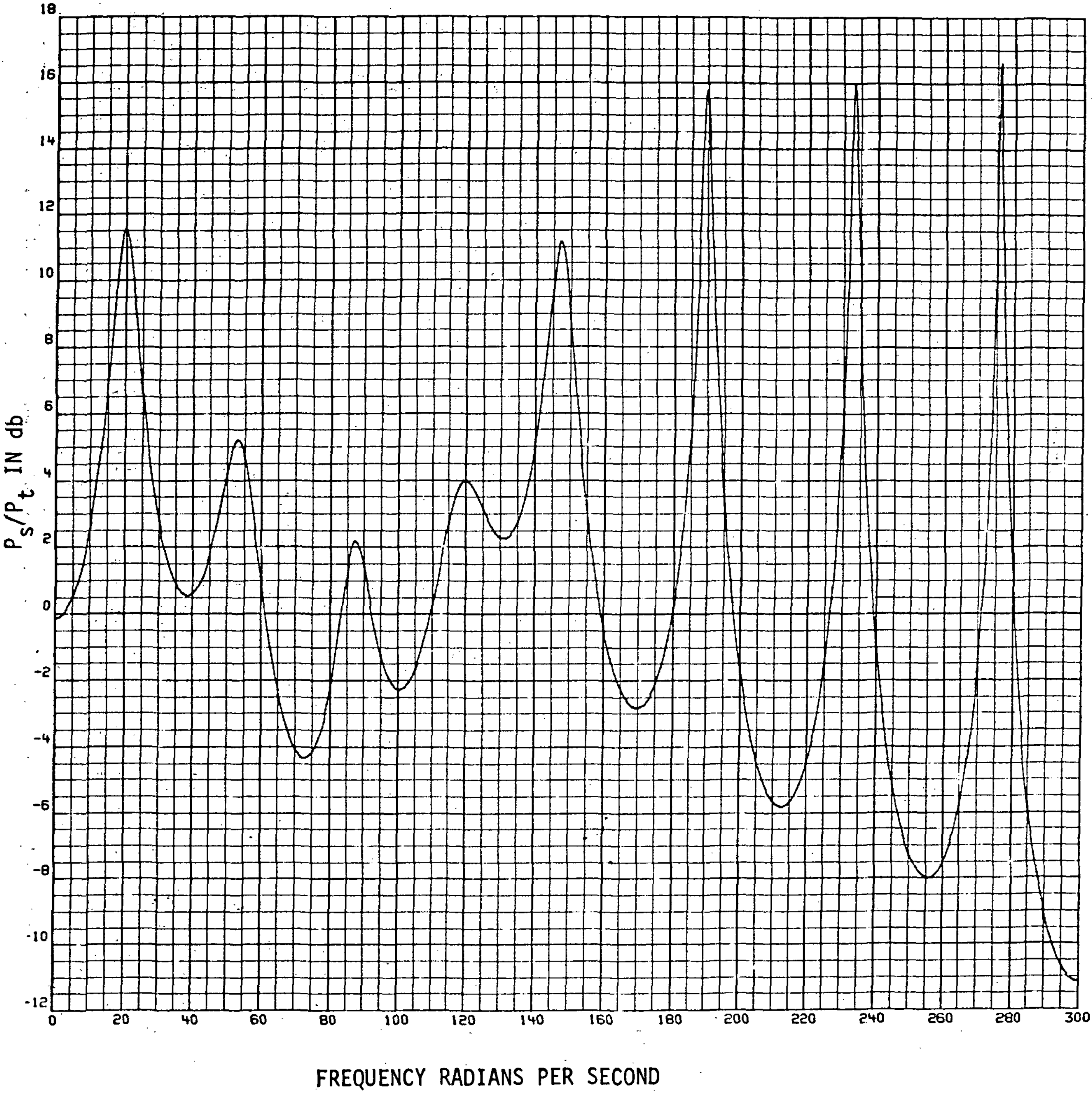

Figure 62 Shuttle Orbiter Feedline Product Series (240th Order)

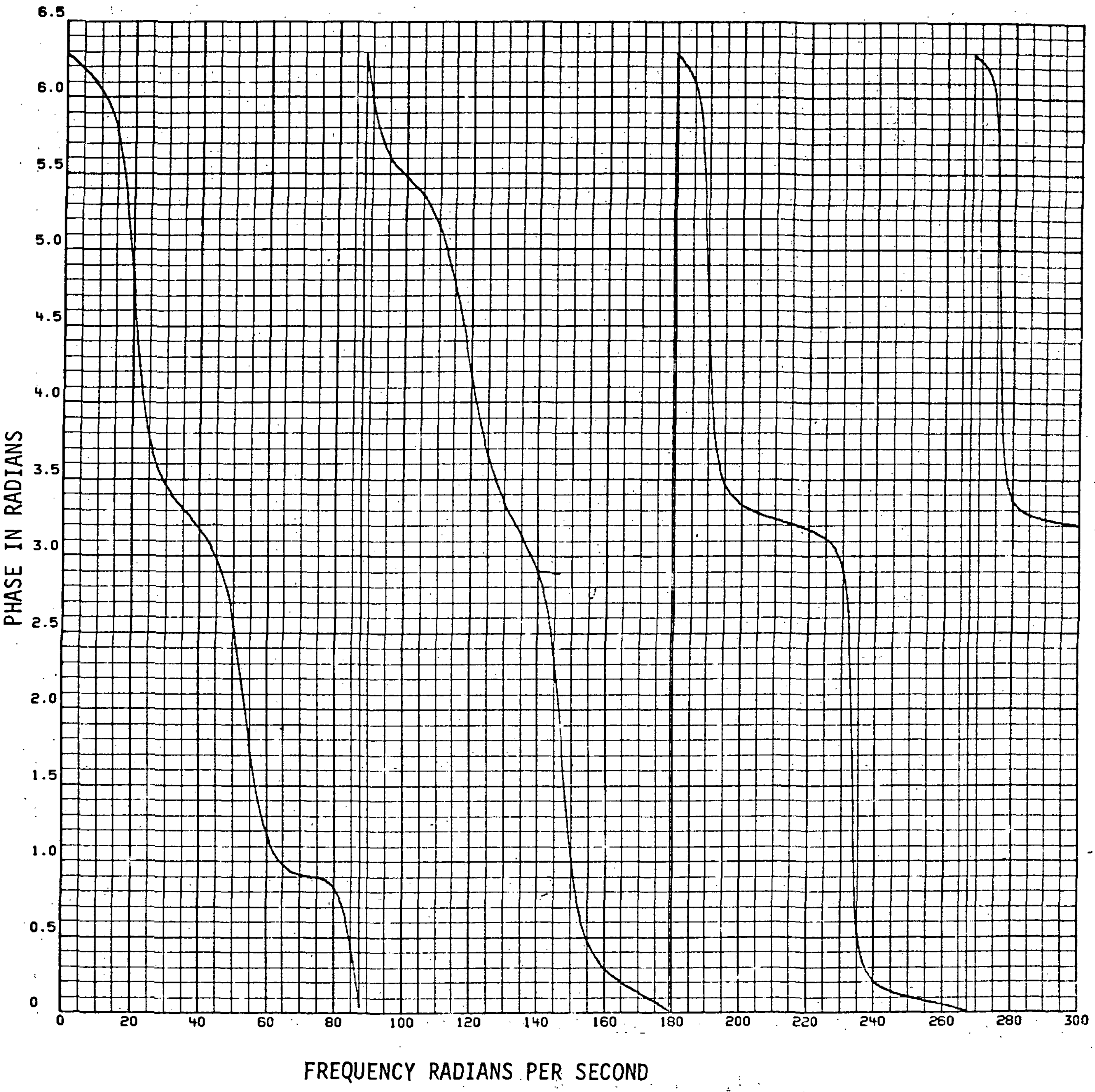

Figure 63 Shuttle Orbiter Feedline
Product Series (240th Order)

Table 3 Shuttle Orbiter Feedline Peak Gains (db)

	"EXACT"	POWER ORDER				PRODUCT ORDER			
		60	120	180	240	60	120	180	240
1	11.477 (20.1)*	11.56	11.56	11.56	11.56	11.415	11.447	11.54	11.54
2	5.368 (53.1)*	5.304	5.304	5.304	5.304	4.941	5.155	5.159	5.159
3	2.717 (88.8)*	2.47	2.46	2.463	2.463	1.497	2.111	2.068	2.168
4	4.167 (119.7)*	4.609	4.551	4.549	4.549	1.920	3.064	3.808	3.995
5	12.807 (148.8)*	12.25	12.0	11.99	11.99	9.314	11.093	10.87	11.15
6	17.013 (192.3)*	17.97	17.1	17.1	17.1	11.124	14.161	15.261	15.738
7	17.594 (234.3)*	20.77	18.2	18.05	18.02	8.670	13.237	15.26	15.975
8	19.860 (276.5)*	26.6	19.36	19.73	19.6	7.608	13.866	15.56	16.59

* FREQUENCY IN RAD/SEC

Page Intentionally Left Blank

V. EIGENVALUES AND THE SOLUTION VECTOR

The stability equations have been reduced to a system of linear homogeneous equations with constant coefficients. They are represented by the following equation:

$$f(D)\,y = 0$$

where y represents a vector whose components are the dependent variables appearing in the stability equation and $f(D)$ is a matrix whose elements $f_{ij}(D)$ are polynomials in the differential operator D. Letting $y = z e^{\lambda t}$ we obtain:

$$f(\lambda)\,y = 0$$

For a non-trivial solution, it is required that $|f(\lambda)| = 0$. The order of the characteristic equation $|f(\lambda)| = 0$ determines the number of arbitrary constants in the solution.

The eigenvalues λ_K of the characteristic equation are obtained using a program currently available at NR and has successfully been used for POGO stability studies. The analysis need only consider the case in which all the eigenvalues are distinct. The system of equations $f(D)y = 0$ can be reduced to a system of linear differential equations with constant coefficients such as $\frac{dx}{dt} = Ax$ such that one could then obtain the eigenvectors associated with the matrix A. For the purpose of the present problem, it is more meaningful to obtain the solution vector y for each of the characteristic values λ_K obtained from the solution of the characteristic equation. Letting $F(\lambda_K)$ be the adjoint of $f(\lambda_K)$ we then have: (Ref. 4).

$$f(\lambda)\ F(\lambda) = \Delta(\lambda)$$

for $\lambda = \lambda_K$ where $\Delta(\lambda_K) = 0$

$$f(\lambda_K)\ F(\lambda_K) = 0$$

The rank of F (λ_K) is 1 so that the matrix F (λ_K) has only one independent column vector. It is clear then that the solution vector y is proportional to any non-null column of the adjoint matrix F (λ_K). (For the case of multiple degeneracy, the adjoint matrix is null. This case, however, is only of academic interest for the POGO stability problem and will not be considered). For the system of equations given for the Shuttle stability analysis, the solution vector y can most easily be obtained by simply choosing $y_1(\lambda_K) = T = e^{\lambda_K t}$ and directly solving for $y_i(\lambda_K)$ where $y_i(\lambda_K)$ represents the remaining dependent variables P_S, P_T, etc.

Performing the indicated operations one obtains:

$$P_s = \frac{1}{H(s)} T$$

$$q_i = \frac{1}{s^2 + \zeta_i \omega_i s + \omega_i^2} \left[\frac{4\,\phi_i(x_g)}{\mathcal{M}_i} \right] (T - P_s A)$$

$$x_o = \frac{4}{s^2 M} (T - P_s A)$$

$$x_g = x_o + \sum \phi_i(x_g)\, q_i$$

$$\ddot{W}_s = P_s / G(s)$$

$$P_T = \sum \gamma_i \ddot{q}_i + \rho h \ddot{x}_o$$

$$H(s) = \bar{C}\,\bar{h}(s)\ ; \quad \bar{C} = 150\ \text{in.}^2 \quad (.0964\ \text{m.}^2)$$

where
$$\bar{h}(s) = \frac{(0.1 + 1.1 \times 10^{-2} s)}{(1 + 5.79 \times 10^{-2} s)(1 + 7.96 \times 10^{-3} s + 1.58404 \times 10^{-5} s^2)}$$

The gain and phase measurements obtained from flight data occur at the characteristic frequency of the system. Comparison of these results with the solution vector should give a check on the accuracy of the POGO model.

The structural data used in the stability analysis is summarized below:

generalized mass	$\mathcal{M}_i = .224 \times 10^3$ SLUGS (3.28×10^3 KGM)
natural frequency	$\omega_1 = 2.6994$ Hz.
damping	$\zeta_1 = 0.005$
modal displacement at gimbal	$\phi_1(x_g) = 1.0694$
modal displacement at sump	$\phi_1(x_T) = -.5795$
liquid LO_2 level	$h = 300$ IN. (7.62 M.)
modal pressure	$\gamma_1 = \rho h \phi_1(x_T)$

The eigenvalues were obtained by solving the system equations with the currently available stability program. Because of the size limitations of the program, power and product series approximations to the 60th order were utilized. The stability analysis was performed using only one structural mode in which the bulkhead was treated using a spring-mass analogy. For a more accurate stability analysis, the bulkhead must be modeled using a multi degree of freedom hydro-elastic model.

For the purpose of the present study which is concerned primarily with numerical methods in treating the propellant line, the simplified treatment of the bulk-head was deemed adequate. It should be emphasized the results will be applicable only in the frequency bandwidth where the feedline transfer function obtained from either the power or product series approximation is valid.

The closed loop roots and the associated solution vectors have been obtained with and without the convective acceleration terms and are given in Tables 4 and 6. The undamped natural frequency and the damping are given in Table 5. The results indicate the convective acceleration terms were of minor importance. Since only one structural mode was used it should be emphasized that only the first root has significance. For this reason the solution vector has been tabulated for only the first characteristic value.

In order to perform the stability analysis using the product series expansion for the transmission parameter it was necessary to alter the model from that used to obtain the Bode plot shown in Figure 56 and 57. The damping due to the bend at B (see Figure 45) was included with the entrance losses at A. This was done to reduce the number of equations in order to make the feedline model acceptable to the stability program. The order of the product series approximation, however, was kept at 60th order. The effect of this model change can be seen by comparing the original Bode plot (Figure 56) with the amended one with the bend damping lumped at the entrance given in Figures 64 and 65.

The largest effect appears to occur at the first mode where the decrease in gain has the effect of increasing the damping from 2.8 percent to 3.3 percent. Although the remaining results are not too meaningful, since only one structural mode was used in the analysis, the first five closed loop roots obtained from the power and product series methods are in substantial agreement. In order to get agreement in a higher frequency range, higher order approximations are required.

The computer time required to obtain the closed loop roots was from 3-4 CPU minutes when the feedline was modeled with either power or product series expansion. Bode plots of the feedline transfer function of the Shuttle Orbiter configurations for each of the polynomial approximations utilized about 0.3 CPU minutes. The computations were performed on an IBM Model 165 computer.

Nyquist diagrams were not presented because the numerical procedures used are not meaningful beyond a given frequency. An instability at 100 Hz for example would result in an instability in the Nyquist diagram. It should be again emphasized that the stability results are only valid in the range where the Bode plots of the approximate feedline transfer functions are in agreement with the "exact" results.

Table 4 Closed Loop Roots

POWER (With Convective Acceleration Term)		POWER (Without Convective Acceleration Term)		PRODUCT (With Convective Acceleration Term)	
Real (a)	Imag. (b)	Real (a)	Imag. (b)	Real (a)	Imag. (b)
-0.4438	15.6770	-0.4552	15.6690	-0.5300	15.6390
-3.2967	22.3788	-3.1861	22.3620	-3.2782	21.6792
-5.4490	52.4634	-5.1763	52.5776	-5.2298	53.0062
-5.1954	88.2370	-5.3191	88.5178	-5.4043	87.8790
-7.2478	119.5710	-7.3445	119.0430	-7.0554	119.4860
-4.3405	148.5320	-3.6360	148.6460	-4.3813	148.0730
-1.7258	193.3330	-0.6566	193.3430	-1.8756	191.3470

Table 5 Undamped Natural Frequency and Damping

POWER (With Convective Acceleration Term)		POWER (Without Convective Acceleration Term)		PRODUCT (With Convective Acceleration Term)	
ω_0 (RAD/SEC)	ζ	ω_0 (RAD/SEC)	ζ	ω_0 (RAD/SEC)	ζ
15.6	.028	15.6	.029	15.6	.033
22.6	.145	22.5	.141	21.9	.149
52.7	.103	52.8	.098	53.2	.098
88.3	.058	88.6	.059	88.0	.061
119.	.029	119.	.061	119.	.058
148.	.008	148.	.024	148.	.029
193.	.011	193.	.003	191.	.010

Table 6 Solution Vector for 1st Root

	GAIN	PHASE	GAIN	PHASE	GAIN	PHASE
$\dot{X}_o/T$	$0.9487\ 10^{-4}$	1.5425	$0.9492\ 10^{-4}$	1.5417	$0.9509\ 10^{-4}$	1.5369
q/T	$0.3699\ 10^{-1}$	0.2633	$0.3671\ 10^{-1}$	0.2695	$0.3539\ 10^{-1}$	0.3131
P_T/T	$0.18274\ 10^{-1}$	0.3208	$0.1811\ 10^{-1}$	0.3285	$0.1739\ 10^{-1}$	0.3819
$\dot{X}/T$	0.3363	-1.2792	0.3335	-1.2722	0.3210	-1.2238
P_s/T	$0.5147\ 10^{-1}$	-0.6662	$0.5146\ 10^{-1}$	-0.6669	$0.5137\ 10^{-1}$	-0.6700
$\dot{W}_{so}/T$	$0.1495\ 10^{-1}$	-0.1391	$0.1494\ 10^{-1}$	-0.1396	$0.1488\ 10^{-1}$	-0.1419
$\dot{W}_s/T$	3.5604	-1.2754	3.5309	-1.2684	3.3989	-1.2200
P_s/P_t	2.8169	-0.9870	2.8415	-0.9954	2.9526	-1.0525

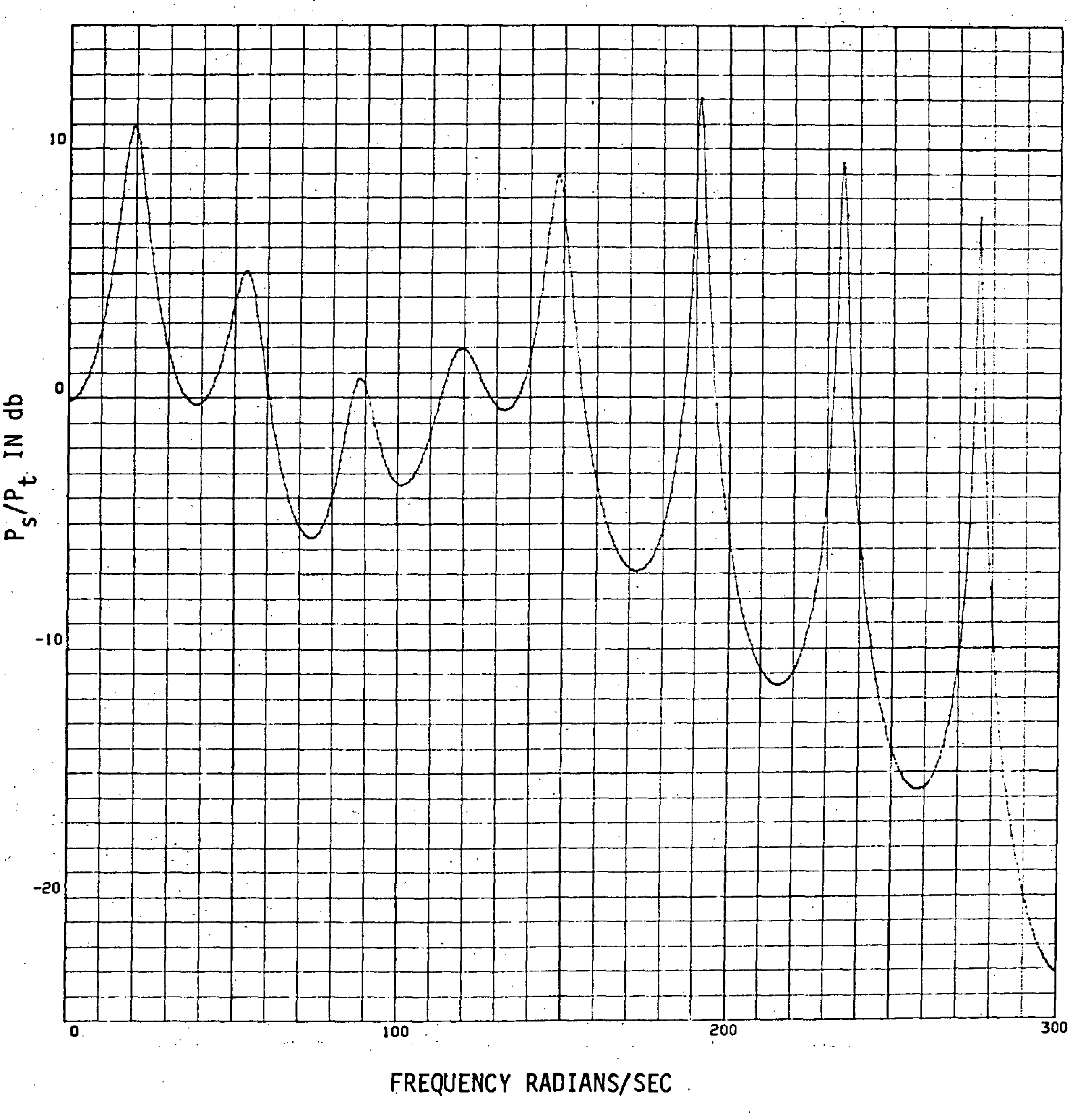

Figure 64 Shuttle Orbiter Feedline Product Series (60th Order)

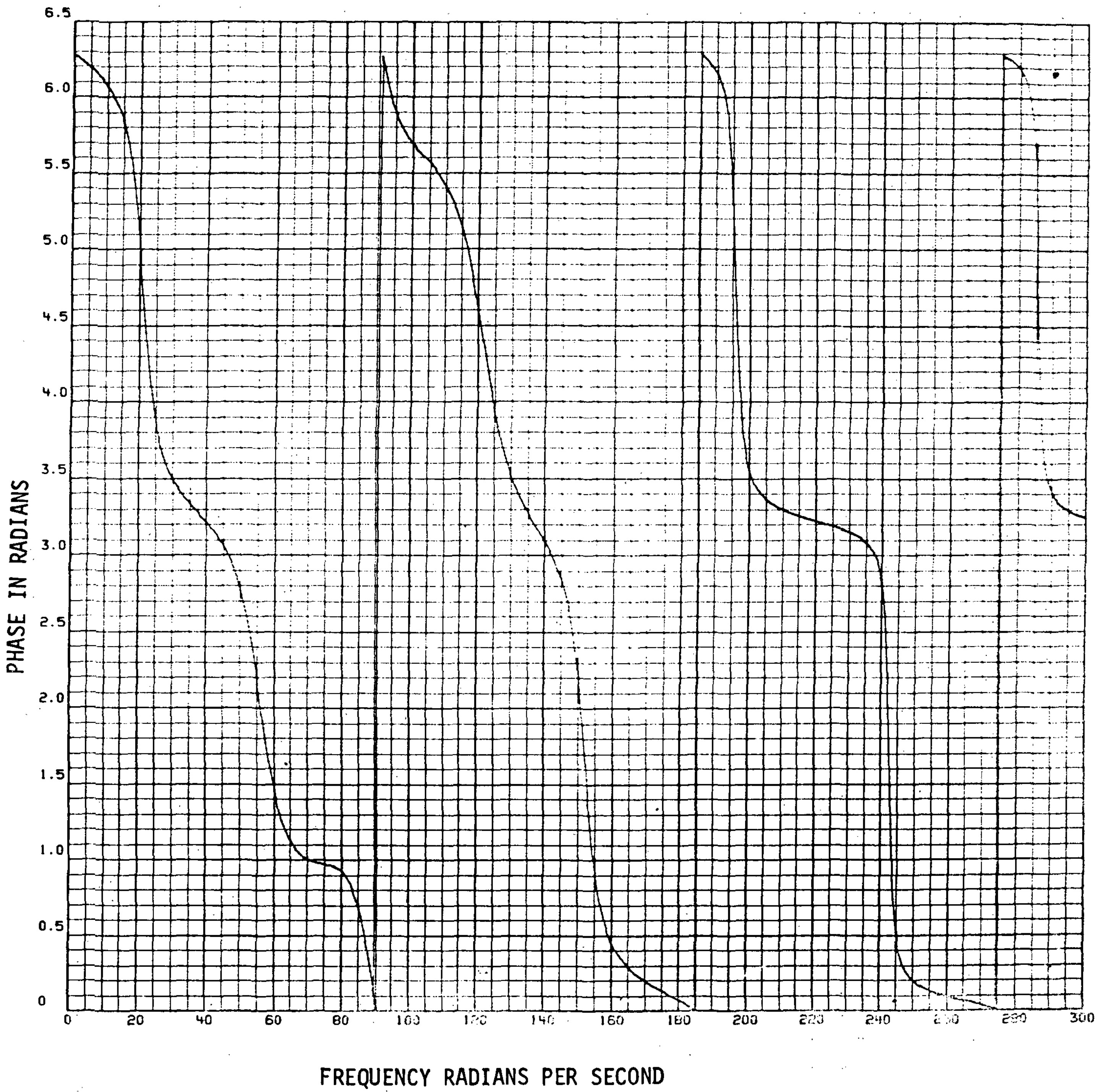

Figure 65 Shuttle Orbiter Feedline Product Series (60th Order)

VI. CONCLUSIONS AND RECOMMENDATIONS

The results of this study show that the Shuttle Orbiter feedline may be modeled adequately by using polynomial approximations to transcendental functions appearing in the transmission parameters. The adequacy of the approximations may be determined by a comparison of the Bode plots of the feedline transfer function obtained from either the power or product series approximations with the "exact" solution obtained using the transcendental functions. For complex feedline with multiple bends this study indicates the power series method is to be preferred over the product series. This study has also shown that the line damping may be adequately approximated by lumped damping provided the elemental sections are made sufficiently small. When using the power series method this is automatically accomplished by the requirement that the nondimensional frequency $\frac{\omega l}{a}$ of the largest elemental section be less than one.

Procedures have been developed for including the effect of the convective acceleration terms in the feedline representation. It has been shown that the sole effect of this term is to cause a phase shift of $\frac{u_o}{a} \cdot \frac{\omega l}{a}$ in the feedline transfer function. For the Shuttle Orbiter configuration this is quite small and may be neglected. This term, however, was included in the feedline transfer function and the stability analysis.

The Shuttle Orbiter line was modeled using polynomial approximation of up to the 240th order. Using the NR stability program the closed loop roots were obtained using a 60th order polynomial approximation for the line.

The system equations used for obtaining these results did not include the hydrogen system and only one LO_2 bulkhead mode was used in the analysis. The stability results therefore, as well as the solution vector, should only be used for comparing the results of different numerical procedures.

The computer time required to obtain the closed loop roots was from 3-4 CPU minutes when the feedline was modeled with either power or product series expansion. Bode plots of the feedline transfers function of the Shuttle Orbiter configurations for each of the polynomial approximations utilized about 0.3 CPU minutes.

The procedures developed in this study for obtaining the approximate and the "exact" Bode plots of the feedline transfer functions are completely general, although they were used for a specific feedline geometry. These procedures should be automated in a digital program so as to handle an arbitrary feedline with branches, bends, pumps, etc., to obtain the required dynamic feedline characteristics. The dynamic characteristics may then be obtained using a Taylor series approximation for the elemental sections and the results checked with the "exact" solution. Having modeled the feedline to the required degree of accuracy necessary one can then proceed to determine the closed loop roots and the associated solution vector by incorporating the feedline model into the system equations.

VII. REFERENCES

1. Titchmarsh, E. C. The Theory of Functions, Oxford University Press (1939).

2. LeVine, Dickey Root Finding Techniques for a Transcendental Function. M.S. Thesis, Purdue University (1968).

3. Jolley, L. B. W. Summation of Series, Dover Publications, Inc. New York.

4. Frazer, R. A., Duncan, W. J., Collar, A. R. Elementary Matrices, Cambridge at the University Press (1960).

APPENDIX A

DETERMINATION OF TRANSMISSION PARAMETERS

The equations of motion of a compressible fluid in an elastic pipe may be obtained from the following three equations:

1. Continuity Equation

$$\frac{d}{dt}\int_{V(t)} \rho \, dV = \int_V \frac{\partial \rho}{\partial t} dV + \int_S \rho \, (\bar{v}\cdot\hat{n})\, dS = 0$$

2. Momentum Equation

$$\frac{d}{dt}\int_{V(t)} \rho \bar{v} \, dV = \int_V \rho \bar{F} \, dV + \int_S \bar{t} \, dS$$

3. Equation of State

$$\rho = \rho_o \left(1 + \frac{P - P_o}{\beta}\right)$$

where S is the surface of V, $\bar{v}\cdot\hat{n}$ is the component of $\bar{v}$ along the outward normal to S and $\frac{\partial}{\partial x}$ denotes differentiation with V held fixed.

The differential form of the equations of motion may be obtained by using a tubular element as shown in Figure 66.

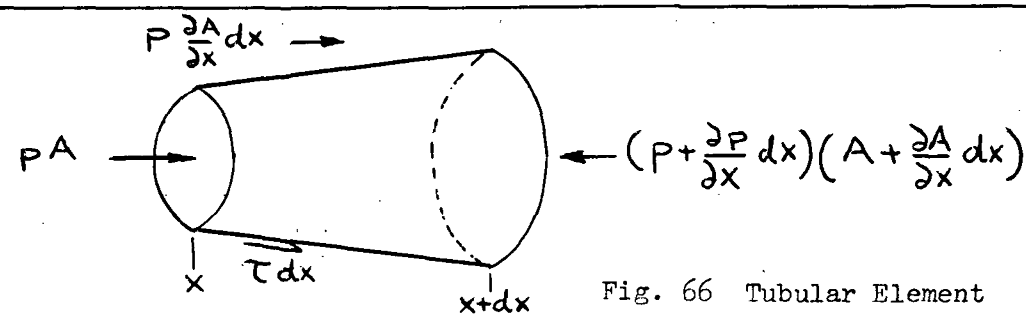

Fig. 66 Tubular Element

Since we are concerned with turbulent flow ($N_R = 10^7$) the shear stress is given by the following formula:

$$\tau = \frac{\rho f V^2}{8}$$

where f is the Darcy Weisbach constant.

Evaluating the integral equations (1) and (2) for the elemental volume shown in Figure 66 results in the following differential equations:

5. Continuity Equation $\frac{\partial}{\partial x}(\rho u A) + \frac{\partial}{\partial t}(\rho A) = 0$

6. Momentum Equation $\frac{\partial}{\partial t}(\rho u A) + \frac{\partial}{\partial x}(\rho u^2 A) + \frac{\partial p}{\partial x} A + \frac{f \rho u^2 \pi D}{8} = 0$

The pressure area relationship required to further reduce the above equation depends on the end conditions for the pipe. The area of the pipe is given by: $A = \pi R^2 \; ; \; R = R_o(1 + \epsilon_1)$

where ϵ_1 is the hoop strain.

<u>Case I</u>

Pipe with end closed such that hoop stress is twice axial stress.

$$\sigma_1 = pR/t \qquad \epsilon_1 = \frac{pD}{2Et}\left(1 - \frac{\mu}{2}\right)$$
$$\sigma_2 = pR/2t$$

<u>Case II</u>

Pipe constrained from having axial motion

$$\epsilon_2 = 0 \; ; \; \sigma_2 - \mu\sigma_1 = 0$$
$$\epsilon_1 = \frac{\sigma_1 - \mu^2\sigma_1}{E} = \frac{\sigma_1}{E}(1 - \mu^2) = \frac{pD}{2Et}(1 - \mu^2)$$

<u>Case III</u>

Pipe with one end free such that

$$\sigma_1 = pR/t \qquad \epsilon_1 = \frac{pD}{2Et}$$
$$\sigma_2 = 0$$

Using these three expressions for hoop strain one obtains the following expression for $\frac{\partial A}{\partial p}$:

Case I $\frac{\partial A}{\partial p} = A\left(1 - \frac{\mu}{2}\right)\frac{D}{Et}$

Case II $$\frac{\partial A}{\partial P} = \frac{AD}{Et}$$

Case III $$\frac{\partial A}{\partial P} = A(1-\mu^2)\frac{D}{Et}$$

Substituting the above into the continuity equation one obtains:

(7) $$\frac{u}{\beta_e}\frac{\partial P}{\partial x} + \frac{\partial u}{\partial x} + \frac{1}{\beta_e}\frac{\partial P}{\partial t} = 0$$

(8) where $$\frac{1}{\beta_e} = \frac{1}{\beta} + \frac{1}{A}\frac{\partial A}{\partial P}$$

For Case I which will be used in this study, one obtains for the effective bulk modulus:

(9) $$\frac{1}{\beta_e} = \frac{1}{\beta} + \left(1-\frac{\mu}{2}\right)\frac{D}{Et}$$

The momentum equation becomes:

(10) $$\frac{\partial u}{\partial t} + \frac{u}{\beta_e}\frac{\partial P}{\partial t} + 2u\frac{\partial u}{\partial x} + \left(\frac{1}{\rho} + \frac{u^2}{\beta_e}\right)\frac{\partial P}{\partial x} + \frac{f u^2}{2D} = 0$$

Combining equation (7) and (10) one obtains

(11) $$\frac{\partial u}{\partial t} + u\frac{\partial u}{\partial x} + \frac{1}{\rho}\frac{\partial P}{\partial x} + \frac{f u^2}{2D} = 0$$

Equations (7) and (11) constitute two nonlinear equations of motion which govern the motion of compressible turbulent flow in a flexible pipe. There are methods of handling nonlinear equations in the time domain, such as the method of characteristics, but we are here concerned only with linear methods which may be used for POGO stability analysis. Linear perturbation equations may be obtained by removing the steady state terms.

$$u = u_0 + \tilde{u} \quad ; \quad P = p_0 + \tilde{p}$$

Substituting into equations (7) and (11) we obtain the following equations for the perturbed values. (The perturbed values $\tilde{u}$, $\tilde{p}$, have now been redefined as u and p).

(12) $$u_o \frac{\partial P}{\partial x} + \beta_e \frac{\partial u}{\partial x} + \frac{\partial P}{\partial t} = 0$$

(13) $$\frac{\partial u}{\partial t} + u_o \frac{\partial u}{\partial x} + \frac{1}{\rho} \frac{\partial P}{\partial x} + c u = 0$$

where $c = \dfrac{f\, u_o}{D\left(1 + .866\sqrt{f}\right)}$

Taking the Laplace Transform of (12) and (13), one can arrive at the following expressions:

(14) $$\frac{\partial^2 u}{\partial x}\left[1 - \left(\frac{u_o}{a}\right)^2\right] - \frac{\partial u}{\partial x}\left(\frac{u_o}{a}\right)\left(\frac{2S+C}{a}\right) - \frac{S(S+C)}{a^2}\, u = 0$$

(15) $$\frac{\partial^2 P}{\partial x}\left[1 - \left(\frac{u_o}{a}\right)^2\right] - \frac{\partial P}{\partial x}\left(\frac{u_o}{a}\right)\left(\frac{2S+C}{a}\right) - \frac{S(S+C)}{a^2}\, P = 0$$

(16) $$a^2 = \frac{\beta_e}{\rho}$$

Letting $u = e^{Rx}$ one obtains:

(17) $$R = \frac{\frac{u_o}{a}\left(\frac{2S+C}{a}\right) \pm \sqrt{\left(\frac{u_o}{a}\right)^2\left(\frac{C}{a}\right)^2 + \frac{4(S^2 - SC)}{a^2}}}{2\left[1 - \left(\frac{u_o}{a}\right)^2\right]}$$

Letting R_1 and R_2, respectively, be the roots associated with positive and negative signs in front of the radical, one obtains the following expressions for the pressure P and the velocity U.

(18) $$P = A_1 e^{R_1 x} + A_2 e^{R_2 x}$$

(19) $$U = B_1 e^{R_1 x} + B_2 e^{R_2 x}$$

where

$$\frac{A_1}{B_1} = \frac{-\beta R_1}{S + u_o R_1} \overset{DF}{=} \frac{1}{\alpha_1}$$

$$\frac{A_2}{B_2} = \frac{-\beta R_2}{S + u_o R_2} \overset{DF}{=} \frac{1}{\alpha_2}$$

Letting
$$P_A = P \quad \text{AT} \quad X = 0$$
$$U_A = U \quad \text{AT} \quad X = 0$$
$$P_B = P \quad \text{AT} \quad X = \ell$$
$$U_B = U \quad \text{AT} \quad X = \ell$$

one obtains:

(20)
$$P_A = \frac{1}{\alpha_1 - \alpha_2}\left[\alpha_1 e^{-R_2\ell} - \alpha_2 e^{-R_1\ell}\right] P_B - \left[\frac{e^{-R_2\ell} - e^{-R_1\ell}}{\rho a(\alpha_1 - \alpha_2)}\right]\rho a U_B$$

(21)
$$\rho a U_A = \frac{\rho a \alpha_1 \alpha_2}{\alpha_1 - \alpha_2}\left[e^{-R_2\ell} - e^{-R_1\ell}\right] P_B + \left[\frac{\alpha_2 e^{-R_2\ell}}{\alpha_1 - \alpha_2} - \frac{\alpha_1 e^{-R_1\ell}}{\alpha_1 - \alpha_2}\right]\rho a U_B$$

The results as they now stand are rather unwieldy and can be simplified considerably by making use of the fact that $\frac{U_c}{a} << 1$ and $\frac{c\ell}{a} << 1$. By neglecting second order terms in $\frac{u_c}{a}$ and $\frac{c\ell}{a}$ we obtain the following simplified version of equations (20) and (21).

(20)
$$\begin{Bmatrix} P_A \\ \rho a U_A \end{Bmatrix} = \begin{bmatrix} A & B \\ C & D \end{bmatrix} \begin{Bmatrix} P_B \\ \rho a U_B \end{Bmatrix}$$

$$A = \exp.\left\{-\frac{u_o}{a}\left(\frac{2S+C}{2}\right)\frac{\ell}{a}\right\}\left\{ch\sqrt{S(S+C)}\left(\frac{\ell}{a}\right) + \left(\frac{1}{2}\frac{u_o}{a}\frac{c}{s}\sqrt{\frac{s}{s+c}}\right) sh\sqrt{S(S+C)}\left(\frac{\ell}{a}\right)\right\}$$

$$B = \exp.\left\{-\frac{u_o}{a}\left(\frac{2S+C}{2}\right)\frac{\ell}{a}\right\}\left\{\sqrt{\frac{S+C}{S}}\left(sh\sqrt{S(C+S)}\right)\frac{\ell}{a}\right\}$$

$$C = \exp.\left\{-\frac{u_o}{a}\left(\frac{2S+C}{2}\right)\frac{\ell}{a}\right\}\left\{\sqrt{\frac{S}{S+C}}\left(sh\sqrt{S(S+C)}\right)\left(\frac{\ell}{a}\right)\right\}$$

$$D = \exp.\left\{-\frac{u_o}{a}\left(\frac{2S+C}{2}\right)\frac{\ell}{a}\right\}\left\{ch\sqrt{S(S+C)}\left(\frac{\ell}{a}\right) - \frac{1}{2}\frac{u_o}{a}\frac{c}{s}\, sh\sqrt{S(S+C)}\left(\frac{\ell}{a}\right)\right\}$$

The above expressions may be further simplified by eliminating product terms in $\frac{u_o}{a}$ and $\frac{c\ell}{a}$. The exponential term thereby reduces to exp $\left(-\frac{u_o}{a}\cdot\frac{s\ell}{a}\right)$. The second expression in A and B behaves as $\frac{u_o}{2a}\cdot\frac{c\ell}{a}$ as $\omega \to 0$. For large values of ω the expression $\frac{c}{2\omega} << 1$ and the product $\frac{u_o}{2a}\cdot\frac{c}{2\omega}$ can be neglected. The resulting simplified transmission parameters are:

$$A = \exp\left\{-\frac{u_o}{a}\cdot\frac{s\ell}{a}\right\} ch\left[\sqrt{s(s+c)}\left(\frac{\ell}{a}\right)\right]$$

$$B = \exp\left\{-\frac{u_o}{a}\cdot\frac{s\ell}{a}\right\}\left(\sqrt{\frac{s+c}{s}}\right) sh\left[\sqrt{s(s+c)}\left(\frac{\ell}{a}\right)\right]$$

$$C = \exp\left\{-\frac{u_o}{a}\cdot\frac{s\ell}{a}\right\}\left(\sqrt{\frac{s}{s+c}}\right) sh\left[\sqrt{s(s+c)}\left(\frac{\ell}{a}\right)\right]$$

$$D = \exp\left\{-\frac{u_o}{a}\cdot\frac{s\ell}{a}\right\} ch\left[\sqrt{s(s+c)}\left(\frac{\ell}{a}\right)\right]$$

If one is interested in the frequency range $\omega > 1$ Hz and notes that for the Shuttle feedlines $c \cong .1$ rad/sec., the following approximations hold:

$$A(s) \cong \exp\left\{-\frac{u_o}{a}\cdot\frac{s\ell}{a}\right\} ch\left[\frac{s\ell}{a}\left(1+\frac{c}{2s}\right)\right]$$

$$B(s) \cong \exp\left\{-\frac{u_o}{a}\cdot\frac{s\ell}{a}\right\}\left(1+\frac{c}{2s}\right) sh\left[\frac{s\ell}{a}\left(1+\frac{c}{2s}\right)\right]$$

$$C(s) \cong \exp\left\{-\frac{u_o}{a}\cdot\frac{s\ell}{a}\right\} sh\left[\frac{s\ell}{a}\left(1+\frac{c}{2s}\right)\right] \Big/ \left(1+\frac{c}{2s}\right)$$

$$D(s) \cong \exp\left\{-\frac{u_o}{a}\cdot\frac{s\ell}{a}\right\} ch\left[\frac{s\ell}{a}\left(1+\frac{c}{2s}\right)\right]$$

APPENDIX B

MERMORPHIC FUNCTIONS

THE MITTAG - LEFFLER'S EXPANSION THEOREM

Consider a class of functions $f(z)$ whose only singularities in the finite part of the plane are simple poles a_1, a_2, a_3........, where $|a_1| \leqslant |a_2| \leqslant |a_3|$... . Let b_1, b_2, b_3........ be the residues at these poles and let it be possible to choose a sequence of circles C_m (the radius of C_m being R_m) with center 0, not passing through any poles, such that $|f(z)|$ is bounded on C_m. Then it can be shown that [Reference (1)]

$$f(z) = f(0) + \sum_{n=1}^{\infty} b_n \left\{ \frac{1}{z-a_n} + \frac{1}{a_n} \right\}$$

INFINITE PRODUCT EXPANSION

The expansion theorem of integral functions into a product series follows directly from the Mittag-Leffler's Expansion Theorem. Let $f(z)$ be an integral function with simple poles at a_1, a_2........ and suppose that $f'(z)/f(z)$ is a function satisfying all the conditions of the Mittag-Leffler Theorem. It can be shown that:

$$f(z) = f(0) \exp. \left\{ z \frac{f'(0)}{f(0)} \right\} \prod_{n=1}^{\infty} \left(1 - \frac{z}{a_n}\right) \exp. \frac{z}{a_n}$$

Applying the above theorem to the functions $\frac{\sin z}{z}$, $\cos z$, $\frac{\operatorname{sh} z}{z}$ and $\operatorname{ch} z$ one obtains:

$$\sin z = z \prod_{n=1}^{\infty} \left(1 - \frac{z^2}{n^2 \pi^2}\right) \quad ; \quad \operatorname{sh} z = \prod_{n=1}^{\infty} \left(1 + \frac{z^2}{n^2 \pi^2}\right)$$

$$\cos z = \prod_{n=1}^{\infty} \left(1 - \frac{z^2}{(2n-1)^2 \pi^2}\right) \quad ; \quad \operatorname{ch} z = \prod_{n=1}^{\infty} \left(1 + \frac{4z^2}{(2n-1)^2 \pi^2}\right)$$

The exponential terms are missing because (1) the roots appear in pairs $\pm a_1, \pm a_2$ such that $\prod_{n=1}^{\infty} e^{z/a_n} = e^0 = 1$, and (2) $\frac{f'(0)}{f(0)} = 0$ so that $e^{\frac{f'(0)}{f(0)}z} = 1$.

Letting f(a) = A ch z + BZ sh Z the same situation arises. The roots to this equation are given by the following formula: (Reference 2).

$$X = 0 \quad ; \quad \cot y = \frac{B}{A} y$$

where Z = $X + jy$

The roots of the above equation occur in pairs. Denoting these roots by $\pm y_1$, $\pm y_2$, and noting that $\frac{f'(0)}{f(0)} = 0$, we obtain the following product expansion for Ach Z + BZ sh Z :

$$A \operatorname{ch} z + Bz \operatorname{sh} z = \prod_{n=1}^{\infty} \left\{ 1 + \frac{z^2}{y_n^2} \right\}$$

APPENDIX C

PRODUCT SERIES EXPANSION OF THE FEEDLINE TRANSFER FUNCTION

The feedline transfer function for a straight feedline with a simple compliance pump has already been obtained and is given by the following expression:

$$\frac{P_s}{P_t} = \frac{\exp.\left\{\frac{u_o}{a}\cdot\frac{s\ell}{a}\right\}}{ch\sqrt{s(s+c)}\left(\frac{\ell}{a}\right)+\Gamma\sqrt{s(s+c)}\left(\frac{\ell}{a}\right)sh\sqrt{s(s+c)}\left(\frac{\ell}{a}\right)}$$

Letting $Z = \sqrt{s(s+c)}\left(\frac{\ell}{a}\right)$; $\frac{u_o}{a} = 0$

$$\frac{P_s}{P_t} = \frac{1}{ch\,z + \Gamma z(sh\,z)}$$

Because of the special nature of the roots of the feedline transfer function, it may be expanded into a product series.

$$\frac{P_s}{P_t} = \frac{1}{\prod_{n=1}^{\infty}\left\{1+\frac{z^2}{y_n^2}\right\}}$$

where $\cot y = \Gamma y$

The solution of this transcendental equation for $\Gamma = .208$ has been obtained and a few roots are given below.

$y_1 = 1.308$

$y_2 = 4.023$

$y_3 = 6.898$

$y_4 = 9.883$

A Bode plot of Ps/Pt has been obtained using the first 20 roots of y_n and is shown in Figs. 67 and 68. This is a similar curve to that shown in Fig. 10. Because of the plotting techniques used the peak gains should not be read off the curve shown in Fig. 64. It is clear though that the gain drops down with increasing frequency in the product expansion. This is the same phenomena that occurred in the more complex Shuttle Orbiter feedline when product expansions of the transmission parameters were used.

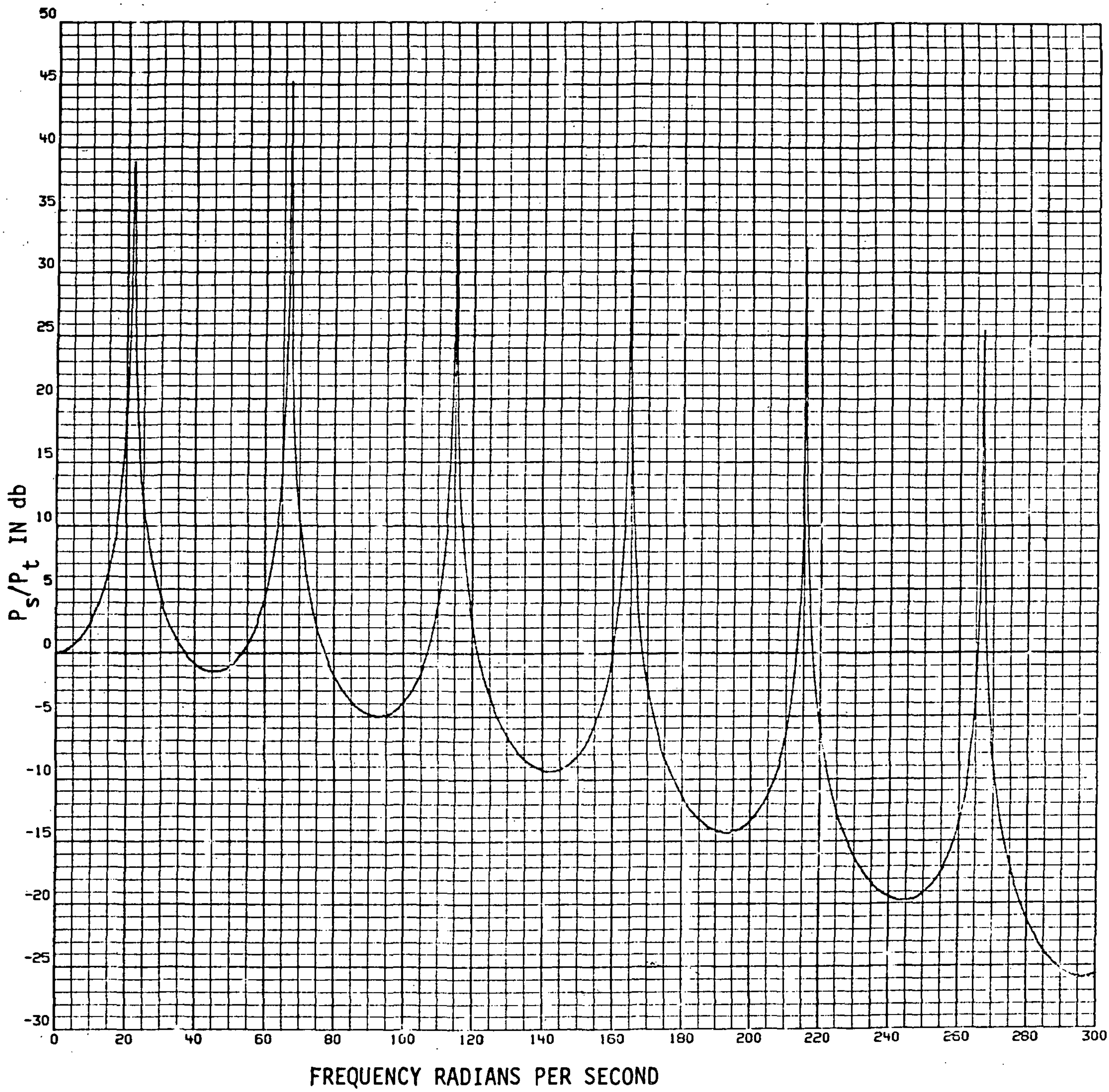

Figure 67 Straight Line with Single Compliance Pump

$$\frac{P_s}{P_t} = \frac{1}{\prod_{n=1}^{20}\left[1 + \frac{z^2}{y_n^2}\right]}$$

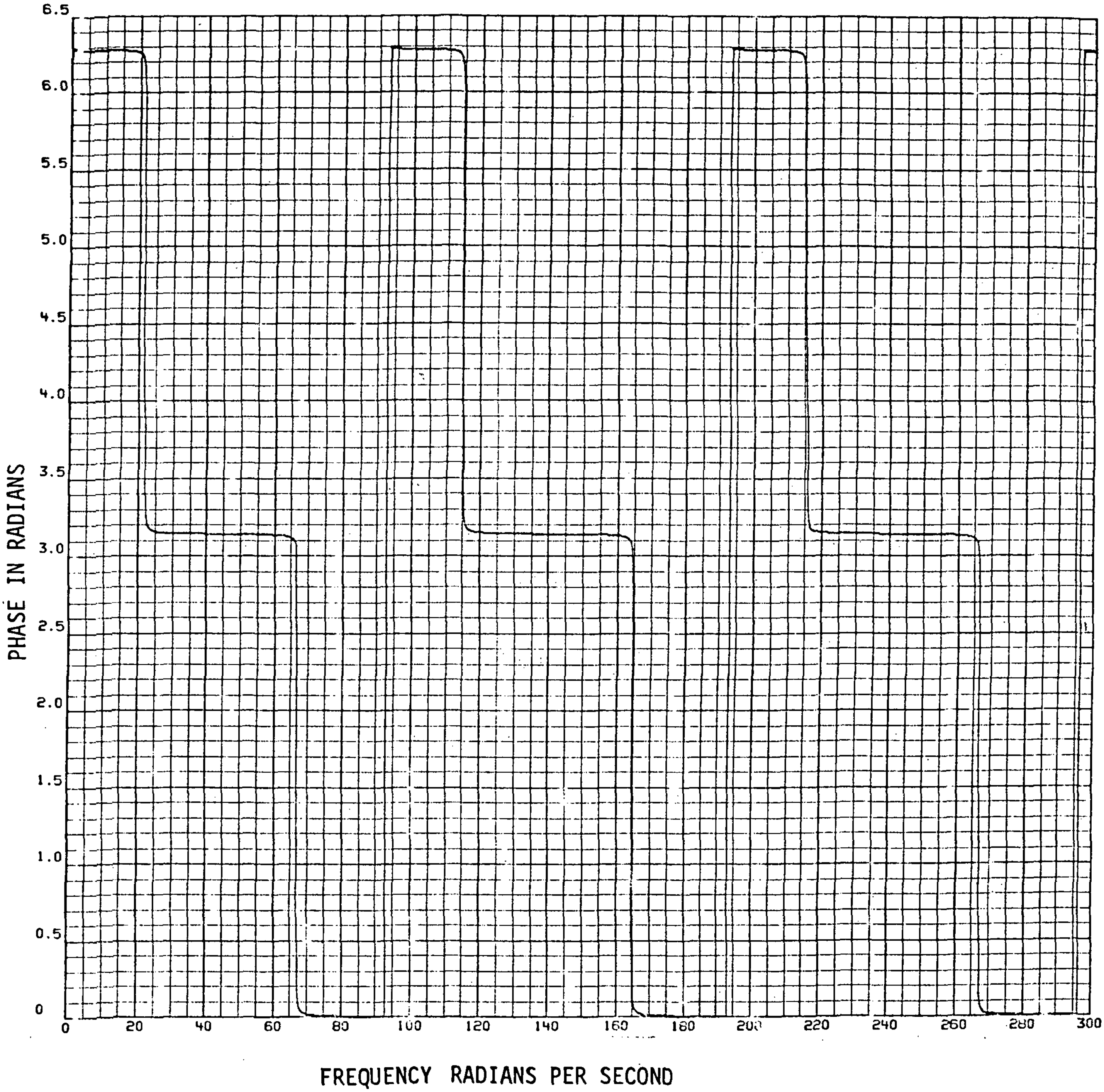

Figure 68 Straight Line with Single Compliance Pump

APPENDIX D

LIST OF SYMBOLS

A	Area of feedline
D	Diameter
M	Mass of vehicle
P	Pressure
R	Damping constant
T	Thrust
A(s), B(s), C(s), D(s)	Transmission parameters
G(s)	Pump termination impedance $P_s/\dot{W}_s$
N_R	Reynolds number
P_s	Pump section pressure
P_t	Tank bottom pressure
P_s/P_t	Feedline transfer function
Teff	Effective thrust
U_o	Nominal flow velocity
$\dot{W}_s$	Flow rate*
a	Acoustic velocity
c	Distributed damping constant $f U_o/D$
f	Darcy Weisbach constant
g	Acceleration of gravity
h	Height of liquid in LO_2 tank
l	Length
s	Complex variable in Laplace transform
q_i	Generalized coordinate
x_g	Displacement of engine gimbal point
x_o	Displacement of orbiter c. g.
β	Bulk modulus
β_e	Effective bulk modulus
ϕ_i	Modal displacement
	Mass density
γ_i	Modal pressure
λ_i	Characteristic value
ρ	Frequency
$\frac{\omega l}{a}$	Nondimensional frequency
μ_i	Generalized mass

*$\dot{W}_s$ is weight flow in English units and mass flow in Metric System.

$\dot{W}_s \stackrel{Df}{=} \rho A U_s g$ ENGLISH SYSTEM

$\dot{W}_s \stackrel{Df}{=} \rho A U_s$ METRIC SYSTEM

This causes some constants to have different units in each system (e. g., damping R is sec/in.^{2} in English units and 1/meter sec in the Metric System).